CHAPTER 2

Wake Fields and Impedances

A charged particle beam interacts electromagnetically with its vacuum chamber surroundings in an accelerator. As a first step in our treatment of the beam-surroundings system (1.1), we will study the properties of the wake electromagnetic fields generated by the beam in the vacuum chamber. For this purpose, the beam is considered to be rigid and unaffected by the wake field it generates (and therefore to show no collective instabilities). The beam is assumed to move with the speed of light. The wake field we are most interested in is that seen by a test charge that follows the beam at a fixed relative distance. In the relativistic limit, causality dictates that there will be no electromagnetic field in front of the beam; thus the term "wake."

The effect of the wake fields on the beam motion—the beam dynamics—will be treated in later chapters. The rigid beam picture adopted in this chapter is not self-consistent, but is an excellent approximation for relativistic beams as far as the calculation of the wake fields is concerned. Materials developed in this chapter serve as inputs to the later chapters.

In Section 1.2, we showed that a relativistic beam does not generate wake fields in a perfectly conducting smooth pipe. If the vacuum chamber is not a smooth pipe or if it is smooth but not perfectly conducting, a beam will generate behind it an electromagnetic wake. See Figure 2.1. We will first work out in some detail in Section 2.1 the wake field for the case of a smooth cylindrical pipe with a resistive wall. In the process, we will point out the general features of all wake fields. The general wake fields are then discussed in Section 2.2.

It is necessary that the concept of impedance also be introduced. This is done in Section 2.3. The wake field, a time domain quantity, and the

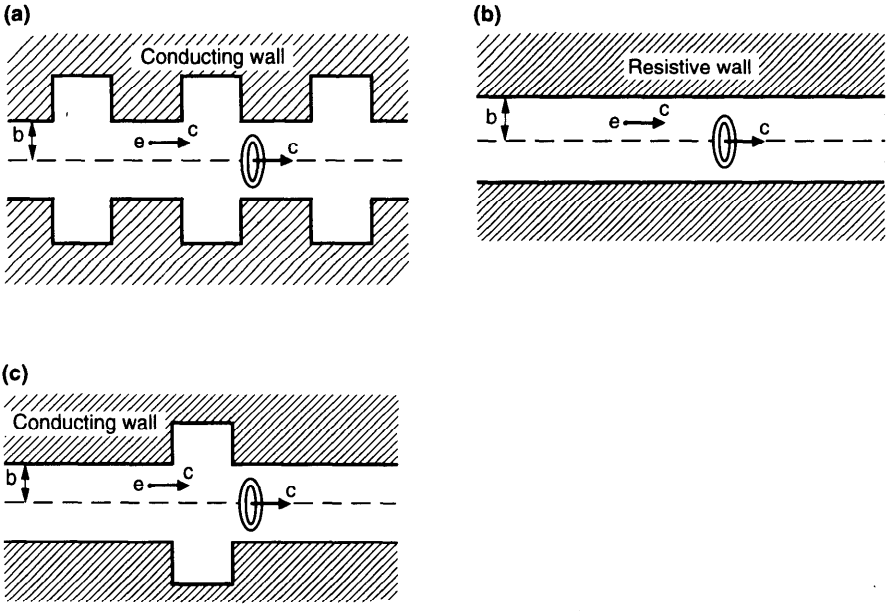

Figure 2.1. Examples of vacuum chamber pipe that generates wake fields. The beam is represented here as a ring possessing a multipole moment with $\cos m\theta$ distribution. A test charge e following the beam at a fixed distance is shown. (a) Periodic structure. (b) Resistive wall. (c) Single structure.

impedance, a frequency domain quantity, are related by Fourier transforms. We will investigate the properties of impedances. Calculation of wake fields and impedances is an important research activity. Two approaches—one in the time domain, one in the frequency domain—are mentioned in Section 2.4. Finally, in Section 2.5, we will discuss the parasitic energy loss—the energy source that feeds all collective instabilities—from the beam to the surroundings.

In the design stage of an accelerator, it is often necessary to budget a total impedance that is consistent with the beam intensity requirements. This total budget is then carefully allocated to individual vacuum chamber components.[1] The topic of how to measure the impedance or wake field of individual vacuum chamber components off-line before they are installed in an acceler-

[1]A possible list of these components: rf cavities, beam position monitors, bellows, flanges, special magnets, beam collimators, vacuum pump ports, vacuum valves, resistive wall, ceramic wall, synchrotron radiation shields, curvature of the pipe, and direct space charge. See the various accelerator design reports, and King Yuen Ng, *AIP Proc.* **184**, *Phys. Part. Accel.*, Fermilab 1987 and Cornell, 1988 p. 472.

ator is an important research and development area not treated in this volume.[2]

2.1 RESISTIVE WALL

In this section, the case of a resistive pipe wall [Figure 2.1(b)] will be worked out in detail. For simplicity, we assume the pipe wall has infinite thickness. We also assume the beam moves with the speed of light and has a distribution given by Eq. (1.7).[3] In this case, the wake field forms a fixed pattern behind the beam, and this pattern moves down the pipe with a phase velocity (not group velocity) c.

Let us first explicitly write down the Maxwell equations, component by component, in cylindrical coordinates:

$$
\begin{aligned}
\frac{1}{r}\frac{\partial(rE_r)}{\partial r} + \frac{1}{r}\frac{\partial E_\theta}{\partial \theta} + \frac{\partial E_s}{\partial s} &= 4\pi\rho, \\
\frac{1}{r}\frac{\partial B_s}{\partial \theta} - \frac{\partial B_\theta}{\partial s} - \frac{1}{c}\frac{\partial E_r}{\partial t} &= \frac{4\pi}{c} j_r, \\
\frac{\partial B_r}{\partial s} - \frac{\partial B_s}{\partial r} - \frac{1}{c}\frac{\partial E_\theta}{\partial t} &= \frac{4\pi}{c} j_\theta, \\
\frac{1}{r}\frac{\partial(rB_\theta)}{\partial r} - \frac{1}{r}\frac{\partial B_r}{\partial \theta} - \frac{1}{c}\frac{\partial E_s}{\partial t} &= \frac{4\pi}{c} j_s, \\
\frac{1}{r}\frac{\partial(rB_r)}{\partial r} + \frac{1}{r}\frac{\partial B_\theta}{\partial \theta} + \frac{\partial B_s}{\partial s} &= 0, \\
\frac{1}{r}\frac{\partial E_s}{\partial \theta} - \frac{\partial E_\theta}{\partial s} + \frac{1}{c}\frac{\partial B_r}{\partial t} &= 0, \\
\frac{\partial E_r}{\partial s} - \frac{\partial E_s}{\partial r} + \frac{1}{c}\frac{\partial B_\theta}{\partial t} &= 0, \\
\frac{1}{r}\frac{\partial(rE_\theta)}{\partial r} - \frac{1}{r}\frac{\partial E_r}{\partial \theta} + \frac{1}{c}\frac{\partial B_s}{\partial t} &= 0.
\end{aligned}
\tag{2.1}
$$

[2]A. Faltens et al., *Proc. 8th Int. Conf. High Energy Accel.*, Geneva, 1971, p. 338; P. B. Wilson, J. B. Styles, and K. L. F. Bane, IEEE Trans. Nucl. Sci. **NS-24**, 1496 (1977); G. Nassibian and F. Sacherer, CERN Report ISR-TH/77-61 (1977); H. Hahn and F. Pedersen, BNL Report 50870 (1978); G. Lambertson, LBL Report 29148 (1990); G. Jackson, *Proc. Workshop Fermilab III Instabilities*, Fermilab, 1990, p. 245; F. Caspers, *Frontiers of Particle Beams: Intensity Limitations*, Lecture Notes in Phys. **400**, Springer-Verlag, 1990, p. 80.

[3]Different treatments of the resistive wall problem can be found in P. L. Morton, V. K. Neil, and A. M. Sessler, J. Appl. Phys. **37**, 3875 (1966); K. W. Robinson, *Proc. Storage Ring Summer Study, 1965*, SLAC Report 49, p. 32; M. J. Lee, F. E. Mills, and P. L. Morton, SLAC Report 76 (1967); R. Briggs, SSC Laboratory Report 512 (1992); Robert L. Gluckstern, Johannes van Zeijts, and Bruno Zotter, Phys. Rev. E **47**, 656 (1993).

Given that ρ and j_s are proportional to $\cos m\theta$, the angular θ-dependence of the field components can be obtained by inspection: E_r, E_s, and B_θ are proportional to $\cos m\theta$, while E_θ, B_r, and B_s are proportional to $\sin m\theta$. One also expects the dependence on s and t to be such that all quantities depend on the combined variable $z \equiv s - ct$, which is the relative longitudinal displacement from the moving $\cos m\theta$ ring beam; $z > 0$ is ahead of the beam, and $z < 0$ is behind the beam. We then write the field components in terms of Fourier transformations[4]

$$\begin{aligned}(E_r, E_s, B_\theta) &= \cos m\theta \int_{-\infty}^{\infty} \frac{dk}{2\pi} e^{ikz}\left(\tilde{E}_r, \tilde{E}_s, \tilde{B}_\theta\right), \\ (E_\theta, B_r, B_s) &= \sin m\theta \int_{-\infty}^{\infty} \frac{dk}{2\pi} e^{ikz}\left(\tilde{E}_\theta, \tilde{B}_r, \tilde{B}_s\right),\end{aligned} \tag{2.2}$$

where $\tilde{E}_r$, etc. are complex quantities and are functions of k and r. Due to causality, our solution must satisfy the condition that no wake field is produced ahead of the beam, i.e., in the region $z > 0$. This requires that $\tilde{E}$ and $\tilde{B}$ components do not have singularities in the upper complex k-plane.

The $m = 0$ Wake

We will first work out the case $m = 0$. The beam considered is a thin ring with total charge q. The field components E_θ, B_r, and B_s vanish. Setting $m = 0$ in Eq. (2.2) and substituting the result, together with Eq. (1.7), into Eq. (2.1), we obtain three equations. [There are eight equations in (2.1), but five of them are redundant.] They are rather easy to solve, yielding

$$\begin{aligned}\tilde{E}_s &= A, \qquad r < b, \\ \tilde{E}_r = \tilde{B}_\theta &= \begin{cases} -ikA\dfrac{r}{2}, & r < a, \\ -ikA\dfrac{r}{2} + \dfrac{2q}{r}, & a < r < b, \end{cases}\end{aligned} \tag{2.3}$$

where A is a constant that depends only on k and is yet to be determined.

Note that there is a discontinuity in $\tilde{E}_r$ and $\tilde{B}_\theta$, but no discontinuity of $\tilde{E}_s$ at $r = a$. Note also that $\tilde{E}_s$, and therefore E_s, does not depend on r; the longitudinal component of the electric wake field at a given longitudinal position z relative to the ring beam is independent of the transverse position r and θ. This is a remarkable result, particularly since we have not yet imposed the boundary conditions. The $2q/r$ term in $\tilde{E}_r$ and $\tilde{B}_\theta$ is the pancake field due to direct space charge. The quantity A is closely related to something called the impedance, to be discussed in Section 2.3. [See Eq. (2.75).]

[4]There is a theorem stating when you have only a partial knowledge of the solution to a differential equation and do not know what to do next, make a Fourier transformation. This theorem is one reason why impedance is such a useful quantity.

For a perfectly conducting wall, $\tilde{E}_s$ vanishes at $r = b$; this means $A = 0$, and an inverse Fourier transform of Eq. (2.3) gives Eqs. (1.4) and (1.5). In case the wall is resistive, one needs to obtain A from the boundary conditions at $r = b$, and to do that, the fields inside the wall, $r > b$, need to be found.

To find the field in the metal wall, we first need a definition of metal. For our purposes, a metal is a material that obeys the conditions[5]

$$\rho = 0 \quad \text{and} \quad \vec{j} = \sigma \vec{E}, \tag{2.4}$$

where σ is the conductivity, assumed to be a constant, independent of k. Equation (2.4) says that a metal is charge free but not current free. Charges, if any, will have to stay on the metal surface. This property of metals leads to the fact (see Exercise 2.4) that the magnetic field tends to penetrate deeper into the metal than the electric field.

Substituting Eq. (2.2) into the Maxwell equation (2.1) and applying Eq. (2.4), we again obtain three nonredundant equations,

$$\begin{aligned} &\frac{1}{r}\frac{\partial}{\partial r}\left(r\frac{\partial \tilde{E}_s}{\partial r}\right) + \lambda^2 \tilde{E}_s = 0, \\ &\tilde{E}_r = \frac{ik}{\lambda^2}\frac{\partial \tilde{E}_s}{\partial r}, \\ &\tilde{B}_\theta = \left(1 + \frac{\lambda^2}{k^2}\right)\tilde{E}_r, \end{aligned} \tag{2.5}$$

where we have defined a parameter

$$\lambda = \sqrt{\frac{2\pi\sigma|k|}{c}}\,[i + \operatorname{sgn}(k)] \tag{2.6}$$

with $\lambda^2 = 4\pi i\sigma k/c$. The sign of λ is chosen so that its imaginary part $\operatorname{Im}\lambda > 0$. The parameter λ^{-1} has the dimensionality of length; it is related to the *skin depth* as a function of frequency $\omega = kc$ inside the metal wall:

$$\delta_{\text{skin}} = \frac{1}{\operatorname{Im}\lambda} = \frac{c}{\sqrt{2\pi\sigma|\omega|}}. \tag{2.7}$$

The procedure in solving Eq. (2.5) is to solve the first equation for $\tilde{E}_s$, then solve for the rest of the field components using the other two equations. This

[5]The definition (2.4) is not arbitrary. For example the equation of continuity must be satisfied, and is satisfied because $\nabla \cdot \vec{j} + \partial\rho/\partial t = \nabla \cdot \vec{j} = \sigma \nabla \cdot \vec{E} = 4\pi\sigma\rho = 0$.

procedure of solving for the longitudinal field components first is common in waveguide analysis. Typical values of σ at room temperature are

$$\sigma = \begin{cases} 3.2 \times 10^{17}\ \mathrm{s}^{-1} \\ 5.4 \times 10^{17} \\ 1.3 \times 10^{16} \end{cases} = \begin{cases} 3.5 \times 10^{7}\ \Omega^{-1}\ \mathrm{m}^{-1}, & \text{aluminum,} \\ 5.9 \times 10^{7}, & \text{copper,} \\ 1.4 \times 10^{6}, & \text{stainless steel.}^{6} \end{cases} \tag{2.8}$$

In what follows, we will assume $|\lambda|$ is much larger than $1/b$, i.e., the skin depth is much shorter than the pipe radius b. This assumption is good if wave number $|k|$ is much greater than $c/4\pi\sigma b^2$, or equivalently, if we are interested in the region

$$|z| \ll \frac{b}{\chi}, \tag{2.9}$$

where χ is a small dimensionless parameter defined by

$$\chi \equiv \frac{c}{4\pi\sigma b}. \tag{2.10}$$

For example, if $b = 5$ cm and the wall is made of aluminum, we have $\chi = 1.5 \times 10^{-9}$ and our approximation breaks down at a distance $\gtrsim 3 \times 10^7$ m behind the beam.

In case the vacuum chamber wall has a finite thickness t, our approximation also requires $|\lambda| \gg 1/t$. If $t = 3$ mm, the approximation breaks down at distance $\gtrsim 1 \times 10^5$ m. The corresponding low-frequency field components leak through the pipe wall, leading to the Laslett analysis of tune shifts (1.30–1.31).

Under the approximation $|\lambda| \gg 1/b$, the equation for $\tilde{E}_s$ in (2.5) becomes $\partial^2\tilde{E}_s/\partial r^2 + \lambda^2\tilde{E}_s = 0$, which has the solution[7]

$$\tilde{E}_s = A\, e^{i\lambda(r-b)}, \tag{2.11}$$

where the coefficient A is the same as that appearing in Eq. (2.3) to assure continuity of $\tilde{E}_z$. From Eq. (2.5), we then have

$$\begin{aligned} \tilde{E}_r &= -\frac{k}{\lambda} A\, e^{i\lambda(r-b)}, \\ \tilde{B}_\theta &= -\frac{k}{\lambda}\left(1 + \frac{\lambda^2}{k^2}\right) A\, e^{i\lambda(r-b)}. \end{aligned} \tag{2.12}$$

[6] We assume 18% chromium, 8% nickel.

[7] If we do not assume $|\lambda| \gg b^{-1}$, $\tilde{E}_s$ will be written in terms of Bessel functions. This complication is not required for our purposes. A slightly more accurate approximation would be to include an additional factor $\sqrt{b/r}$ in the field expressions (2.11–2.12).

The coefficient A is determined by the continuity of $\tilde{B}_\theta$ at $r = b$, yielding the result

$$A = \frac{2q/b}{\frac{ikb}{2} - \frac{\lambda}{k}}, \tag{2.13}$$

where a term $-k/\lambda$ in the denominator has been dropped because it is much smaller than the term $ikb/2$. Note that it would be incorrect to demand continuity of $\tilde{E}_r$ at $r = b$, because there is a surface charge on the wall pipe.

What we will have to do next is to make inverse Fourier transforms on $\tilde{E}_r$, $\tilde{E}_z$, and $\tilde{B}_\theta$ to obtain the fields. The exact expressions will be given later, but first, investigate the region where $|\lambda/k| \gg |kb|$. This condition on k in frequency space is equivalent to requiring in physical space the condition

$$|z| \gg \chi^{1/3} b. \tag{2.14}$$

Again taking an aluminum pipe with $b = 5$ cm, this condition excludes the study of wake fields within a distance $\lesssim 0.06$ mm behind the beam.

Under the assumptions (2.9) and (2.14), i.e., in the region $b/\chi \gg |z| \gg \chi^{1/3} b$, the quantity A becomes

$$A \approx -\frac{2qk}{b\lambda}. \tag{2.15}$$

The inverse Fourier transform can then be readily performed for the region $r < b$. The results for $z < 0$, i.e., behind the beam, are

$$\begin{aligned} E_s &= \frac{q}{2\pi b}\sqrt{\frac{c}{\sigma}}\,\frac{1}{|z|^{3/2}}, \\ B_\theta = E_r &= -\frac{3}{4}\frac{q}{2\pi b}\sqrt{\frac{c}{\sigma}}\,\frac{r}{|z|^{5/2}}. \end{aligned} \tag{2.16}$$

The fields vanish for $z > 0$ due to causality. In the region $a < r < b$, E_r and B_θ contain the additional pancake terms (1.4) and (1.5), but they are dropped because they are excluded by the condition (2.14). In deriving Eq. (2.16), we have used the formulas given in Table 2.1. Equation (2.16) shows that E_s decreases algebraically as $|z|^{-3/2}$ and is uniform in the transverse dimension (independent of r and θ), while the transverse field components decrease faster, with a $|z|^{-5/2}$ dependence, and are proportional to r.

Table 2.1. Fourier transform pairs $F(z) = \int_{-\infty}^{\infty}(dk/2\pi)e^{ikz}\tilde{F}(k)$. The quantity λ is given by Eq. (2.6). The function $F(z)$ vanishes for $z > 0$.

$\tilde{F}(k)$	$F(z)\,(z < 0)$
$1/k$	$-i$
$1/k^2$	z
$1/k^{n+1}$	$-(i/n!)(iz)^n$
λ/k^2	$-4i\sqrt{\sigma/c}\,\lvert z\rvert^{1/2}$
λ/k^3	$-(8/3)\sqrt{\sigma/c}\,\lvert z\rvert^{3/2}$
$1/\lambda$	$-(i/2\pi)\sqrt{c/\sigma}\,\lvert z\rvert^{-1/2}$
k/λ	$-(1/4\pi)\sqrt{c/\sigma}\,\lvert z\rvert^{-3/2}$
k^2/λ	$(3/8\pi)i\sqrt{c/\sigma}\,\lvert z\rvert^{-5/2}$
$e^{i\alpha\lambda}$ $(\alpha > 0)$	$\sqrt{\sigma/c}\,\alpha\lvert z\rvert^{-3/2}\exp(-\pi\sigma\alpha^2/c\lvert z\rvert)$

Exercise 2.1 The impedance per unit length, $Z_0^{\parallel}/L$, is related to A by $Z_0^{\parallel}/L = -A/qc$, as given by Eq. (2.75) below. Show that $\tilde{E}_s/\tilde{B}_\theta = -k/\lambda$ at $r = b^-$, and therefore, using Eq. (2.15),

$$\frac{Z_0^{\parallel}}{L} = \frac{Z_0}{2\pi b}\frac{\tilde{E}_s}{\tilde{B}_\theta}\bigg|_{r=b^-}, \tag{2.17}$$

where $Z_0 = 377\ \Omega$, as defined in Eq. (1.2). Equation (2.17) relates the impedance to the ratio of $\tilde{E}_s$ and $\tilde{B}_\theta$ at the pipe wall, as is often encountered in the analysis of waveguides.

Exercise 2.2 Consider a pipe with finite thickness t and conductivity σ. Follow the analysis of the text to show that, inside the pipe region, and for distances $b/\chi \gg |z| \gg \chi^{1/3}b$,

$$\tilde{E}_s = -\frac{2qk}{b\lambda}\frac{1 - e^{2i\lambda t}}{1 + e^{2i\lambda t}}. \tag{2.18}$$

Show that Eq. (2.17) is valid in this case also.

Exercise 2.3 Table 2.1, with the exception of the last entry, can be obtained by considering a general $F(z) = e^{\epsilon z}|z|^{p-1}$ for $z < 0$ and 0 for $z > 0$, where $\epsilon > 0$. Show that

$$\tilde{F}(k) = \Gamma(p)\left(\frac{i}{k + i\epsilon}\right)^p,$$

where $\Gamma(x)$ is the gamma function.[8] Show that this Fourier transform pair satisfies the Parseval theorem, Eq. (2.26).

Exercise 2.4 In the pipe wall ($r > b$) and in the region where $|z|$ is of the order of pipe radius b behind the beam, show that $B_\theta \gg E_s \gg E_r$ and that each is greater than the next by a factor of the order of $\chi^{-1/2}$. The magnetic field penetrates better into the metal than the electric field, and the component of the electric field perpendicular to the metal surface is stopped most effectively by the surface charge on the metal surface.

Exercise 2.5 Perform an inverse Fourier transformation on Eq. (2.11), using Table 2.1, to obtain E_s in the pipe wall:

$$E_s = \frac{q}{2\pi b}\sqrt{\frac{c}{\sigma}}\,|z|^{-3/2}\left[1 - \frac{2\pi\sigma(r-b)^2}{c|z|}\right]\exp\left[-\frac{\pi\sigma(r-b)^2}{c|z|}\right]. \quad (2.20)$$

The fields penetrate into the wall to a depth of the order of

$$\delta r = \sqrt{\frac{c|z|}{\pi\sigma}}\,. \quad (2.21)$$

This penetration depth, increasing as $\sqrt{|z|}$, is the time domain description of the skin depth effect.

Note that in the region of interest the field components are continuous across $r = a$ and, in fact, are even independent of a. By taking the limit $a \to 0$, we see that the results are also applicable to the case when the beam is represented as a point charge.

There is something disturbing about Eq. (2.16). Consider a test charge trailing the beam at a certain distance $|z|$. The sign of the longitudinal electric field E_s is such that the test charge gets *accelerated* if it has the same sign as q. If this were true for $|z| \to 0$, one would expect the point charge q to *gain* energy as it travels down the resistive pipe due to its own wake field. To make sure this unphysical phenomenon does not happen, we have to

[8]Gamma functions are generalized factorials. One is of course familiar with the factorials of integers; the gamma function defines how to take factorials of fractional numbers as well. Some properties of the gamma function that will be handy later are listed below:

$$\begin{aligned}
&\Gamma(n+1) = n!, \qquad \Gamma(x+1) = x\Gamma(x),\\
&\Gamma(x)\Gamma(1-x) = \frac{\pi}{\sin \pi x},\\
&\Gamma\left(\tfrac{1}{2}\right) = \sqrt{\pi}, \qquad \Gamma\left(\tfrac{1}{4}\right) = 3.626,\\
&\lim_{x\to\infty}\frac{\Gamma(x+a)}{\Gamma(x)} = x^a.
\end{aligned} \quad (2.19)$$

compute the field at very short distances behind the beam, which so far has been excluded by the condition (2.14).

To do this, we could perform the inverse Fourier transformations using the complete expression (2.13) for $A(k)$.[9] The derivation, which involves taking branch cuts in complex variables, is omitted here. The results in the pipe region are

$$E_s = -\frac{16q}{b^2}\left(\frac{1}{3}e^u\cos\sqrt{3}u - \frac{\sqrt{2}}{\pi}\int_0^\infty dx\frac{x^2 e^{ux^2}}{x^6+8}\right),$$

$$E_r = B_\theta = \frac{8qr}{(2\chi)^{1/3}b^3}\left(\frac{1}{3}e^u\cos\sqrt{3}u - \frac{1}{\sqrt{3}}e^u\sin\sqrt{3}u - \frac{\sqrt{2}}{\pi}\int_0^\infty dx\frac{x^4 e^{ux^2}}{x^6+8}\right), \tag{2.22}$$

where $u = z/(2\chi)^{1/3}b < 0$. The behavior of the fields at small $|z|$ can be obtained from Eq. (2.22).

Alternatively, we can take the opposite limit to Eq. (2.14), i.e., we can take the limit $|\lambda/k| \ll |kb|$, or equivalently $|z| \ll \chi^{1/3}b$. The parameter A then is approximately given by[10]

$$A \approx \frac{4q}{ikb^2}\left(1 - i\frac{2\lambda}{k^2 b} + \cdots\right). \tag{2.23}$$

Using Table 2.1, we perform inverse Fourier transformations to obtain, for a point charge with $a = 0$, in the pipe region $r < b$,

$$E_s \approx -\frac{4q}{b^2} + \frac{64}{3}\frac{q}{b^3}\sqrt{\frac{\sigma}{c}}|z|^{3/2},$$

$$E_r = B_\theta \approx \frac{2q}{b}\left(\frac{b}{r} - \frac{r}{b}\right)\delta(z) + 16\frac{q}{b^3}r\sqrt{\frac{\sigma}{c}}|z|^{1/2}. \tag{2.24}$$

Again these expressions are valid for $z < 0$; the fields vanish for $z > 0$. For very small $|z| \ll \chi^{1/3}b$, the first terms in Eq. (2.24) dominate. One finds that, immediately behind the charge q, E_s is indeed decelerating, that $E_s(0^-) = -4q/b^2$, and that E_r and B_θ contain only the "pancake" terms proportional to $\delta(z)$. The strength of E_s is uniform across the entire pancake plane, while $E_r = B_\theta$ decreases with increasing r and vanishes as r reaches the pipe radius b, as if the field is leaking out of the pancake region. This leakage, in fact, is what *becomes* the nonvanishing E_s.

[9]Karl L. F. Bane, SLAC Report AP-87 (1991); H. Henke and O. Napoly, *Proc. Euro. Part. Accel. Conf.*, Nice, 1990, p. 1046; O. Henry and O. Napoly, Part. Accel. **35**, 235 (1991).

[10]The short range behavior of the wake field depends on the assumption that the beam moves with the speed of light. The upper range of k in reality has a cutoff around γ/b. This introduces the condition that in order for Eq. (2.23) to be valid, the beam energy must be high enough so that $\gamma \gg \chi^{-1/3}$.

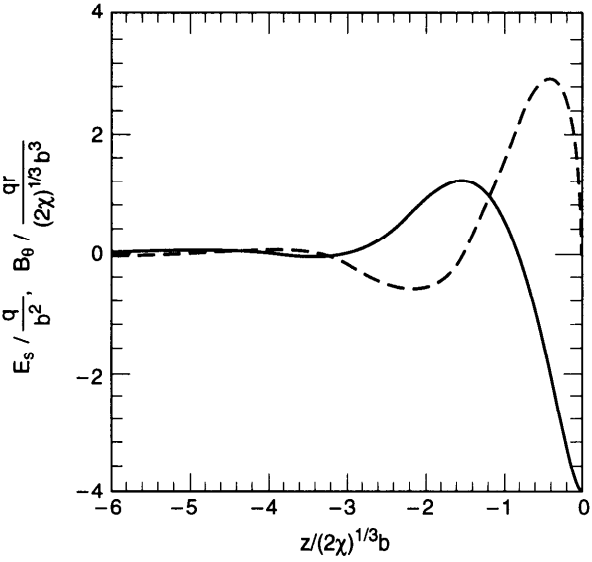

Figure 2.2. The short range wake field components due to a resistive wall are shown as functions of $u = z/(2\chi)^{1/3}b$. Solid and dashed curves are for E_s and $E_r = B_\theta$, normalized by q/b^2 and $qr/(2\chi)^{1/3}b^3$, respectively. The fields vanish for $z > 0$.

Note that although $E_s(0^-)$ is independent of the wall conductivity σ, the range of validity of Eq. (2.24) does depend on σ. In the limit $\sigma \to \infty$, a beam with finite length or a point charge with $v < c$, of course, does not lose energy to the vacuum chamber.

Figure 2.2 shows the fields immediately following the point charge calculated using the exact expressions (2.22). The transverse field components E_r and B_θ are much larger than the longitudinal component E_s, but decay faster with increasing $|z|$.[11] All field components switch signs three times following the point charge, and approach the power law behavior (2.16) asymptotically when $|z| \gg \chi^{1/3}b$. The fields $E_r = B_\theta = 0$ when E_s reaches its maxima, but $E_s \neq 0$ when $E_r = B_\theta$ reach their maxima. Figure 2.3 shows the electric field pattern in the pipe region.

Exercise 2.6 Derive the approximate expressions (2.16) and (2.24) in the proper limits using the exact formula (2.22). It is interesting to observe how fractional powers of u appear in the asymptotic forms starting from the innocent-looking Eq. (2.22).

[11] Be reminded of the fact that the transverse *force* vanishes even though the transverse *fields* are large.

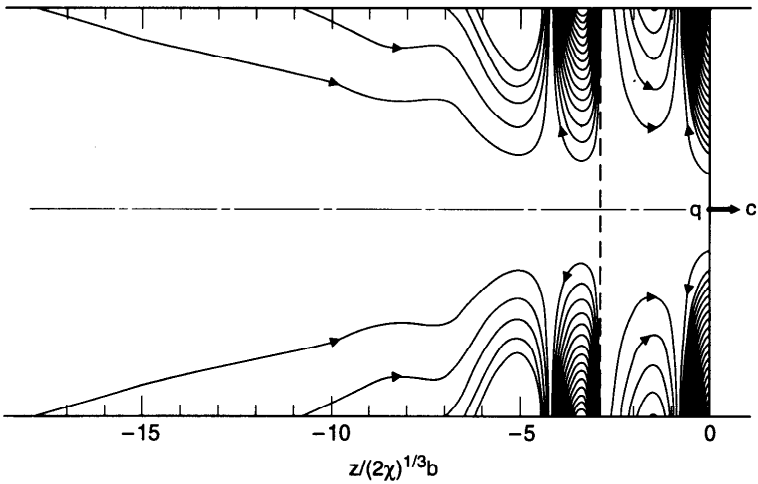

Figure 2.3. Wake electric field lines in a resistive wall pipe generated by a point charge q. The field pattern shows oscillatory behavior in the region $|z| \lesssim 5(2\chi)^{1/3}b$ (or $|z| \lesssim 0.35$ mm for an aluminum pipe with $b = 5$ cm). The field line density to the left of the dashed line has been magnified by a factor of 40. (Courtesy Karl Bane, 1991.)

One can obtain the rate of energy loss of the charge q by equating it to the heat generated in the resistive wall. This gives

$$\begin{aligned}\frac{d\mathscr{E}}{ds} &= -\frac{1}{c}\int_{\text{wall}} dV\vec{j}\cdot\vec{E} = -\frac{1}{c}\int_{\text{wall}} dV\,\sigma\vec{E}^2 \\ &= -\frac{\sigma}{c}\int_b^\infty 2\pi b\,dr\int_{-\infty}^\infty dz\left(E_s^2 + E_r^2\right) \\ &= -\frac{\sigma}{c}\int_b^\infty b\,dr\int_{-\infty}^\infty dk\left(|\tilde{E}_s|^2 + |\tilde{E}_r|^2\right),\end{aligned} \tag{2.25}$$

where we have used the Parseval theorem that

$$\int_{-\infty}^\infty dz\,F^2(z) = \int_{-\infty}^\infty \frac{dk}{2\pi}\left|\tilde{F}(k)\right|^2 \tag{2.26}$$

for Fourier transform pairs $F(z)$ and $\tilde{F}(k)$. Using the expressions (2.11) and (2.12) for $\tilde{E}_s$ and $\tilde{E}_r$ in the metal wall and Eq. (2.13) for A, and making the approximation that $\chi = c/4\pi\sigma b \ll 1$, we find[12]

$$\frac{d\mathscr{E}}{ds} = -\frac{2q^2}{b^2}. \tag{2.27}$$

[12]The algebra simplifies if one notes the contribution from $\tilde{E}_r$ is small.

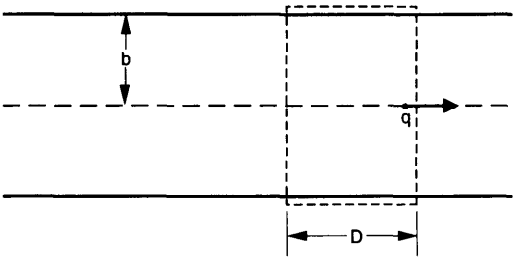

Figure 2.4. A box for computing the image charge using Gauss's law.

If we then associate this energy loss with an equivalent electric field as seen by the charge q, we find that it is exactly equal to half of the value of $E_s(z)$ in the limit $|z| \to 0$, given by Eq. (2.24). That is,

$$E_s\big|_{\text{seen by } q} = \tfrac{1}{2} E_s\big|_{z \to 0^-}. \tag{2.28}$$

Exercise 2.7 Equation (2.27), and thus Eq. (2.28), can be shown in different ways.

(a) Evaluate $E_s(0) = \int_{-\infty}^{\infty} (dk/2\pi) A(k)$ explicitly to show it is equal to $-2q/b^2$.

(b) Use the parasitic loss formula (2.103), combined with the resistive wall impedance (2.75) and $\tilde{\rho}(\omega) = q$ for a point charge.

(c) The energy flux into the wall is determined by the radial component of the Poynting vector $S_r = -cE_s B_\theta / 4\pi$. Calculate $d\mathscr{E}/ds$ by integrating S_r over the wall surface.

Exercise 2.8

(a) The surface charge density Σ on the pipe wall is related to the discontinuity of E_r at $r = b$. Show that the total charge on the wall surface is $-q$ by integrating Σ over the wall surface.

(b) Draw a box like Figure 2.4 and apply Gauss's law. Show that the total image charge contained between $|z| = 0$ and $|z| = D \gg \chi^{1/3} b$ behind the point charge q, to order $1/\sqrt{\sigma}$, is given by

$$-q\left(1 + \frac{b}{8\pi}\sqrt{\frac{c}{\sigma}}\, D^{-3/2}\right). \tag{2.29}$$

Note that the magnitude of this charge is larger than q.

Equation (2.28) actually is a general result, referred to as the *fundamental theorem of beam loading*.[13] The factor $\frac{1}{2}$ comes from the fact that charges in a beam see the wake produced only by those charges in front of it and as a result see on the average only half of the total beam charge.

[13] Perry B. Wilson, *AIP Proc.* **87**, *Phys. High Energy Accel.*, Fermilab, 1981, p. 450.

To prove Eq. (2.28) in general, consider a beam with short but finite length that has an otherwise arbitrary longitudinal charge density $\rho(z)$. The beam loses energy at a rate

$$\frac{d\mathscr{E}}{ds} = -\int_{-\infty}^{\infty} dz'\,\rho(z')\int_{z'}^{\infty} dz\,\rho(z)E_s(z'-z) \tag{2.30}$$

where $E_s(z'-z)$ is the wake produced by a unit point charge and seen by another point charge a distance $|z'-z|$ behind in an arbitrary vacuum chamber environment. If the bunch length is short enough that E_s behaves like a step function within the bunch distribution, Eq. (2.30) becomes

$$\frac{d\mathscr{E}}{ds} \approx -E_s(0^-)\int_{-\infty}^{\infty} dz'\,\rho(z')\int_{z'}^{\infty} dz\,\rho(z). \tag{2.31}$$

By a change of variable from z to $u = \int_z^{\infty} dz'\,\rho(z')$, Eq. (2.31) gives

$$\frac{d\mathscr{E}}{ds} \approx -E_s(0^-)\int_0^q u\,du = -\frac{q^2}{2}E_s(0^-), \tag{2.32}$$

which proves Eq. (2.28). The derivation assumed nothing but causality.

The $m \geq 1$ Wake

So far, electromagnetic wake fields have been obtained for the case $m = 0$. The fields are excited as the charge (i.e., the monopole moment) of the beam interacts with the resistive wall surroundings. If the beam possesses higher moments ($m = 1$ for dipole, $m = 2$ for quadrupole, etc.) in its transverse distribution, it will interact differently and generate different wake field patterns. In the following, we will work out the wake fields for cases $m \geq 1$.

Substituting Eqs. (1.7) and (2.2) into the Maxwell equation (2.1), we obtain the following results in the region $r < b$:

$$\begin{aligned}
\frac{\partial \tilde{E}_s}{\partial r} &= -\frac{m}{r}\tilde{B}_s,\\
\frac{\partial \tilde{B}_s}{\partial r} &= -\frac{m}{r}\tilde{E}_s,\\
\frac{1}{r}\frac{\partial}{\partial r}(r\tilde{E}_r) - \frac{m}{r}\tilde{B}_r &= \frac{4I_m}{a^{m+1}}\delta(r-a) - i\left(k + \frac{m^2}{kr^2}\right)\tilde{E}_s,\\
\frac{1}{r}\frac{\partial}{\partial r}(r\tilde{B}_r) - \frac{m}{r}\tilde{E}_r &= -i\left(k + \frac{m^2}{kr^2}\right)\tilde{B}_s,\\
\tilde{B}_\theta &= \tilde{E}_r - i\frac{m}{kr}\tilde{B}_s,\\
\tilde{E}_\theta &= -\tilde{B}_r + i\frac{m}{kr}\tilde{E}_s.
\end{aligned} \tag{2.33}$$

The first two of these equations are used to obtain $\tilde{E}_s$ and $\tilde{B}_s$; the second pair can then be solved for $\tilde{E}_r$ and $\tilde{B}_r$; then $\tilde{E}_\theta$ and $\tilde{B}_\theta$ are found from the last two expressions. The longitudinal components are easy to find,

$$\begin{aligned} \tilde{E}_s &= Ar^m, \qquad r < b, \\ \tilde{B}_s &= -Ar^m, \qquad r < b, \end{aligned} \tag{2.34}$$

where A is some coefficient that depends on k. Note that $\tilde{E}_s$ and $\tilde{B}_s$ are continuous across $r = a$.

Knowing $\tilde{E}_s$ and $\tilde{B}_s$, the solution for the other field components is not difficult to obtain. One needs only to observe that they generally can be written as polynomials in r, each containing three terms proportional to r^{m-1}, r^{m+1}, and r^{-m-1}, respectively. By properly choosing the coefficients for each of the terms for the two regions $r < a$ and $a < r < b$, the solution is found to be

$$\tilde{E}_r = \begin{cases} -\dfrac{ikA}{2(m+1)} r^{m+1} + \dfrac{1}{2}\left(-\dfrac{imA}{k} + B - \dfrac{4I_m}{a^{2m}} \right) r^{m-1}, \\ \dfrac{2I_m}{r^{m+1}} - \dfrac{ikA}{2(m+1)} r^{m+1} + \dfrac{1}{2}\left(-\dfrac{imA}{k} + B \right) r^{m-1}, \end{cases}$$

$$\tilde{E}_\theta = \begin{cases} -\dfrac{ikA}{2(m+1)} r^{m+1} + \dfrac{1}{2}\left(\dfrac{imA}{k} - B + \dfrac{4I_m}{a^{2m}} \right) r^{m-1}, \\ \dfrac{2I_m}{r^{m+1}} - \dfrac{ikA}{2(m+1)} r^{m+1} + \dfrac{1}{2}\left(\dfrac{imA}{k} - B \right) r^{m-1}, \end{cases} \tag{2.35}$$

$$\tilde{B}_r = \begin{cases} \dfrac{ikA}{2(m+1)} r^{m+1} + \dfrac{1}{2}\left(\dfrac{imA}{k} + B - \dfrac{4I_m}{a^{2m}} \right) r^{m-1}, \\ -\dfrac{2I_m}{r^{m+1}} + \dfrac{ikA}{2(m+1)} r^{m+1} + \dfrac{1}{2}\left(\dfrac{imA}{k} + B \right) r^{m-1}, \end{cases}$$

$$\tilde{B}_\theta = \begin{cases} -\dfrac{ikA}{2(m+1)} r^{m+1} + \dfrac{1}{2}\left(\dfrac{imA}{k} + B - \dfrac{4I_m}{a^{2m}} \right) r^{m-1}, \\ \dfrac{2I_m}{r^{m+1}} - \dfrac{ikA}{2(m+1)} r^{m+1} + \dfrac{1}{2}\left(\dfrac{imA}{k} + B \right) r^{m-1}, \end{cases}$$

where the upper and lower entries of each field component refer to the regions $r < a$ and $a < r < b$, respectively. The field components in the region $r < a$ do not contain r^{-m-1} terms, since they are unphysical at $r = 0$. The coefficient A appeared in Eq. (2.34), while B is a new coefficient. Both A and B are yet to be determined.

In the case of a perfectly conducting wall, $A = 0$ because $\tilde{E}_s$ must vanish at $r = b$. The condition that $\tilde{E}_\theta = 0$ at $r = b$ gives $B = 4I_m/b^{2m}$. An inverse Fourier transform then establishes Eq. (1.8).

To find A and B for the resistive-wall case, we need to solve for the fields in the metal wall. Inserting again Eq. (2.2) into the Maxwell equations and setting $\vec{j} = \sigma\vec{E}$ and $\rho = 0$, we obtain

$$
\begin{aligned}
&\frac{1}{r}\frac{\partial}{\partial r}\left(r\frac{\partial \tilde{E}_s}{\partial r}\right) + \left(\lambda^2 - \frac{m^2}{r^2}\right)\tilde{E}_s = 0,\\
&\frac{1}{r}\frac{\partial}{\partial r}\left(r\frac{\partial \tilde{B}_s}{\partial r}\right) + \left(\lambda^2 - \frac{m^2}{r^2}\right)\tilde{B}_s = 0,\\
&\tilde{E}_r = \frac{c}{4\pi\sigma}\left(\frac{m}{r}\tilde{B}_s + \frac{\partial \tilde{E}_s}{\partial r}\right),\\
&\tilde{E}_\theta = -\frac{c}{4\pi\sigma}\left(\frac{m}{r}\tilde{E}_s + \frac{\partial \tilde{B}_s}{\partial r}\right),\\
&\tilde{B}_r = \frac{c}{4\pi\sigma}\frac{\partial \tilde{B}_s}{\partial r} + \left(\frac{c}{4\pi\sigma} + \frac{i}{k}\right)\frac{m}{r}\tilde{E}_s,\\
&\tilde{B}_\theta = \frac{c}{4\pi\sigma}\frac{m}{r}\tilde{B}_s + \left(\frac{c}{4\pi\sigma} + \frac{i}{k}\right)\frac{\partial \tilde{E}_s}{\partial r}.
\end{aligned}
\tag{2.36}
$$

After the first pair of equations are solved for $\tilde{E}_s$ and $\tilde{B}_s$, the other field components are obtained from the remaining four equations. The quantity λ was defined in Eq. (2.6).

Following the analysis for the $m = 0$ case, we assume again that the skin depth is much smaller than b, i.e., we are interested in the region specified by Eq. (2.9). The first two equations in (2.36) then have the solution

$$
\tilde{E}_s = -\tilde{B}_s = Ab^m e^{i\lambda(r-b)}, \qquad r > b. \tag{2.37}
$$

Knowing $\tilde{E}_s$ and $\tilde{B}_s$, the rest of the field components are found to be

$$
\begin{aligned}
\tilde{E}_r = \tilde{E}_\theta &= -\frac{k}{\lambda}Ab^m e^{i\lambda(r-b)},\\
\tilde{B}_\theta &= -\left(\frac{k}{\lambda} + \frac{\lambda}{k}\right)Ab^m e^{i\lambda(r-b)},\\
\tilde{B}_r &= \left(\frac{k}{\lambda} + \frac{im}{kb}\right)Ab^m e^{i\lambda(r-b)}.
\end{aligned}
\tag{2.38}
$$

The requirement that $\tilde{E}_\theta$, $\tilde{B}_r$, and $\tilde{B}_\theta$ be continuous at $r = b$ (the component $\tilde{E}_r$ is not continuous across $r = b$, due to a surface charge on the wall) gives

$$A = \frac{4I_m}{b^{2m+1}\left(\dfrac{ikb}{m+1} - \dfrac{\lambda}{k} - \dfrac{im}{kb}\right)},$$
$$B = -\frac{\lambda}{k} bA. \tag{2.39}$$

If we further restrict our interest to the region specified by Eq. (2.14), the coefficients A and B become

$$A \approx -\frac{4I_m k}{b^{2m+1}\lambda},$$
$$B \approx \frac{4I_m}{b^{2m}}\left[1 + i\frac{k^2 b}{(m+1)\lambda} - \frac{im}{b\lambda}\right]. \tag{2.40}$$

Table 2.1 can then be used to find the field components, yielding

$$E_s = \frac{I_m}{\pi b^{2m+1}}\sqrt{\frac{c}{\sigma}}\, r^m \cos m\theta \frac{1}{|z|^{3/2}},$$
$$E_r = -\frac{3I_m}{4\pi b^{2m+1}}\sqrt{\frac{c}{\sigma}}\frac{1}{(m+1)} r^{m-1}\cos m\theta\,(r^2 + b^2)\frac{1}{|z|^{5/2}},$$
$$E_\theta = -\frac{3I_m}{4\pi b^{2m+1}}\sqrt{\frac{c}{\sigma}}\frac{1}{(m+1)} r^{m-1}\sin m\theta\,(r^2 - b^2)\frac{1}{|z|^{5/2}},$$
$$B_s = -\frac{I_m}{\pi b^{2m+1}}\sqrt{\frac{c}{\sigma}}\, r^m \sin m\theta \frac{1}{|z|^{3/2}}, \tag{2.41}$$
$$B_r = -E_\theta - \frac{2I_m}{\pi b^{2m+1}}\sqrt{\frac{c}{\sigma}}\, m r^{m-1}\sin m\theta \frac{1}{|z|^{1/2}},$$
$$B_\theta = E_r - \frac{2I_m}{\pi b^{2m+1}}\sqrt{\frac{c}{\sigma}}\, m r^{m-1}\cos m\theta \frac{1}{|z|^{1/2}}.$$

These expressions are valid for regions behind the beam and inside the pipe. Again, the field vanishes in front of the beam. Note that the beam dimension a does not appear explicitly in the fields, indicating that for a given mth moment of the beam, the wake field is independent of the detailed shape of the beam distribution. See Figure 2.5.

According to Eq. (2.41), the longitudinal electric field component E_s behaves like $|z|^{-3/2}$ and the transverse electric field components behave like

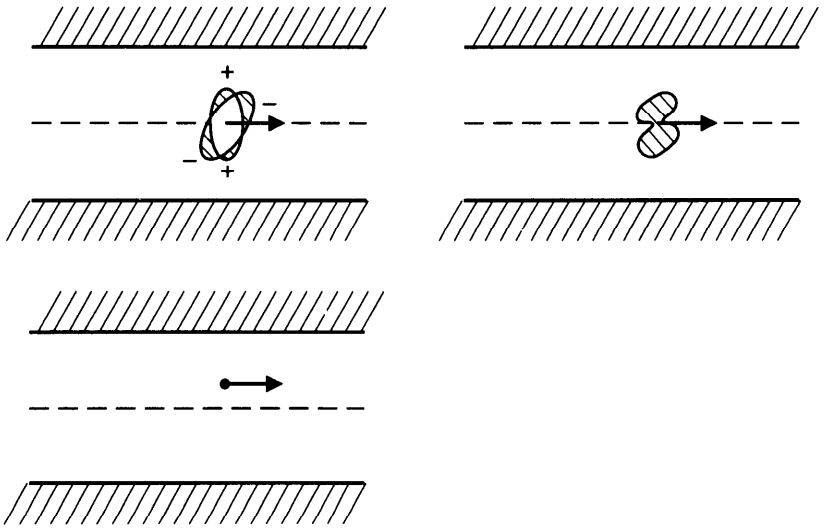

Figure 2.5. The wake field is independent of the detailed beam distribution. The same wake field is generated as long as the beam has the same mth moment. Cases shown are for $m = 2$.

$|z|^{-5/2}$, similarly to the $m = 0$ case, Eq. (2.16); but the magnetic field behaves very differently from the $m = 0$ case. First, B_s no longer vanishes. Second, the magnitude of the transverse magnetic field is comparable to the transverse electric field at distances $|z| \lesssim b$ behind the beam, but, having a long $|z|^{-1/2}$ tail, dominates at distances $|z| \gtrsim b$.

Equation (2.41) is obtained assuming I_m is a constant as it moves down the resistive pipe with $s = ct$. In case I_m changes with s, the wake field observed at a fixed location $s' < s$ in the accelerator is given by replacing I_m in Eq. (2.41) with its value $I_m(s')$ at the moment when it was passing by position s', and replacing z with $s' - s$.

Exercise 2.9 Verify that Eqs. (2.16), (2.22), (2.24), and (2.41) satisfy the Maxwell equations.

The electromagnetic field components can also be computed in the short range $|z| \ll \chi^{1/3}b$ for the case $m \geq 1$. The component E_s, for example, is determined by

$$A \approx -i\frac{4I_m(m+1)}{kb^{2m+2}}, \tag{2.42}$$

which gives

$$E_s(0^-) = -\frac{4I_m(m+1)}{b^{2m+2}}r^m \cos m\theta. \tag{2.43}$$

Compared with Eq. (2.41), E_s has to switch sign in the region $0 > z \gtrsim -\chi^{1/3}b$.

A point mth moment I_m, with charge density given by Eq. (1.7), going down the resistive wall pipe, thus loses energy at a rate

$$\frac{d\mathscr{E}}{ds} = \int dV \rho_m \frac{E_s(0^-)}{2}$$
$$= \int_0^{2\pi} d\theta \frac{I_m}{\pi a^m} \cos m\theta \frac{E_s(0^-)}{2} = -\frac{2I_m^2(m+1)}{b^{2m+2}}, \qquad (2.44)$$

where $E_s(0^-)$ is divided by 2 to take into account the fundamental theorem of beam loading.

Exercise 2.10 Consider an off-centered point charge described by superposition of moments, Eqs. (1.6–1.7). Show that this particle loses energy in the resistive pipe at a rate

$$\frac{d\mathscr{E}}{ds} = -\frac{2q^2b^2}{(b^2-a^2)^2}. \qquad (2.45)$$

Compared with a centered charge, the energy loss rate is faster by a factor of $b^4/(b^2-a^2)^2$, which diverges as a approaches b, i.e., as the point charge approaches the resistive wall.

2.2 WAKE FUNCTIONS

In Figure 2.1, we showed examples of environments in which a beam with a multipole moment can excite a wake electromagnetic field behind it. Consider now a test charge e trailing behind the $\cos m\theta$ ring beam in one such environment. The test charge experiences an electromagnetic wake force. The vacuum chamber pipe is considered to be axially symmetric, and both the beam and the trailing test charge travel with the speed of light c.

Consider first the case of resistive wall. The Lorentz force $\vec{F} = e(\vec{E} + \hat{s} \times \vec{B})$ experienced by the test charge has the components

$$F_\parallel = eE_s,$$
$$F_\theta = e(E_\theta + B_r), \qquad (2.46)$$
$$F_r = e(E_r - B_\theta).$$

Substituting from Eq. (2.41), Eq. (2.46) gives

$$F_\parallel = \frac{eI_m}{\pi b^{2m+1}(1+\delta_{m0})}\sqrt{\frac{c}{\sigma}}\, r^m \cos m\theta \frac{1}{|z|^{3/2}},$$
$$\vec{F}_\perp = \frac{2\,eI_m}{\pi b^{2m+1}}\sqrt{\frac{c}{\sigma}}\, mr^{m-1}\frac{1}{|z|^{1/2}}(\hat{r}\cos m\theta - \hat{\theta}\sin m\theta). \qquad (2.47)$$

These expressions also give the correct answer for $m = 0$ if we set $I_0 = q$. [See Eq. (2.16).] For $m = 0$, we have $\vec{F}_\perp = 0$, as one would also expect by symmetry.

It is interesting to observe that the $|z|^{-5/2}$ terms in the transverse fields (2.41) do not contribute to the transverse force, and that the transverse force comes solely from the $|z|^{-1/2}$ terms of the magnetic field. What happens is that the image current penetrates into the metal wall and, as it slowly resurfaces, drives the $|z|^{-1/2}$ tail of the magnetic field. The same thing does not happen to the electric field because the image charges stay on the wall surface without penetration into the metal.

Because of the translational symmetry in the case of resistive wall, the force seen by the test charge, Eq. (2.47), depends on s and t through the combination $s - ct = z$, which is the longitudinal separation of the test charge from the $\cos m\theta$ ring beam. The wake force pattern does not change as the beam and the test charge travel down the pipe. This is no longer true in the environments shown in Figure 2.1(a) and (c). In Figure 2.1(a), the force seen by the test charge varies periodically with the period of the structure. In Figure 2.1(c), the force occurs more or less as an impulse when the test charge passes by the wall structure. In these cases without translational symmetry, the wake force becomes much more complicated; it depends on s and t separately instead of the combined variable $z = s - ct$.

However, at high energies, the trajectory of the beam and the test charge is not perturbed much as they travel a distance over a wall structure. The net effect on the test charge can be obtained by integrating the force through a distance longer than the wall structure, and one considers quantities

$$\int_{-L/2}^{L/2} ds f \equiv \bar{f}, \tag{2.48}$$

where f represents the components of the force $\vec{F}$ (or the fields $\vec{E}$ and $\vec{B}$) seen by the test charge, and L is a distance of interest. For Figure 2.1(a), L is the structure period. For Figure 2.1(c), L is chosen to be a convenient distance much longer than the wall structure. For Figure 2.1(b), the wake force is independent of s and we have simply $\bar{f} = fL$.

The quantities $\bar{f}$, when properly integrated over s, are smoothed out so that the detailed s- and t-dependences combine into a z-dependence. As we will see next, the fact that we are interested only in the *integrated impulses* (2.48), rather than the detailed instantaneous forces, allows the problem at hand be drastically simplified. This simplification is possible because we are only interested in high energy beams.

There actually exists a general form of the wake force once it is integrated over the structure period; Eq. (2.47) is only a special case for the resistive wall. To obtain the general form, the Maxwell equations (2.1) are linearly combined into equations for the quantities $\bar{F}_\parallel$, $\bar{F}_r$, $\bar{F}_\theta$, and $e\bar{B}_s$, which are

functions of r, θ, and z. The result in the pipe region $r < b$ is surprisingly simple:

$$
\begin{aligned}
-\frac{e}{r}\frac{\partial}{\partial\theta}\bar{B}_s &= \frac{\partial}{\partial z}\bar{F}_r = \frac{\partial}{\partial r}\bar{F}_{\parallel}, \\
e\frac{\partial}{\partial r}\bar{B}_s &= \frac{\partial}{\partial z}\bar{F}_\theta = \frac{1}{r}\frac{\partial}{\partial\theta}\bar{F}_{\parallel}, \\
\frac{\partial}{\partial r}(r\bar{F}_r) &= -\frac{\partial}{\partial\theta}\bar{F}_\theta, \\
\frac{\partial}{\partial r}(r\bar{F}_\theta) &= \frac{\partial}{\partial\theta}\bar{F}_r.
\end{aligned}
\tag{2.49}
$$

In deriving Eq. (2.49), we have used the fact that in the region $r < b$ the source terms satisfy $j_r = j_\theta = 0$ and $j_s = c\rho$. Note that Eq. (2.49) does not contain source terms explicitly; neither does it depend on the boundary conditions.

Recalling that, for an axially symmetric environment, $F_{\parallel}$ and F_r are proportional to $\cos m\theta$ and B_s and F_θ are proportional to $\sin m\theta$, Eq. (2.49) can easily be solved to yield

$$
\begin{aligned}
\int_{-L/2}^{L/2} ds\,\vec{F}_\perp &= -eI_m W_m(z) m r^{m-1}(\hat{r}\cos m\theta - \hat{\theta}\sin m\theta), \\
\int_{-L/2}^{L/2} ds\,F_{\parallel} &= -eI_m W_m'(z) r^m \cos m\theta, \\
\int_{-L/2}^{L/2} ds\,eB_s &= eI_m W_m'(z) r^m \sin m\theta,
\end{aligned}
\tag{2.50}
$$

where W_m is a function of z yet to be determined, and W_m' is the derivative of W_m with respect to z. The case $m = 0$ is included provided we set $I_0 = q$. Causality dictates that the test charge does not experience a wake force if it is ahead of the ring beam. This requires $W_m(z) = 0$ if $z > 0$.

In the present ultrarelativistic approximation, the integrated wake force impulses (2.50) are applied to the test charge at the location where the wake fields are generated, i.e., at the location of the wall structure. Note that there is no transverse wake force when $m = 0$, because $\int ds\,\vec{F}_\perp = 0$. Note also that one can define a quantity V so that

$$
\begin{aligned}
\int_{-L/2}^{L/2} ds\,\vec{F} &= -\nabla V, \\
V &= eI_m W_m(z) r^m \cos m\theta.
\end{aligned}
\tag{2.51}
$$

The explicit form of W_m, of course, can only be determined after imposing the boundary conditions as was done for the resistive wall. It is interesting, however, that all the explicit r, θ, and z dependences in Eq. (2.50) are derived without referring to the boundary conditions at all, except that the boundary is axially symmetric.[14]

The function $W_m(z)$ in Eq. (2.50) is called the *wake function*; it describes the shock response of the vacuum chamber environment to a δ-function beam which carries an mth moment. Mathematically, W_m resembles a Green's function. Sometimes it may be more convenient to call $W_m(z)$ the transverse wake function and $W_m'(z)$ the longitudinal wake function, for reasons that should be obvious from Eq. (2.50). The dimensionality of W_m is L^{-2m} in cgs units. In analogy with the concept of the electric potential, the integrals on the left hand side of Eq. (2.50) are called the *wake potentials*.

In general, the wake functions are solely determined by the properties of the vacuum chamber environment; they are independent of the beam properties. The property (2.50) applies to the force components and not to the electromagnetic field components. Fortunately, it is the force components, not the field components, that we need.

The result (2.50) can be combined to say that the transverse gradient of the longitudinal wake potential is equal to the longitudinal gradient of the transverse wake potential,

$$\nabla_\perp \int_{-L/2}^{L/2} ds\, F_\parallel = \frac{\partial}{\partial z} \int_{-L/2}^{L/2} ds\, \vec{F}_\perp \,. \tag{2.52}$$

This expression is sometimes referred to as the *Panofsky-Wenzel theorem*.[15]

For the special case of a resistive wall, the wake function over a distance L is, for $z < 0$,

$$W_m(z) = -\frac{2}{\pi b^{2m+1}(1+\delta_{m0})} \sqrt{\frac{c}{\sigma}} \frac{1}{|z|^{1/2}} L. \tag{2.53}$$

The range of validity of Eq. (2.53) is $b/\chi \gg |z| \gg \chi^{1/3} b$, where χ is the small parameter defined in Eq. (2.10). In the range $|z| \ll \chi^{1/3} b$, we also have, from Eq. (2.24) for $m = 0$,

$$\frac{W_0(z)}{L} = \frac{4}{b^2} z + \frac{128}{15} \frac{1}{b^3} \sqrt{\frac{\sigma}{c}} |z|^{5/2}. \tag{2.54}$$

It was mentioned before that the wake functions are properties of the vacuum chamber environment, and are independent of the beam properties.

[14] In case the boundary is not axially symmetric, modes of different m's will couple. The $\cos m\theta$ and $\sin m\theta$ patterns no longer form an eigenmode. The analysis becomes more complicated.

[15] W. K. H. Panofsky and W. A. Wenzel, Rev. Sci. Instr. 27, 967 (1956).

Equation (2.50) was derived under the ultrarelativistic assumption $\gamma \to \infty$. The space charge forces, which are nonrelativistic in nature, are excluded from the treatment. It turns out, however, that the space charge forces can almost fit into the wake function framework, and when that is done, the wake functions will depend on beam properties such as the transverse beam size a and the beam energy γ. For a $\cos m\theta$ ring beam, the transverse and longitudinal space charge forces, Eqs. (1.32) and (1.51), in the region $r < a$ can be cast in the framework of (2.50) if we let

$$W_m(z) = \frac{2L}{\gamma^2}\delta(z)\begin{cases} \ln\dfrac{b}{a} & \text{if} \quad m = 0, \\ \dfrac{1}{m}\left(\dfrac{1}{a^{2m}} - \dfrac{1}{b^{2m}}\right) & \text{if} \quad m > 0, \end{cases} \tag{2.55}$$

although the third member of Eq. (2.50) is not satisfied.

For a uniform disk beam, the space charge forces (1.35), (1.44), and (1.53) cannot be cast in the wake function framework. However, it is often convenient to insist on it at least for the $m = 0$ longitudinal case. To do so, consider $r = 0$ and write

$$W_0(z) = \frac{2L}{\gamma^2}\delta(z)\left(\ln\frac{b}{a} + \frac{1}{2}\right). \tag{2.56}$$

As mentioned, Eqs. (2.55–2.56) depend on the beam properties a and γ.

If one considers a rigid uniform disk beam executing a small transverse dipole motion, the space charge force is a superposition of that of an $m = 0$ uniform disk beam force and an $m = 1$ ring-beam force. In this case, one can use Eq. (2.55) with $m = 1$ and Eq. (2.56) for $m = 0$ as the space charge wake functions. This model is the one used in most of our applications later.

Exercise 2.11 Equation (2.50) relates the *force* components to wake functions. For a general m, there are no simple a priori relations for the individual *field* components. However, Eq. (2.49) does not exhaust the information contained in the Maxwell equations without explicit knowledge of the boundary conditions. Show that, for $m = 0$ and in the free space behind the beam, the Maxwell equations give the additional relations

$$\bar{E}_r = \bar{B}_\theta = \frac{q}{2} r W_0''(z). \tag{2.57}$$

Confirm this with the resistive-wall case, Eqs. (2.16) and (2.24).

Immediately following the beam, we expect to see a longitudinal electric field that retards the beam, regardless of vacuum chamber properties. This

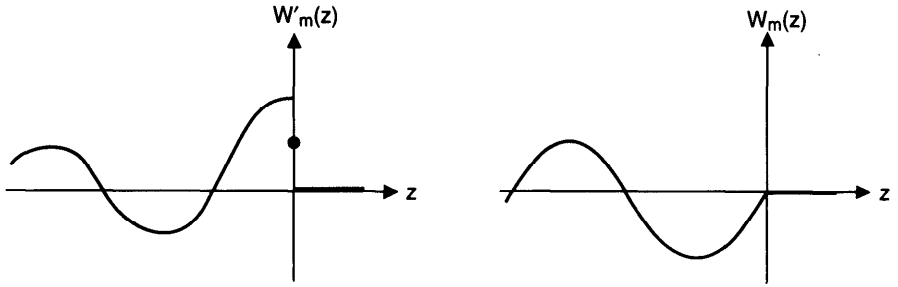

Figure 2.6. Sketches of the longitudinal wake function $W'_m(z)$ and the transverse wake function $W_m(z)$. Both W_m and W'_m vanish if $z > 0$. The value of $W'_m(z)$ at $z = 0$ is indicated by a solid dot and it sits exactly midway between the values of $W'_m(0^+) = 0$ and $W'_m(0^-) > 0$, according to the fundamental theorem of beam loading.

means the quantity $j_s F_{\|}$ must be negative definite, which implies

$$W'_m(z) > 0 \qquad \text{for} \quad z \to 0^-. \tag{2.58}$$

It follows that the longitudinal wake function $W'_m(z)$ of a resistive wall must switch sign in the range between $z = 0$ and $z \approx -\chi^{1/3} b$, since W'_m obtained from Eq. (2.53) is negative.

Another consequence of Eq. (2.58) is that the transverse wake function $W_m(z)$ is negative for $z < 0$, and its magnitude increases monotonically with $|z|$, at least initially, starting from $W_m = 0$ at $z = 0^+$. In other words, the longitudinal wake function is cosinelike and the transverse wake function is sinelike, as sketched in Figure 2.6. It follows that a point charge does not experience a deflecting force due to its own transverse wake. This is in contrast to the longitudinal dimension, in which a point charge does see its own retarding wake force. This property leads to a preference for short beams when the transverse wake effects dominate, while longer bunches are preferred when the main concern is the longitudinal wake effects.

There are several interesting properties of the wake functions. One has been listed in Eq. (2.58). Some of these properties for the longitudinal wake function $W'_m(z)$ are given in Exercise 2.12 below. Here let us demonstrate how property (c) can be shown; the other properties can be shown similarly. Consider a point charge q followed by another point charge q at a distance $|z|$ behind. After traveling a distance L, the first q loses an energy $\frac{1}{2}q^2 W'_0(0^-)$ due to the wake generated by itself, where the factor of $\frac{1}{2}$ is due to the fundamental theorem of beam loading. The trailing q loses an energy $\frac{1}{2}q^2 W'_0(0^-) + q^2 W'_0(z)$, where the second term is due to the wake left by the leading q. Physically, the two-charge system can never gain energy; this means $W'_0(z) \geq -W'_0(0^-)$ for any z. Similarly, if the second charge is $-q$ rather than q, one proves $W'_0(z) \leq W'_0(0^-)$. Property (c) is thus established for $m = 0$. From this property, it follows that $W'_m(0^-)$ is the maximum value

the function $W_m'(z)$ ever reaches, and $W_m'(0^-) = 0$ necessarily gives the trivial case when the entire wake potential vanishes.

Exercise 2.12 Show that the longitudinal wake function $W_m'(z)$ is unphysical unless the following properties are satisfied:

(a) $W_m'(z) = 0$ if $z > 0$.

(b) $W_m'(0^-) \geq 0$.

(c) $W_m'(0^-) \geq |W_m'(z)|$ for all z.

(d) If $W_m'(-D) = W_m'(0^-)$ for some D, then $W_m'(z)$ is periodic with period D, i.e., $W_m'(z - D) = W_m'(z)$ for any $z < 0$. [Hint: Consider three

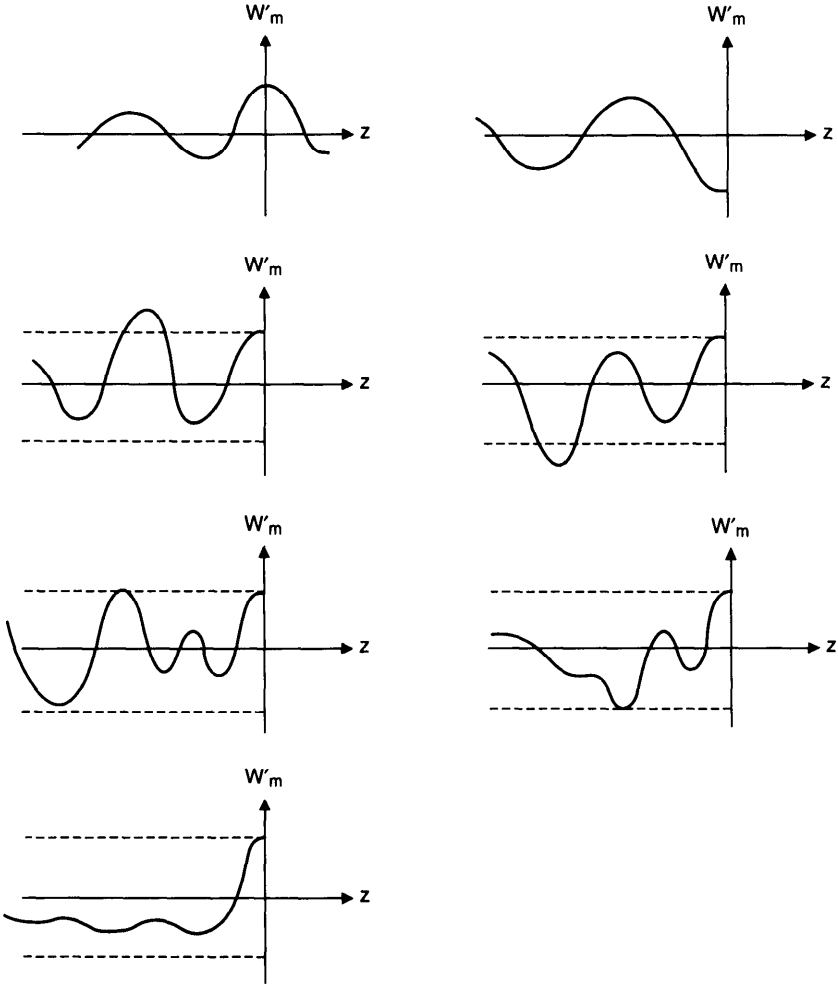

Figure 2.7. Sketches of some unphysical wake functions $W_m'(z)$.

charges q_1, q_2, and $-q_2$, with spacing z between q_1 and q_2, and spacing D between q_2 and $-q_2$.]

(e) If $W'_m(-D) = -W'_m(0^-)$ for some D, then $W'_m(z - D) = -W'_m(z)$.

(f) $\int_{-\infty}^{0} W'_m(z)\,dz \geq 0$, i.e., the area under $W'_m(z)$ is positive. [Hint: Consider a test charge in a continuous beam in steady state.]

(g) $1 \geq W'_m(z_1)W'_m(z_2)W'_m(z_1 + z_2)/[W'_m(0^-)]^3 \geq -\frac{1}{8}$ for any z_1, z_2.

Use these results to show that the wake functions sketched in Figure 2.7 are unphysical.

We now define a Cartesian coordinate system with $x = r\cos\theta$ and $y = r\sin\theta$, and orient the charge density in the x-y system at an angle θ_0 [i.e., in the expression (1.7) for ρ_m, $\cos m\theta$ is replaced by $\cos m(\theta - \theta_0)$]. In this Cartesian system, the beam now has two components of mth moments—one normal and another skewed. Table 2.2 lists the two moments (first the normal moment and then the skewed moment) and the associated wake potentials. A bracket $\langle\ \rangle$ means averaging over the transverse distribution of the beam; $\hat{x}$ and $\hat{y}$ are the unit vectors in the x- and y-directions. The wake potentials are those seen by a test charge e with transverse coordinates x, y that follows the beam at distance $|z|$ behind.

The transverse wake force experienced by the test charge for $m = 1$ listed in Table 2.2 behaves like the bending force seen in a horizontal or vertical dipole magnet. Similarly, the wakes act like quadrupole and skew quadrupole magnets for $m = 2$, sextupole and skew sextupole magnets for $m = 3$, etc. The $m = 0$ case does not have a transverse wake force, because the longitudinal wake potential does not have a transverse gradient.

Table 2.2. The longitudinal and transverse wake potentials $\int_{-L/2}^{L/2} ds\, F_{\parallel}$ and $\int_{-L/2}^{L/2} ds\, \vec{F}_{\perp}$ seen by a test charge e a distance $|z|$ behind a beam which possesses an mth moment.

m	Distribution Moments of Beam	Longitudinal Wake Potential	Transverse Wake Potential
0	q	$-eqW'_0(z)$	0
1	$q\langle x\rangle$	$-eq\langle x\rangle xW'_1(z)$	$-eq\langle x\rangle W_1(z)\hat{x}$
	$q\langle y\rangle$	$-eq\langle y\rangle yW'_1(z)$	$-eq\langle y\rangle W_1(z)\hat{y}$
2	$q\langle x^2 - y^2\rangle$	$-eq\langle x^2 - y^2\rangle(x^2 - y^2)W'_2(z)$	$-2eq\langle x^2 - y^2\rangle W_2(z)(x\hat{x} - y\hat{y})$
	$q\langle 2xy\rangle$	$-eq\langle 2xy\rangle 2xyW'_2(z)$	$-2eq\langle 2xy\rangle W_2(z)(y\hat{x} + x\hat{y})$
3	$q\langle x^3 - 3xy^2\rangle$	$-eq\langle x^3 - 3xy^2\rangle(x^3 - 3xy^2)W'_3(z)$	$-3eq\langle x^3 - 3xy^2\rangle W_3(z) \times[(x^2 - y^2)\hat{x} - 2xy\hat{y}]$
	$q\langle 3x^2y - y^3\rangle$	$-eq\langle 3x^2y - y^3\rangle(3x^2y - y^3)W'_3(z)$	$-3eq\langle 3x^2y - y^3\rangle W_3(z) \times[2xy\hat{x} + (x^2 - y^2)\hat{y}]$

If the wake forces come from cavity structures which are of a size similar to the pipe radius b, we will show later [see Eq. (2.114)] that W'_m/L scales as b^{-2m-2} and W_m/L scales as b^{-2m-1}. The longitudinal wake force, according to Table 2.2, scales as $a^{2m}W'_m/L \sim (a/b)^{2m}(1/b^2)$, and the transverse wake force scales as $a^{2m-1}W_m/L \sim (a/b)^{2m-1}(1/b^2)$, where a is the transverse beam size. Since typically $b \gg a$, the lower modes usually dominate, i.e., the $m = 0$ mode dominates the longitudinal wake effects, and the $m = 1$ mode dominates the transverse wake effects. The wake W'_0 therefore is often loosely referred to as *the* longitudinal wake function, although only the $m = 0$ member is being considered. Similarly, W_1 is sometimes referred to as *the* transverse wake function.

The longitudinal ($m = 0$) and transverse ($m = 1$) wake forces scale with b as b^{-2} and b^{-3}, respectively. In application to linear colliders, where there is a tendency to make the cavity structures small to save cost, the transverse wake effects tend to dominate. It then follows from the discussion following Eq. (2.58) that a short beam bunch is preferred in these applications.

One can also say something about the polarity of the transverse wake forces using Table 2.2. To do that, imagine a short beam traveling down the accelerator with a displacement in x. The head of the beam bunch will generate a wake force that kicks the particles that are in the tail further away from the accelerator axis, since $W_1(z) < 0$ if $|z|$ is short enough. Similarly, if the beam has an elliptical shape in its transverse distribution and thus possesses a quadrupole moment, the transverse wake force is such that it

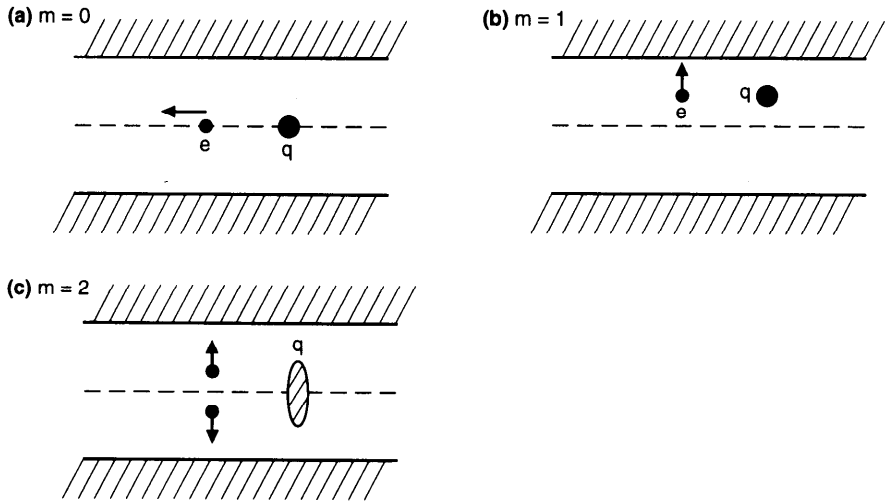

Figure 2.8. The polarity of the wake field always hurts a short beam. For $m = 0$, the longitudinal wake force is retarding. For $m = 1$, the transverse wake force further deflects the test charge e. For $m = 2$, the tail portion of an elliptical beam becomes further elongated. Arrows represent the wake force.

tends to elongate the ellipse further in the bunch tail. In general, one finds that the polarity of the transverse wake forces is such that it always hurts a short beam. See Figure 2.8.

As $|z|$ increases, W'_m and W_m may change signs and the wake forces become beneficial. In particular, W'_0 may become negative at some finite distance behind the head of the beam. Therefore, if one injects two beam bunches into the accelerator and if the separation of the two bunches is chosen strategically, the trailing bunch can be *accelerated* by the wake field of the leading bunch. This leads to the idea of *wake field accelerators*. We will not discuss such accelerators,[16] but as an illustration of the property of the wake functions, we will show below that a straightforward application of the wake field acceleration idea in which a short leading bunch is followed by a short trailing bunch traveling down the *same* path would not work very well.

To show this, consider a wake field accelerator consisting of a short leading bunch of charge $N_1 e$ and a short trailing bunch of charge $N_2 e$ a distance $|z|$ behind the leading bunch. After a distance L, the leading bunch loses an energy

$$\Delta \mathscr{E}_1 = -\tfrac{1}{2} N_1^2 e^2 W'_0(0^-). \tag{2.59}$$

To maximize the energy gain by the trailing bunch, we design the wake potential and choose the relative position of the two bunches in such a way that $W'_0(z) = -W'_0(0^-)$. The energy of the trailing bunch then changes by

$$\Delta \mathscr{E}_2 = \left(-\tfrac{1}{2} N_2^2 + N_1 N_2\right) e^2 W'_0(0^-), \tag{2.60}$$

where the first term is the energy loss due to self-field, and the second term comes from the accelerating wake field left behind by the leading bunch. For a given N_2, the acceleration rate of the trailing bunch can be made arbitrarily large by having a large N_1. However, a large N_1 also means the leading bunch is decelerated rapidly. In fact, let E_1 and E_2 be the energies of a single particle in the leading and trailing bunches; then the leading bunch will come to a full stop when it has exhausted all its energy, i.e., when $\Delta \mathscr{E}_1 = -N_1 E_1$. At this point, the energy of a particle in the trailing bunch has increased by an amount

$$\Delta E_2 = \frac{\Delta \mathscr{E}_2}{N_2} = \left(2 - \frac{N_2}{N_1}\right) E_1 < 2E_1. \tag{2.61}$$

[16]G.-A. Voss and T. Weiland, DESY Report 82-074 (1982); R. J. Briggs, T. J. Fessenden, and V. K. Neil, *Proc. 9th Int. Conf. High Energy Accel.*, SLAC, 1974, p. 278; M. Friedman, Phys. Rev. Lett. **31**, 1107 (1973); E. A. Perevedentsev and A. N. Skrinsky, *Proc. 6th All-Union Conf. Charged Part. Accel.*, Dubna, 1978, Vol. 2, p. 272; Andrew M. Sessler, *AIP Proc.* **91**, *Laser Accel. of Part.*, Los Alamos, 1982, p. 154; P. Chen, R. W. Huffad, and J. M. Dawson, Bull. Am. Phys. Soc. **29**, 1355 (1984); Yongho Chin, *Proc. Lin. Accel. Conf.*, Seeheim/Darmstadt, 1984, p. 159.

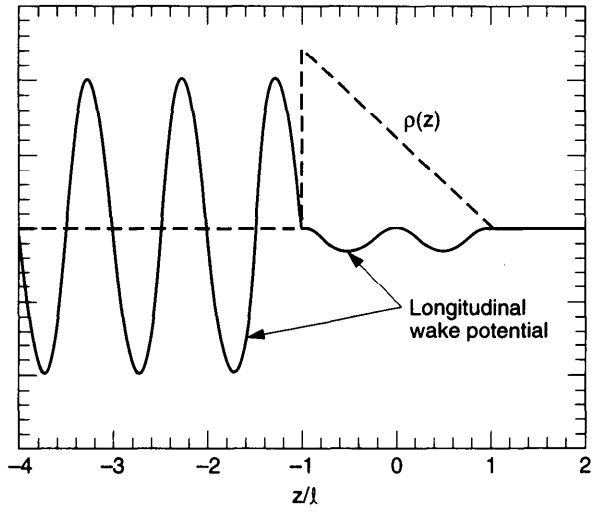

Figure 2.9. The longitudinal wake potential (solid curve) produced by the beam discussed in Exercise 2.13 as a function of z/l. The dashed curve gives $\rho(z)$. The vertical scales are unspecified.

An intense leading bunch indeed induces a large acceleration rate for the trailing bunch, but the total energy gained by each particle in the trailing bunch cannot exceed $2E_1$, no matter how intense the leading bunch is; most of the energy contained in the leading beam would be wasted. The *transformer ratio* $\Delta E_2/\Delta E_1$ cannot exceed 2.[17] To accelerate the trailing beam by 2 GeV, for instance, one has to prepare a 1 GeV leading beam first. Such a wake field accelerator is not very efficient. Note that this conclusion applies regardless of details of the wake field mechanism, whether it is provided by a resistive wall, cavity structures, or a plasma medium.

To improve the transformer ratio, one can consider two beams in *different* paths. This is the approach of klystrons, as well as many of the new generation of wake field accelerator concepts. In these devices, the wake field is generated in a special-purpose chamber, optimized, and sent by waveguides to accelerate another beam in a different vacuum chamber. The transformer ratio can then be made much larger than 2.

Exercise 2.13 The discussion leading to Eq. (2.61) assumes a short leading bunch. It is in fact possible, in principle at least, to defeat this limit on the transformer ratio by using a longer leading bunch. The wake potential of a long bunch can be obtained by superposition. As an illustration, consider a wake $W_0'(z < 0) = W_0 \cos kz$ and a leading bunch with a triangular-shaped

[17] J. Seeman, IEEE Trans. Nucl. Sci. **NS-30**, 3180 (1983); R. D. Ruth, A. W. Chao, P. L. Morton, and P. B. Wilson, Part. Accel. **17**, 171 (1985).

longitudinal charge density $\rho = (Ne/2l)(1 - z/l)$ if $|z| < l$ and 0 otherwise. Let the bunch length $2l$ be n times the wavelength of the wake field, i.e., $kl = \pi n$. Show that by locating a short trailing bunch optimally behind the leading bunch, one can achieve a transformer ratio of $2\pi n$.[18] Figure 2.9 shows the longitudinal wake potential as a function of z for the case of $n = 2$.

2.3 IMPEDANCES

So far the wake fields have been described as a function of time after the passage of a δ-function beam. It is often useful to examine the frequency content of the wake field by performing a Fourier transformation on it. One early indication of the usefulness of this procedure is the fact that we introduced the Fourier transformed quantities $\tilde{E}$ and $\tilde{B}$ when we worked out the case of the resistive wall in Section 2.1. Another indication is that the wake response often contains a number (say, 20) of sharply defined frequencies, which can be revealed by the proper Fourier transforms. Such a situation does not occur for a resistive wall wake, but does occur if the wake is generated by a cavity structure in an otherwise smooth vacuum chamber pipe as shown in Figure 2.1(a) and (c). The Fourier transform of the wake function is called the *impedance*. The idea of representing the accelerator environment by an impedance was introduced by Sessler and Vaccaro.[19]

Needless to say, the descriptions of the wake force in terms of wake functions in the time domain and in terms of impedances in the frequency domain are identical. In most practical applications, for example, the calculation of the wake functions at short distances poses a difficult technical problem. Exactly the same difficulty is encountered in calculating the impedance at high frequencies. It is a matter of taste which approach to take. For many later developments, we find a mixed approach convenient in which we use the time domain description to set up the equations of motion ($F = ma$) and then use the Fourier transform techniques to solve them.

So far we have considered δ-function beams. Wakes produced by other beam distributions can be constructed by superposition using the δ-function result. For example, consider a beam that has a current

$$J_0(s,t) = \hat{J}_0\, e^{i(ks-\omega t)}. \tag{2.62}$$

[18]K. L. F. Bane, P. B. Wilson, and T. Weiland, *AIP Proc.* **127**, *Phys. High Energy Part. Accel.*, BNL/SUNY, 1983, p. 875; K. L. F. Bane, Pisin Chen, and P. B. Wilson, IEEE Trans. Nucl. Sci. **NS-32**, 3524 (1985). Here we have defined the transformer ratio to be the ratio of the energy gain of a particle in the trailing bunch to the average—not the maximum—energy loss of a particle in the leading bunch. This definition is consistent with that used in deriving Eq. (2.61).

[19]A. Sessler and V. Vaccaro, CERN Report ISR-RF/67-2 (1967).

Only the real part of Eq. (2.62) is meaningful. The $m = 0$ wake potential at position s and time t is a superposition of the wakes produced by all charges in the beam that passed by the *same* position s at previous times, i.e.,

$$\begin{aligned}\bar{E}_s(s,t) &= -\frac{1}{c}\int_s^\infty ds' J_0\left(s, t - \frac{s'-s}{c}\right) W_0'(s-s') \\ &= -\frac{1}{c}\int_{-\infty}^0 dz J_0\left(s, t + \frac{z}{c}\right) W_0'(z) \\ &= -\frac{1}{c} J_0(s,t)\int_{-\infty}^\infty dz\, e^{-i\omega z/c} W_0'(z),\end{aligned} \tag{2.63}$$

where $\bar{E}_s(s,t)$ is the E_s integrated according to Eq. (2.48) over a cavity structure.[20] In the second step in Eq. (2.63), we changed variable from s' to $z = s - s'$. In the last step, the upper limit of integration has been extended to ∞, since $W_0' = 0$ for $z > 0$. We have used the fact that the $m = 0$ wake field is insensitive to the cross-sectional area of the beam so we can integrate the current density j_s over the cross section to obtain the beam current J_0.

Let the accelerator section that contains the wake field be of length L. One can define the wake potential across the section due to the wake field by $V(s,t) = \bar{E}_s(s,t)$; we then have the expression, for a sinusoidal current (2.62),

$$V(s,t) = -J_0(s,t) Z_0^{\parallel}(\omega), \tag{2.64}$$

where the quantity $Z_0^{\parallel}(\omega)$ is called the *longitudinal impedance* for the $m = 0$ mode at frequency ω. Comparing Eqs. (2.63) and (2.64) gives

$$Z_0^{\parallel}(\omega) = \int_{-\infty}^\infty \frac{dz}{c} e^{-i\omega z/c} W_0'(z). \tag{2.65}$$

Equation (2.65) says that the impedance $Z_0^{\parallel}$ is related to the wake function W_0' through a Fourier transformation, and so it describes the frequency content of W_0'. Instead of Eqs. (2.62) and (2.64), an alternative view is simply to take Eq. (2.65) as the definition of the impedance. What we have shown is that these two definitions are equivalent.

Note that in spite of the fact that the current (2.62) depends on both ω and k, the impedance is exclusively a function of ω, not k. This is due to the fact that the impedance is localized in space. It assembles the signal from the beam at a fixed location, and such a signal contains only the ω-information, not the k-information.

Exercise 2.14

(a) Consider a conducting material occupying the half space $s < 0$, with a surface current $\vec{K} = \hat{x} K_0 \cos \omega t$ established on its surface. Show that

[20] It is important to note that it is $J_0(s,t')$, not $J_0(s',t')$, where $t' = t - (s-s')/c$, that appears in the first step of Eq. (2.63). Physically, this comes from the fact that the wake field is generated by the current source as it passes by the location of the impedance.

this current source radiates a plane wave in the $s > 0$ region, given by

$$\vec{E} = -\frac{4\pi K_0}{c}\hat{x}\cos\left(\omega t - \omega\frac{s}{c}\right),$$
$$\vec{B} = -\frac{4\pi K_0}{c}\hat{y}\cos\left(\omega t - \omega\frac{s}{c}\right). \tag{2.66}$$

(b) Consider an upright square of side L on the surface $s = 0$. The power consumed to establish the surface current is carried away by the radiation. By identifying this power as $J^2 Z_0 = (KL)^2 Z_0$, show that, to this current source, the unbounded free space acts as a purely resistive impedance $Z_0 = 4\pi/c = 377\ \Omega$, independent of ω.[21]

Similarly, if the beam current possesses a multipole moment

$$J_m(s,t) = \hat{J}_m e^{i(ks-\omega t)}, \tag{2.67}$$

one can define the relationship

$$V = \bar{E}_s = -J_m Z_m^{\parallel} r^m \cos m\theta \tag{2.68}$$

through a longitudinal impedance

$$Z_m^{\parallel}(\omega) = \int_{-\infty}^{\infty}\frac{dz}{c}e^{-i\omega z/c}W_m'(z). \tag{2.69}$$

For the beam (2.67), one can further write the transverse wake force according to

$$\vec{F}_{\perp} = ieJ_m(s,t)mr^{m-1}(\hat{r}\cos m\theta - \hat{\theta}\sin m\theta)Z_m^{\perp}(\omega), \tag{2.70}$$

where $Z_m^{\perp}(\omega)$ is the transverse impedance given by

$$Z_m^{\perp}(\omega) = i\int_{-\infty}^{\infty}\frac{dz}{c}e^{-i\omega z/c}W_m(z). \tag{2.71}$$

In many applications, one is most interested in the $m = 0$ longitudinal effects and the $m = 1$ transverse effects. One then somewhat loosely calls $Z_0^{\parallel}$ the longitudinal impedance and $Z_1^{\perp}$ the transverse impedance. In cgs units, the dimensionality is TL^{-2m-1} for $Z_m^{\parallel}$ and TL^{-2m} for $Z_m^{\perp}$. Sometimes it is more convenient to express the impedances using the ohm as unit, in which case the dimensionality is ΩL^{-2m} for $Z_m^{\parallel}$ and ΩL^{-2m+1} for $Z_m^{\perp}$. For example, $Z_0^{\parallel}$ would be in ohms; $Z_1^{\perp}$ would be in ohms per meter.

[21] In a perfectly conducting smooth vacuum chamber pipe, the pancake fields are truncated by the pipe wall. The environment is not an unbounded free space into which the radiation continues to extract energy from the beam like a black hole, and thus does not present an impedance to the beam.

A minus sign is included in Eqs. (2.64) and (2.68) for the reason that the voltage seen by the beam tends to be retarding, i.e., 180° out of phase with the beam current. Similarly, we have included a factor i in Eq. (2.70) because the transverse force tends to be 90° out of phase with the beam current. These factors are included for convenience only. The impedances are complex quantities in general.

Inverting the Fourier transforms (2.69) and (2.71) allows us to construct the wake functions from the impedances:

$$\begin{aligned} W'_m(z) &= \frac{1}{2\pi}\int_{-\infty}^{\infty} d\omega\, e^{i\omega z/c} Z_m^{\parallel}(\omega), \\ W_m(z) &= \frac{-i}{2\pi}\int_{-\infty}^{\infty} d\omega\, e^{i\omega z/c} Z_m^{\perp}(\omega). \end{aligned} \tag{2.72}$$

The Panofsky-Wenzel theorem, Eq. (2.52), which relates the longitudinal wake function to the derivative of the transverse wake function, also gives a relationship between the longitudinal and transverse impedances for a given m,

$$Z_m^{\parallel}(\omega) = \frac{\omega}{c} Z_m^{\perp}(\omega). \tag{2.73}$$

Exercise 2.15 Equation (2.73) has its origin already imbedded in Eq. (2.33). Show first that the definitions of the impedances can be written in terms of

$$\tilde{E}_\theta + \tilde{B}_r = -icmI_m r^{m-1}\frac{Z_m^{\perp}}{L} \quad \text{and} \quad \tilde{E}_s = -cI_m r^m \frac{Z_m^{\parallel}}{L}. \tag{2.74}$$

Show then that Eq. (2.73) follows from Eq. (2.33).

For a resistive wall, the impedance per unit length is related to the quantity $A(k)$ of Eq. (2.13) for $m = 0$ and Eq. (2.39) for $m \neq 0$:

$$\begin{aligned} \frac{Z_m^{\parallel}(\omega)}{L} &= \frac{\omega}{c}\frac{Z_m^{\perp}(\omega)}{L} = -\frac{1}{cI_m} A\left(\frac{\omega}{c}\right) \\ &= \frac{4/b^{2m}}{(1+\delta_{m0})bc\sqrt{\dfrac{2\pi\sigma}{|\omega|}}\,[1+\operatorname{sgn}(\omega)i] - \dfrac{ib^2}{m+1}\omega + \dfrac{imc^2}{\omega}}. \end{aligned} \tag{2.75}$$

For frequencies $|\omega| \ll \chi^{-1/3}c/b$, Eq. (2.75) becomes

$$\frac{Z_m^{\parallel}(\omega)}{L} = \frac{\omega}{c}\frac{Z_m^{\perp}(\omega)}{L} \approx \sqrt{\frac{2}{\pi\sigma}}\frac{1}{(1+\delta_{m0})b^{2m+1}c}|\omega|^{1/2}[1-\mathrm{sgn}(\omega)i]. \quad (2.76)$$

Equation (2.76) is related to the Fourier transform of Eq. (2.53). In terms of the skin depth (2.7), we have, for the special cases of $m = 0$ and $m = 1$,

$$\frac{Z_0^{\parallel}(\omega)}{L} \approx \frac{1-\mathrm{sgn}(\omega)i}{2\pi b\,\delta_{\mathrm{skin}}\sigma}, \qquad \frac{Z_1^{\perp}(\omega)}{L} \approx \frac{c}{\omega}\frac{1-\mathrm{sgn}(\omega)i}{\pi b^3\,\delta_{\mathrm{skin}}\sigma}. \quad (2.77)$$

The $Z_0^{\parallel}/L$ expression can be understood physically from the fact that the resistivity per unit length is equal to $1/\sigma A$, where A is the cross-sectional area in which the image wall current flows. As sketched in Figure 2.10, $A \approx 2\pi b\delta_{\mathrm{skin}}$. Figure 2.11 shows the resistive-wall impedance for the case of an aluminum pipe. At very high frequencies, $|\omega| \gg \chi^{-1/3}c/b$, the impedance $Z_0^{\parallel}(\omega)/L \approx i4/b^2\omega$.

If the resistive-wall pipe has a finite thickness t,[22] it follows from Eq. (2.18) that

$$\frac{Z_0^{\parallel}(\omega>0)}{L} \approx \frac{1-i}{2\pi b\delta_{\mathrm{skin}}\sigma}\frac{1-\exp[-2(1-i)t/\delta_{\mathrm{skin}}]}{1+\exp[-2(1-i)t/\delta_{\mathrm{skin}}]}. \quad (2.78)$$

For $t \gg \delta_{\mathrm{skin}}$, this reduces to Eq. (2.77). For a thin pipe $t \ll \delta_{\mathrm{skin}}$, we obtain a purely imaginary impedance of $Z_0^{\parallel}/L \approx -i2t\omega/bc^2$. When the resistive-wall pipe is removed, $t = 0$, the impedance vanishes.

For the space charge effect, the wake function (2.55) gives the impedance for a $\cos m\theta$ ring beam. Setting $L = 2\pi R$ gives the total impedance of the circular accelerator,

$$Z_m^{\parallel}(\omega) = \frac{\omega}{c}Z_m^{\perp}(\omega) = iZ_0\frac{R\omega}{c\gamma^2}\begin{cases}\ln\dfrac{b}{a} & \text{if } m=0,\\ \dfrac{1}{m}\left(\dfrac{1}{a^{2m}}-\dfrac{1}{b^{2m}}\right) & \text{if } m>0,\end{cases} \quad (2.79)$$

where $Z_0 = 4\pi/c$. For a uniform disk beam, we have

$$Z_0^{\parallel}(\omega) = iZ_0\frac{R\omega}{c\gamma^2}\left(\ln\frac{b}{a}+\frac{1}{2}\right). \quad (2.80)$$

[22]The pipe is considered to be in an otherwise free space, or inside another larger perfectly conducting pipe.

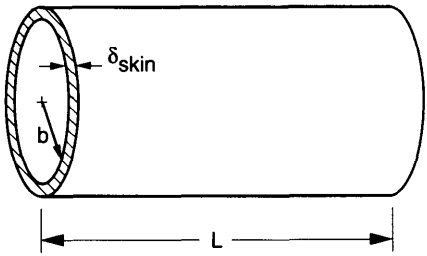

Figure 2.10. Geometry used to estimate the resistive-wall impedance $Z_0^{\parallel}$.

The space charge impedances are purely imaginary. As discussed following Eq. (2.56), a rigid uniform disk beam executing transverse dipole motion can be modeled by taking Eq. (2.80) for the longitudinal impedance and the $m = 1$ member of Eq. (2.79) for the transverse impedance.

The longitudinal impedance $Z_m^{\parallel}$ can often be modeled by an equivalent parallel LRC resonator circuit as shown in Figure 2.12(a).[23] The impedance of the circuit is given by

$$\frac{1}{Z_m^{\parallel}} = \frac{1}{R_S} + \frac{i}{\omega L} - i\omega C, \tag{2.81}$$

which gives

$$Z_m^{\parallel} = \frac{R_S}{1 + iQ\left(\dfrac{\omega_R}{\omega} - \dfrac{\omega}{\omega_R}\right)}, \tag{2.82}$$

where $Q = R_S\sqrt{C/L}$ is the quality factor and $\omega_R = 1/\sqrt{CL}$ is the resonant frequency. This impedance is drawn in Figure 2.12(b) and (c) for $Q = 1$ and 10. The quantity R_S has the dimension of Ω/L^{2m}. The area covered under $\text{Re}\, Z_m^{\parallel}(\omega)$ is

$$\int_0^{\infty} d\omega\, \text{Re}\, Z_m^{\parallel}(\omega) = \frac{\pi R_S \omega_R}{2Q}. \tag{2.83}$$

The width (half width at half maximum) of the resonance peak of $\text{Re}\, Z_m^{\parallel}(\omega)$ is about $\Delta\omega \approx \omega_R/2Q$ if $Q \gg 1$. A sharply peaked impedance has $Q \gg 1$, while a broad-band impedance has $Q \sim 1$.

[23]A. Hofmann, K. Hübner, and B. Zotter, IEEE Trans. Nucl. Sci. **NS-26**, 3514 (1979); P. B. Wilson et al., IEEE Trans. Nucl. Sci. **NS-24**, 1211 (1977); A. Hofmann, *Proc. 11th Int. Conf. High Energy Accel.*, Geneva, 1980, p. 540.

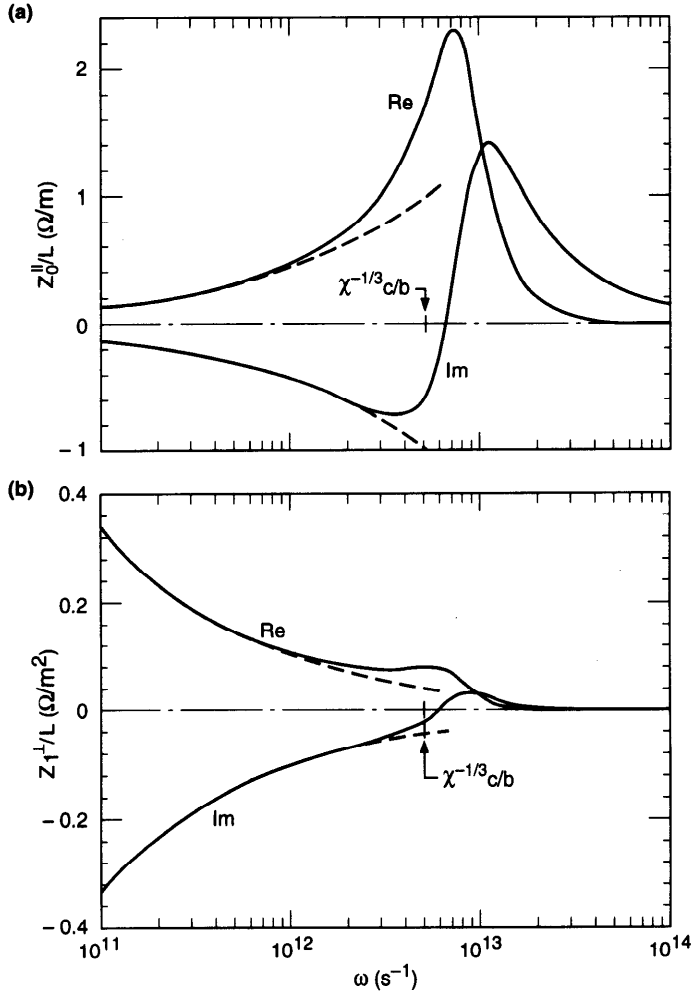

Figure 2.11. (a) Resistive-wall impedance per unit length $Z_0^{\parallel}/L$ as a function of frequency ω according to Eq. (2.75). (b) The same for $Z_1^{\perp}/L$. An aluminum pipe with $\sigma = 3 \times 10^{17}\ s^{-1}$ and $b = 5$ cm is assumed. The dashed curves give the low frequency approximation (2.77). The critical frequency $\chi^{-1/3}c/b$ is indicated.

The wake function $W_m'(z)$ can be obtained by performing a Fourier transformation on the impedance:

$$W_m'(z) = \begin{cases} 0 & \text{if} \quad z > 0, \\ \alpha R_S & \text{if} \quad z = 0, \\ 2\alpha R_S\, e^{\alpha z/c}\left(\cos\dfrac{\bar{\omega} z}{c} + \dfrac{\alpha}{\bar{\omega}}\sin\dfrac{\bar{\omega} z}{c}\right) & \text{if} \quad z < 0, \end{cases} \tag{2.84}$$

where $\alpha = \omega_R/2Q$ and $\bar{\omega} = \sqrt{\omega_R^2 - \alpha^2}$.

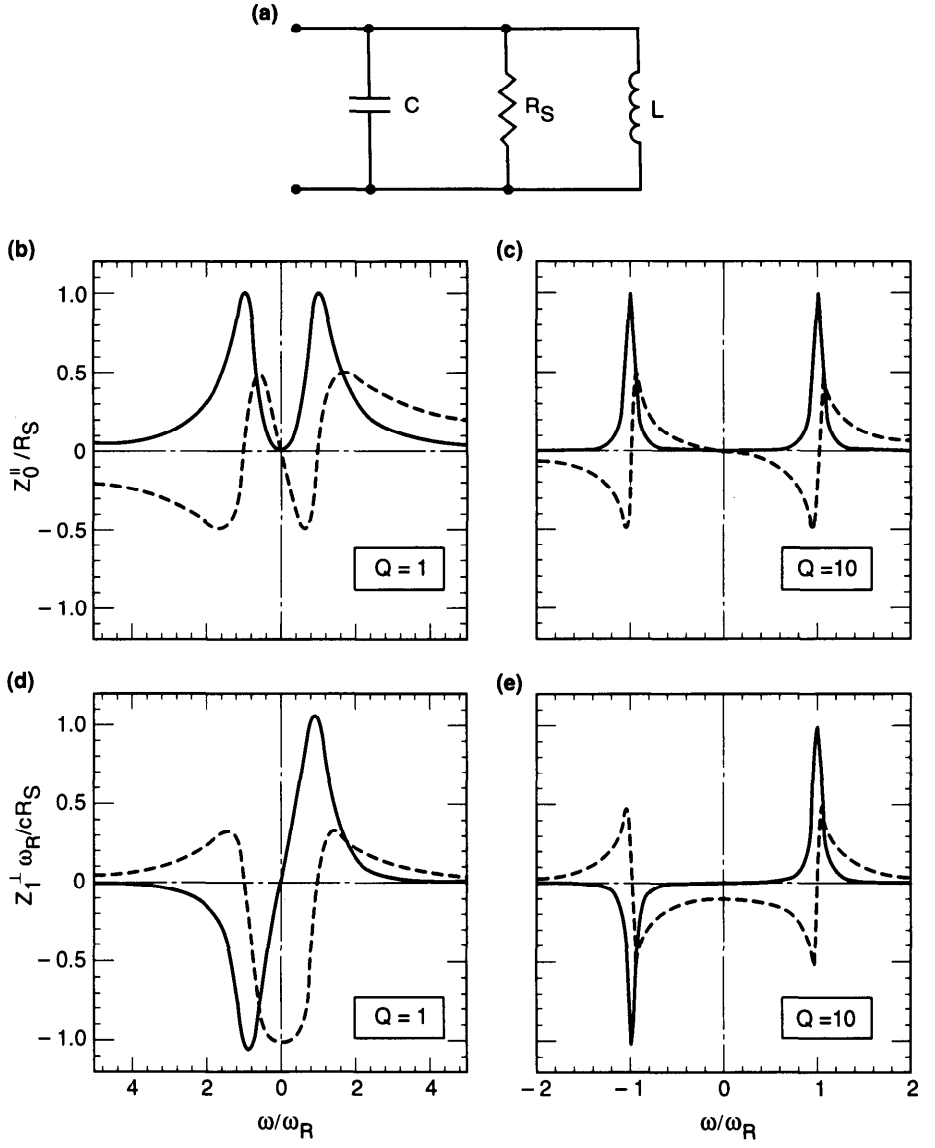

Figure 2.12. (a) An LRC resonator circuit. (b) and (c) are the longitudinal impedance of the circuit for $Q = 1$ and 10. (d) and (e) are the transverse impedance of the circuit for $Q = 1$ and 10. The solid curves give the real parts and the dashed curves give the imaginary parts of the impedances. The quality factor Q is typically ~ 1 for a broad-band resonator, or $\sim 10^4$ for a fine-tuned sharp resonator, or $\sim 10^9$ for a superconducting structure.

A sharply peaked impedance can sometimes be modeled by taking the limit $Q \to \infty$ and $R_S \to \infty$ but keeping R_S/Q fixed, i.e.,

$$\begin{aligned} \operatorname{Re} Z_m^{\parallel} &= \frac{\pi}{2}\frac{R_S\omega_R}{Q}\left[\delta(\omega-\omega_R)+\delta(\omega+\omega_R)\right], \\ \operatorname{Im} Z_m^{\parallel} &= \frac{R_S\omega_R}{2Q}\left(\frac{1}{\omega-\omega_R}+\frac{1}{\omega+\omega_R}\right). \end{aligned} \tag{2.85}$$

The corresponding wake function is

$$W_m'(z) = \frac{R_S\omega_R}{Q}\cos\frac{\omega_R z}{c} \qquad \text{for} \quad z<0. \tag{2.86}$$

Another particularly simple special case of resonator impedance occurs when $Q = 1/2$. See Eq. (2.99).

At low frequencies $|\omega| \ll \omega_R$, the *LRC* resonator impedance $Z_m^{\parallel}(\omega) \approx -i\omega L$ is inductive. For $|\omega| \gg \omega_R$, we have $Z_m^{\parallel}(\omega) \approx i/\omega C$, which is capacitive. Around the resonant frequency ω_R, the impedance $Z_m^{\parallel}(\omega) \approx R_S$ is mostly resistive. Sometimes, one calls an impedance *inductive* or *capacitive* according to the sign of $\operatorname{Im} Z_m^{\parallel}$ in the region $\omega > 0$; and inductive or capacitive impedance then means $\operatorname{Im} Z_m^{\parallel} < 0$ or > 0, respectively. Therefore, the resistive-wall impedance (2.77) is partly inductive and partly resistive, and the space charge impedance (2.80), in spite of the fact that it is proportional to ω like that of an inductance, is referred to as purely capacitive.

The Panofsky-Wenzel theorem requires that the same resonator (2.82) also give a transverse impedance,

$$Z_m^{\perp} = \frac{c}{\omega}\frac{R_S}{1+iQ\left(\dfrac{\omega_R}{\omega}-\dfrac{\omega}{\omega_R}\right)}. \tag{2.87}$$

This impedance is shown in Figure 2.12(d) and (e). The corresponding transverse wake function is (for $z < 0$)

$$W_m(z) = \frac{cR_S\omega_R}{Q\bar{\omega}}e^{\alpha z/c}\sin\frac{\bar{\omega}z}{c}. \tag{2.88}$$

For $Q \to \infty$, $R_S \to \infty$, and fixed R_S/Q, these expressions become

$$\begin{aligned} \operatorname{Re} Z_m^{\perp} &= \frac{\pi c R_S}{2Q}\left[\delta(\omega-\omega_R)-\delta(\omega+\omega_R)\right], \\ \operatorname{Im} Z_m^{\perp} &= \frac{cR_S\omega_R}{2Q\omega}\left(\frac{1}{\omega-\omega_R}+\frac{1}{\omega+\omega_R}\right), \end{aligned} \tag{2.89}$$

and

$$W_m(z) = \frac{cR_S}{Q}\sin\frac{\omega_R z}{c}. \tag{2.90}$$

Properties of Impedances

In addition to Eq. (2.73), there are a few other general properties of impedances which we describe below.

(i) Since the wake functions are real, Eqs. (2.69) and (2.71) imply

$$\begin{aligned} Z_m^{\parallel *}(\omega) &= Z_m^{\parallel}(-\omega), \\ Z_m^{\perp *}(\omega) &= -Z_m^{\perp}(-\omega), \end{aligned} \tag{2.91}$$

i.e., Re $Z_m^{\parallel}$ and Im $Z_m^{\perp}$ are even functions of ω, and Im $Z_m^{\parallel}$ and Re $Z_m^{\perp}$ are odd functions of ω. It follows from Eq. (2.91) and the causality of the wake functions that

$$\begin{aligned} W_m'(z<0) &= \frac{2}{\pi}\int_0^\infty d\omega\ \mathrm{Re}\ Z_m^{\parallel}(\omega)\cos\frac{\omega z}{c}, \\ W_m(z<0) &= \frac{2}{\pi}\int_0^\infty d\omega\ \mathrm{Re}\ Z_m^{\perp}(\omega)\sin\frac{\omega z}{c}. \end{aligned} \tag{2.92}$$

Equation (2.92) exhibits explicitly the cosinelike behavior of W_m' and the sinelike behavior of W_m, as sketched in Figure 2.6.

(ii) In most cases,[24] the transverse wake function satisfies $W_m(0) = 0$, which gives

$$\begin{aligned} \int_0^\infty d\omega\ \mathrm{Im}\ Z_m^{\perp}(\omega) &= 0, \\ \int_0^\infty d\omega \frac{\mathrm{Im}\ Z_m^{\parallel}(\omega)}{\omega} &= 0. \end{aligned} \tag{2.93}$$

It follows that in these cases, Im $Z_m^{\perp}(\omega)$ must not have only one sign in the region $\omega > 0$. Combined with Eq. (2.94) below, this also means Re $Z_m^{\parallel}(0) = 0$.

(iii) To guarantee causality of the wake functions, the impedances must not have singularities in the upper complex ω-plane. It follows from the

[24]One exception is the space charge effect. Another is mentioned later in Eq. (2.110). One also assumes the integrals in Eq. (2.93) converge properly.

Cauchy theorem (See Exercise 2.16 below) that the real and imaginary parts of $Z_m^{\parallel}(\omega)$ must be related by the Hilbert transforms,[25]

$$\begin{aligned} \text{Re } Z_m^{\parallel}(\omega) &= \frac{1}{\pi}\text{P.V.}\int_{-\infty}^{\infty} d\omega' \frac{\text{Im } Z_m^{\parallel}(\omega')}{\omega' - \omega}, \\ \text{Im } Z_m^{\parallel}(\omega) &= -\frac{1}{\pi}\text{P.V.}\int_{-\infty}^{\infty} d\omega' \frac{\text{Re } Z_m^{\parallel}(\omega')}{\omega' - \omega}, \end{aligned} \tag{2.94}$$

where P.V. means taking the principal value of the integral.[26] The same expressions apply to $Z_m^{\perp}$.

An inspection of Eq. (2.95) indicates that the integral (2.95) as a function of a resembles (although it does not equal) $f'(a)$. This is why, in view of Eq. (2.94), Re $Z(\omega)$ as a function of ω often resembles Im $Z'(\omega)$, and Im $Z(\omega)$ often resembles $-$Re $Z'(\omega)$.

The point of Eq. (2.94) is that, in principle, knowing either the real or the imaginary part of the impedance, one can construct the whole impedance and, in turn, the wake function. In practice, this may be a difficult operation and has to be applied with care.

Exercise 2.16 Perform a contour integral of $Z_m^{\parallel}(\omega')/(\omega' - \omega)$ in the complex ω'-plane over the upper half plane along the contour shown in Figure 2.13. Show that if $Z_m^{\parallel}(\omega')$ converges sufficiently fast at $|\omega'| \to \infty$,

$$\text{P.V.}\int_{-\infty}^{\infty} d\omega' \frac{Z_m^{\parallel}(\omega')}{\omega' - \omega} = \pi i Z_m^{\parallel}(\omega). \tag{2.96}$$

Show that Eq. (2.94) follows from Eq. (2.96). The P.V. occurs because the contour around the pole $\omega' = \omega$ is a semicircle.

[25]See for example, Philip M. Morse and Herman Feshbach, *Methods of Theoretical Physics*, McGraw-Hill, New York, 1953.

[26]The integrals (2.94) are undefined without specifying P.V. because of the divergence at $\omega' = \omega$. The trick of P.V. is to utilize the property that the divergences on the side $\omega' < \omega$ and the side $\omega' > \omega$ are of opposite signs and, if the integration is taken *symmetrically* about the singularity so that the divergences on the two sides cancel each other, the integral is actually well defined. Algebraically, this leads to

$$\text{P.V.}\int_{-\infty}^{\infty} dx \frac{f(x)}{x - a} = \int_0^{\infty} du \frac{f(a + u) - f(a - u)}{u}, \tag{2.95}$$

where the expression on the right is well behaved at $u = 0$.

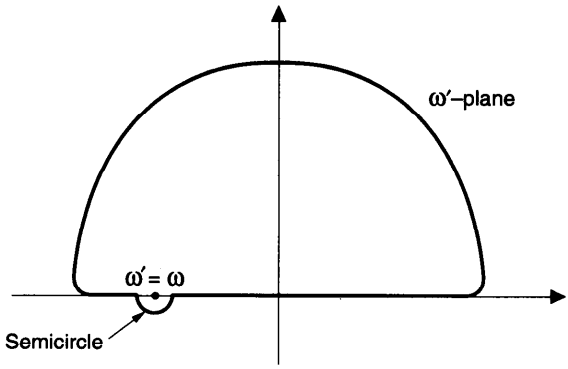

Figure 2.13. Contour in the complex ω'-plane to establish the Hilbert transform relation (2.94) for the impedance.

Exercise 2.17

(a) A simple model of Re $Z_m^{\parallel}$ could be Re $Z_m^{\parallel}(\omega) = R_0$ if $|\omega| < \omega_0$ and 0 if $|\omega| > \omega_0$. Show that the matching Im $Z_m^{\parallel}$ and $W_m'(z)$ are given by

$$\begin{aligned} \text{Im } Z_m^{\parallel}(\omega) &= \frac{R_0}{\pi} \ln \left| \frac{\omega + \omega_0}{\omega - \omega_0} \right|, \\ W_m'(z < 0) &= \frac{2R_0 c}{\pi z} \sin \frac{\omega_0 z}{c}. \end{aligned} \tag{2.97}$$

(b) Show that

$$\begin{aligned} W_m'(z < 0) &= W_0 J_0(\alpha z), \\ Z_m^{\parallel}(\omega) &= \begin{cases} -i \dfrac{W_0 \operatorname{sgn}(\omega)}{c\sqrt{\omega^2 - \alpha^2}} & \text{if} \quad |\omega| > \alpha, \\ \dfrac{W_0}{c\sqrt{\alpha^2 - \omega^2}} & \text{if} \quad |\omega| < \alpha, \end{cases} \end{aligned} \tag{2.98}$$

form a matching wake function and impedance pair.

(c) Show that

$$\begin{aligned} W_m(z < 0) &= W_0 z e^{\alpha z}, \\ Z_m^{\parallel}(\omega) &= \frac{i W_0 \omega}{(\omega + ic\alpha)^2}, \end{aligned} \tag{2.99}$$

form a matching pair. This is in fact a special case (the critically damped case) of the resonator impedance when $Q = 1/2$.

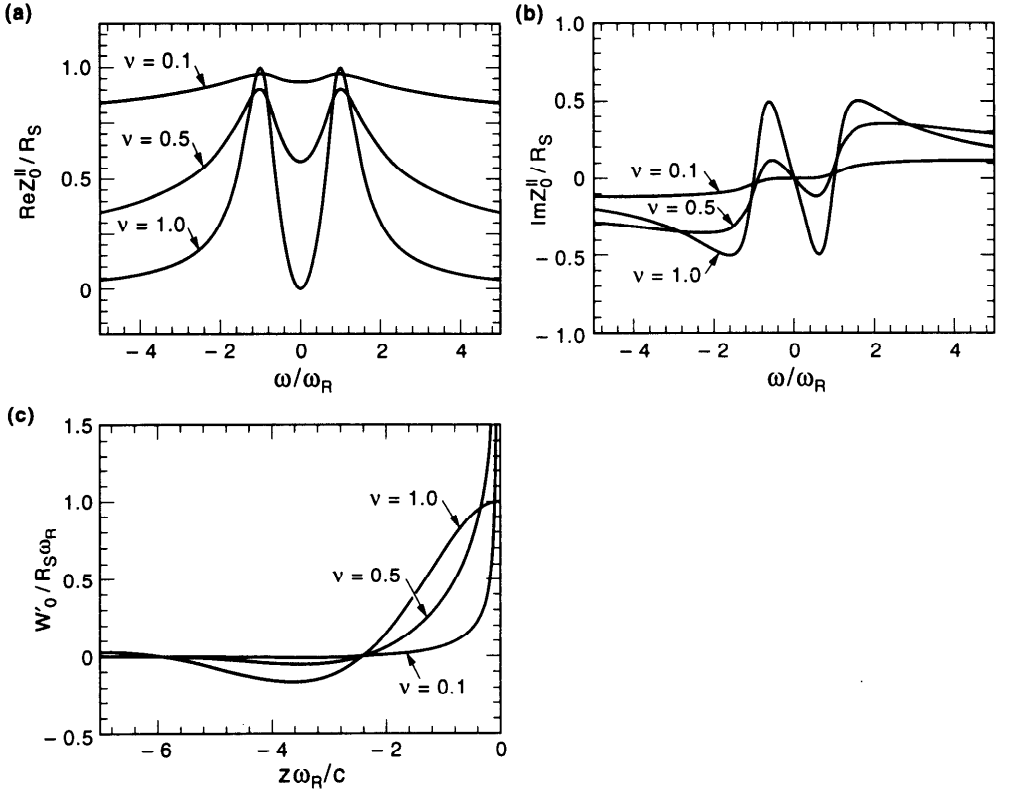

Figure 2.14. Generalized resonator impedance and wake function (2.100) for $\nu = 0.1$, 0.5, and 1. We have assumed $Q = 1$. The case of $\nu = 1$ has been shown in Figure 2.12.

(d) The resonator impedance (2.82) and wake function (2.84) can be generalized. Show that a possible model is given by[27]

$$Z_m^{\parallel}(\omega) = \frac{R_S}{2Q\bar{\omega}}\left[\omega_1\left(\frac{i\omega_R}{\omega-\omega_1}\right)^{\nu} - \omega_2\left(\frac{i\omega_R}{\omega-\omega_2}\right)^{\nu}\right],$$

$$W'_m(z<0) = \frac{R_S\omega_R}{Q\Gamma(\nu)}\left(-\frac{z\omega_R}{c}\right)^{\nu-1} e^{\alpha z/c} \times\left(\cos\frac{\bar{\omega}z}{c} + \frac{\alpha}{\bar{\omega}}\sin\frac{\bar{\omega}z}{c}\right), \tag{2.100}$$

where $\omega_1 = \bar{\omega} - i\alpha$, $\omega_2 = -\bar{\omega} - i\alpha$, $\bar{\omega} = \sqrt{\omega_R^2 - \alpha^2}$, $\alpha = \omega_R/2Q$,

[27]Toshio Suzuki, Yongho Chin, and Kohtaro Satoh, Part. Accel. **13**, 179 (1983). See also Exercise 2.3.

and $0 < \nu \leq 1$. The resonator model (2.82) corresponds to $\nu = 1$. The impedance and wake function (2.100) are shown in Figure 2.14. The impedance behaves as $\propto \omega^{-\nu}$ for large ω, and the wake function $\propto |z|^{\nu-1}$ for small $|z|$. Show that some physical properties are violated if $\nu > 1$.

Exercise 2.18

(a) Using the fact that $\text{P.V.}\int_{-\infty}^{\infty} d\omega'/(\omega' - \omega) = 0$, show from Eqs. (2.91) and (2.94) that

$$\begin{aligned}
\text{Re } Z_m^{\parallel}(\omega) &= \frac{2}{\pi}\text{P.V.}\int_0^{\infty} \frac{d\omega'}{\omega'^2 - \omega^2}\left[\omega' \text{ Im } Z_m^{\parallel}(\omega') - \omega \text{ Im } Z_m^{\parallel}(\omega)\right], \\
\text{Im } Z_m^{\parallel}(\omega) &= -\frac{2\omega}{\pi}\text{P.V.}\int_0^{\infty} \frac{d\omega'}{\omega'^2 - \omega^2}\left[\text{Re } Z_m^{\parallel}(\omega') - \text{Re } Z_m^{\parallel}(\omega)\right], \\
\text{Re } Z_m^{\perp}(\omega) &= \frac{2\omega}{\pi}\text{P.V.}\int_0^{\infty} \frac{d\omega'}{\omega'^2 - \omega^2}\left[\text{Im } Z_m^{\perp}(\omega') - \text{Im } Z_m^{\perp}(\omega)\right], \\
\text{Im } Z_m^{\perp}(\omega) &= -\frac{2}{\pi}\text{P.V.}\int_0^{\infty} \frac{d\omega'}{\omega'^2 - \omega^2}\left[\omega' \text{ Re } Z_m^{\perp}(\omega') - \omega \text{ Re } Z_m^{\perp}(\omega)\right].
\end{aligned} \tag{2.101}$$

(b) Verify that Eq. (2.101) satisfies the conditions (2.73) and (2.91).

(c) Verify that the resistive-wall impedance $Z_m^{\perp}$ of Eq. (2.76) satisfies Eq. (2.101).[28]

(iv) Energy loss consideration gives another general condition on impedance. Consider a beam whose mth moment has a longitudinal distribution $\rho(s - ct)$, normalized so that $\int dz\, \rho(z) = I_m$, the total mth moment of the beam. As this beam travels down the pipe for a distance L, its energy changes by [cf. Eq. (2.30)]

$$\Delta\mathscr{E} = -\int_{-\infty}^{\infty} dz'\, \rho(z') \int_{z'}^{\infty} dz\, \rho(z) W_m'(z' - z). \tag{2.102}$$

[28]The longitudinal impedance $Z_m^{\parallel}$ does not satisfy Eq. (2.94) or (2.101), because of the divergence at $|\omega'| \to \infty$.

This result can also be written in terms of the Fourier transformed quantities:

$$\Delta\mathscr{E} = -\frac{1}{2\pi}\int_{-\infty}^{\infty} d\omega |\tilde{\rho}(\omega)|^2 \operatorname{Re} Z_m^{\parallel}(\omega), \tag{2.103}$$

where

$$\begin{aligned} \tilde{\rho}(\omega) &= \int_{-\infty}^{\infty} dz\, e^{-i\omega z/c}\rho(z), \\ \rho(z) &= \frac{1}{2\pi c}\int_{-\infty}^{\infty} d\omega\, e^{i\omega z/c}\tilde{\rho}(\omega). \end{aligned} \tag{2.104}$$

Only the real part of the impedance contributions to the energy loss of the beam.

Since the beam as a whole cannot gain energy from the pipe structure, and this must be valid for arbitrary ρ and $\tilde{\rho}$, we conclude that[29]

$$\operatorname{Re} Z_m^{\parallel}(\omega) \geq 0 \qquad \text{for all } \omega. \tag{2.105}$$

This is the complete condition that is only partly studied in Figure 2.7. It then follows from Eq. (2.73) that

$$\operatorname{Re} Z_m^{\perp}(\omega)\begin{cases} \geq 0 & \text{if } \omega > 0, \\ \leq 0 & \text{if } \omega < 0. \end{cases} \tag{2.106}$$

(v) The relationship (2.73) holds for a given m. There is no a priori connection between the impedances of different m's. On the other hand, as mentioned before, the most important wake effects are the $m = 0$ longitudinal and the $m = 1$ transverse cases. A rough connection between the two leading impedances $Z_0^{\parallel}$ and $Z_1^{\perp}$ can be very useful if one knows one and wants to have some idea of the other. From a simple dimensionality argument, one expects $Z_1^{\parallel} \sim 2Z_0^{\parallel}/b^2$ and therefore[30]

$$Z_1^{\perp} \sim \frac{2c}{b^2\omega} Z_0^{\parallel}, \tag{2.107}$$

where b is a length characterizing the vacuum chamber structure and is taken to be the radius of the chamber pipe.[31] A factor of 2 is included so that this expression is strictly valid for the resistive-wall case. [See Eq. (2.77).]

[29]One may attempt to cast a feedback system in the impedance framework. In that case, Re $Z_m^{\parallel}$ may become negative.

[30]W. Schnell, CERN Report ISR-RF/70-7 (1970); B. Zotter and F. Sacherer, *Proc. Int. School of Part. Accel.*, Erice, 1976, CERN Report 77-13, p. 175.

[31]Another useful form of Eq. (2.107) in terms of the quantity $Z_0^{\parallel}/n$ is

$$Z_1^{\perp} \sim \frac{2R}{b^2}\frac{Z_0^{\parallel}}{n}, \tag{2.108}$$

where $n = \omega/\omega_0$, ω_0 is the revolution frequency, and $2\pi R$ is the accelerator circumference.

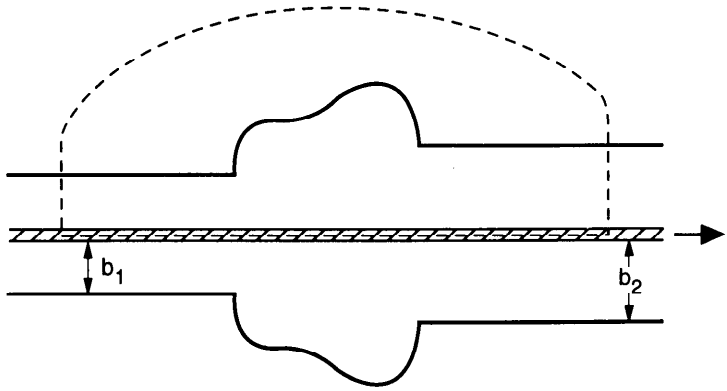

Figure 2.15. Demonstration of Eq. (2.110).

There is also a generalized form of Eq. (2.107),

$$Z_m^{\parallel} \sim \frac{2}{b^{2m}} Z_0^{\parallel} \quad \text{or} \quad Z_m^{\perp} \sim \frac{2c}{b^{2m}\omega} Z_0^{\parallel} . \tag{2.109}$$

The validity of Eqs. (2.107–2.109) rests on the fact that the electrodynamics are all occurring in the neighborhood of the pipe wall $r = b$. This will be the case for the resistive wall and the diffraction model impedance to be discussed later. It will also apply if the discontinuities of the structures on the beam pipe have dimensions $\ll b$. When electromagnetic wake fields penetrate into a cavity-like structure of depth $\gtrsim b$, Eqs. (2.107–2.109) will not be very accurate. In those cases, the relations (2.107–2.109) describe a gross averaged behavior; they apply more or less to frequencies near or above the cutoff frequency c/b and are not to be confused with the exact relationship (2.73).

Exercise 2.19 Consider a steady state continuous beam in a vacuum pipe that contains a transition section from radius b_1 to radius b_2 as illustrated in Figure 2.15. By drawing a circuit as shown by the dashed curve in Figure 2.15 and applying the steady state condition $\oint d\vec{l} \cdot \vec{E} = 0$, show that

$$\text{Re}\, Z_0^{\parallel}(0) = \frac{2}{c} \ln \frac{b_2}{b_1} = \frac{Z_0}{2\pi} \ln \frac{b_2}{b_1} . \tag{2.110}$$

This result apparently contradicts Eqs. (2.93), and (2.105) if $b_2 < b_1$. Explore how these apparent contradictions can be resolved.

Exercise 2.20 A stripline beam-position monitor consists of two striplines diametrically located across the beam pipe. It produces the impedances[32]

$$Z_m^{\parallel}(\omega) = -iR_{Sm} \sin\frac{\omega d}{c} e^{i\omega d/c}, \tag{2.111}$$

where R_{Sm} is the characteristic resistance of the monitor design for the mth mode, $R_{Sm} \approx R_{S0}/b^{2m}$, and d is the length of the monitor.

(a) Show that the longitudinal wake functions are

$$W'_m(z) = \frac{cR_{Sm}}{2}[\delta(z) - \delta(z + 2d)]. \tag{2.112}$$

Each of the striplines receives a signal proportional to

$$I_m W'_m(z) r^m \cos m\theta$$

according to Eq. (2.50), where I_m is the mth moment of the beam, (r, θ) is evaluated at the location of the stripline being considered.

(b) For a beam with longitudinal distribution $\rho(z)$ and a transverse offset of $a \ll b$, the signals received by the two striplines are approximately given by a superposition of the $m = 0$ and $m = 1$ signals. Show that the two signals are proportional to $(R_{S0} \pm abR_{S1})[\rho(z) - \rho(z + 2d)]$. The term $\rho(z)$ comes from a direct beam current; the term $\rho(z + 2d)$ comes from the reflection from the downstream end of the stripline. The sum of the two signals gives information on the beam intensity and the longitudinal beam distribution. The difference of the signals gives information on the transverse beam offset. Note that it is the longitudinal wakes (for both $m = 0$ and $m = 1$) that the monitor is measuring.

(c) Show that the $m = 1$ transverse wake function is given by

$$W_1(z) = -\frac{cR_{S1}}{b^2}\begin{cases} 1 & \text{if } 0 > z > -2d, \\ 0 & \text{otherwise.} \end{cases} \tag{2.113}$$

(d) Demonstrate how four striplines can provide a measurement of the ellipticity of the transverse beam profile. Generalize the result to obtain a device that measures the mth moment of the beam.

Having described the general properties of impedances, it may be instructive next to describe how one can estimate roughly the impedance of a cavity structure in the vacuum chamber. We will start by considering a cavity

[32] D. A. Goldberg and G. R. Lambertson, *AIP Proc.* **249**, *Phys. Part. Accel.*, 1992, Vol. 1, p. 539; Robert E. Shafer, ibid., p. 601.

structure whose dimension and length are of the order of the pipe radius b. In this case, since b is the only length parameter,[33] a simple dimensional analysis tells us that the wake functions per cavity (at distances $z \sim -b$) must be of the order of

$$W'_m(z) \approx \frac{1}{b^{2m+1}}, \qquad W_m(z) \approx \frac{1}{b^{2m}}, \tag{2.114}$$

and the impedances per cavity (at frequency $\omega \sim c/b$) are approximately given by

$$Z_m^{\parallel}(\omega) \approx \frac{b}{c} W'_m \approx \frac{1}{cb^{2m}}, \qquad Z_m^{\perp}(\omega) \approx \frac{b}{c} W_m \approx \frac{1}{cb^{2m-1}}. \tag{2.115}$$

To obtain the quantities per unit longitudinal length, divide the above expressions by $L \sim b$. Note that $1/c = Z_0/4\pi \approx 30\ \Omega$.

To gain more insight beyond the simple dimensional analysis, we will next illustrate Eq. (2.115) more explicitly by introducing two models—the *broad-band resonator model* and the *diffraction model*—which describe the gross features of the cavity impedance. The broad-band resonator model describes the impedance for low frequencies $\omega \lesssim c/b$, and the diffraction model for high frequencies $\omega \gtrsim c/b$.

Broad-Band Resonator Model

We first consider the $m = 0$ impedance $Z_0^{\parallel}$ at frequency $\omega \approx c/b$. To do so, consider a beam bunch of charge q and length b traveling down the pipe through the cavity. The electromagnetic field patterns of the beam are sketched in Figure 2.16. During the passage, wake fields are generated. After the passage, some fields are "scraped off" by the edge of the exit step of the cavity. The energy contained in the wake field scraped off by the cavity is related to the energy lost by the beam. A rough estimate of this energy can be obtained by calculating the field energy contained in the shaded region of

[33]This does not apply for the space charge and resistive-wall cases. In the resistive-wall case, we have another length scale δ_{skin}. This leads to an extra factor of δ_{skin}/b in Eqs. (2.114–2.115) where δ_{skin} is evaluated at $\omega \sim c/b$. Since typically $\delta_{\text{skin}} \ll b$, the resistive-wall wake fields are usually smaller than those due to pipe discontinuities.

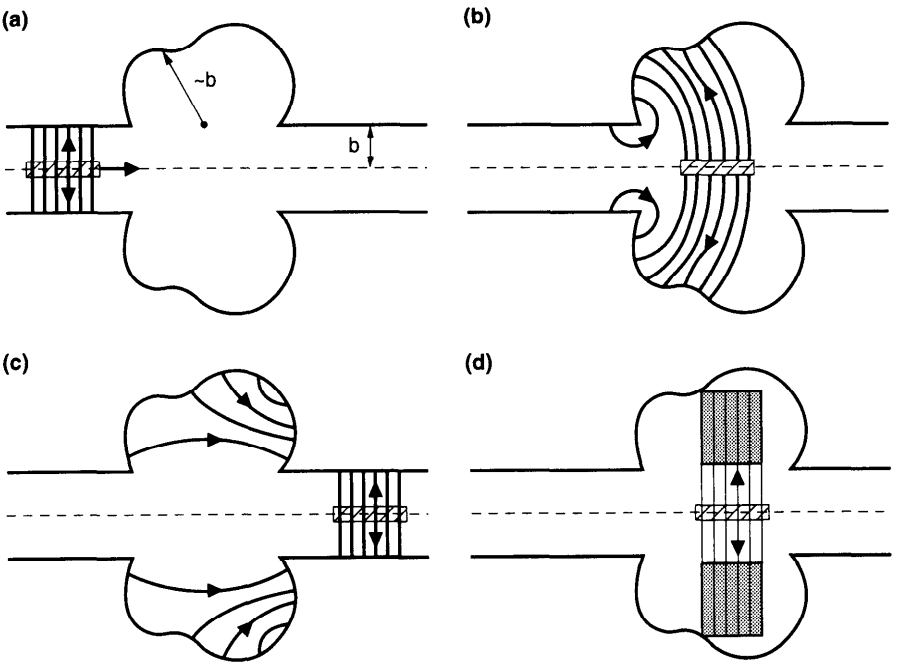

Figure 2.16. (a), (b), and (c), Field patterns as a beam bunch is traversing a cavity structure. (d) The energy loss of the beam can be estimated by calculating the field energy contained in the shaded region. The bunch length and the size of the cavity are both taken to be comparable to the pipe radius b.

Figure 2.16(d), which gives

$$\Delta\mathscr{E} \approx -\frac{1}{8\pi}\int dV\left(E_r^2 + B_\theta^2\right) = -\frac{2q^2}{b}\ln 2, \tag{2.116}$$

where we have used $E_r = B_\theta = 2q/rb$ and the integral over r is from b to $2b$.

Equation (2.116) gives the field energy trapped in the cavity. At high frequencies $\omega \gtrsim c/b$, an equal amount of energy is diffracted into the pipe region by the cavity edges to create the wake fields in the pipe, as sketched later in Figure 2.20.[34] The energy loss of the beam is therefore *twice* that of Eq. (2.116). By equating this energy loss with $-(b/c)J^2Z_0^{\parallel}$, where b/c is the time duration of beam passage, $J^2Z_0^{\parallel}$ is the power of beam energy loss, and

[34]At frequency $\omega \sim c/b$, part of this energy is reabsorbed by the beam. The 80 Ω estimate of Eq. (2.117) for $\omega \sim c/b$ is therefore likely to be a slight over-estimate. This leads to the choice of 60 Ω value in Eq. (2.121), which follows more from Eq. (2.120) than from Eq. (2.117).

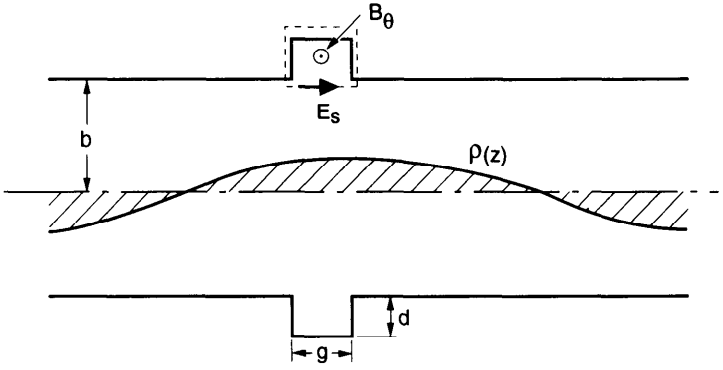

Figure 2.17. The impedance of a small cavity ($g \lesssim d \lesssim b$) is predominantly inductive at low frequencies ($\omega \ll c/b$). The voltage across the cavity gap can be obtained by applying Faraday's law to the dashed circuit.

$J = qc/b$ is the beam current, one obtains, at $\omega \sim c/b$,

$$Z_0^{\parallel} \approx \frac{4}{c} \ln 2 \approx 80\ \Omega. \tag{2.117}$$

We thus conclude that a cavity of the size of the beam pipe radius contributes approximately 80 Ω of impedance $Z_0^{\parallel}$, regardless of its actual size. This gives another proof of Eq. (2.115) for $m = 0$. Fourier transform properties then establish Eq. (2.114).

In deriving Eq. (2.116), the depth of the cavity is taken to be $\sim b$. The result (2.116), however, still applies if the cavity depth is larger than b. This is because the field will not penetrate more than a distance b into the cavity during the beam passage and the cavity region beyond $r = 2b$ is irrelevant to our consideration here.

We have just shown that for a cavity structure of size $\sim$ pipe radius b, the impedance $Z_0^{\parallel} \approx 80\ \Omega$ at $\omega \sim c/b$. At this frequency, the main effect on the beam is an energy loss and the impedance is mostly resistive. To complete the broad-band resonator model, we have yet to consider the regime $\omega \ll c/b$, which can be done by considering a beam with charge density $\rho(z) \propto e^{i\omega z/c}$ where the wavelength $2\pi c/\omega \gg b$.[35] Let the cavity have length g and depth d ($g \lesssim d \lesssim b$) as sketched in Figure 2.17. As the beam passes by, a magnetic field $B_\theta \approx 2\rho/b$ is established in the cavity region. The magnetic flux $\Phi \approx gdB_\theta$ in the cavity region varies slowly with the beam density

[35]Karl L. Bane, *Proc. Euro. Part. Accel. Conf.*, Rome, 1988, p. 637.

$\rho \propto e^{-i\omega t}$, generating a voltage across the cavity gap,

$$V = \int_{\text{gap}} ds\, E_s = -\frac{1}{c}\dot{\Phi} = i\omega \frac{2gd\rho}{cb} \tag{2.118}$$

Relating Eq. (2.118) to $V = -Z_0^{\parallel} J$ with the beam current $J = \rho c$, we obtain for $\omega \ll c/b$

$$Z_0^{\parallel} \approx -i\omega Z_0 \frac{gd}{2\pi bc}. \tag{2.119}$$

The small cavity thus behaves as an inductance $L = Z_0 gd/2\pi bc$ at low frequencies. The inductance is proportional to the cavity cross-sectional area gd. When $g \sim b$ and $d \sim b$, we find

$$Z_0^{\parallel} \approx -i\omega Z_0 \frac{b}{2\pi c} \approx -i\frac{\omega}{c/b} \times 60\ \Omega. \tag{2.120}$$

Combining Eq. (2.117) near $\omega \sim c/b$ and Eq. (2.120) for $\omega \ll c/b$, we recognize that the cavity impedance resembles an LRC resonator [Eq. (2.82) with $m = 0$] with

$$R_S \approx 60\ \Omega, \qquad Q \approx 1, \qquad \omega_R \approx \frac{c}{b}. \tag{2.121}$$

Equation (2.121) is the broad-band resonator model for the $m = 0$ impedance $Z_0^{\parallel}$ of the cavity of size $\sim b$.

The broad-band resonator model does not give an accurate description of the impedance at high frequencies $\omega \gg c/b$; it predicts a purely capacitive impedance, while, as we will show later, a more accurate model—the diffraction model—predicts an impedance which is half capacitive and half resistive. For this reason, the model does not give accurate wake functions at very short ranges $|z| \ll b$.

The broad-band resonator model ignores the possibility of the cavity responding resonantly to sharply defined frequencies, i.e., it ignores the possible existence of cavity modes. These cavity modes occur at frequencies below the cutoff frequency $\sim c/b$, and they give rise to wake functions which ring for long periods of time. Neglecting these long-range contributions, the model also does not give accurate wake functions at very long ranges $|z| \gg b$.

In spite of its limitations, however, the broad-band resonator model gives a good estimate of the impedance near $\omega \sim c/b$ and wake functions near $|z| \sim b$. For applications where the beam bunch length is comparable to the cavity size, it provides a very simple and handy tool.

If one imagines a carelessly built circular accelerator in which the vacuum chamber is filled with all sorts of cavities and discontinuities of approximately the same size as the pipe radius, the total impedance around the circumference is $Z_0^{\parallel} \approx n_{\text{cav}} \times 60\ \Omega$, where $n_{\text{cav}} \approx 2\pi R/2b = \pi R/b$ is the total number of cavities, assuming each cavity occupies a distance $2b$, and ignoring any interference effects of adjacent cavities. As we will show in later chapters, one quantity that characterizes the magnitude of the collective effects in a circular accelerator is $Z_0^{\parallel}/n$, where $n = \omega/\omega_0$ with $\omega_0 = c/R$ the revolution frequency. Setting $\omega \approx c/b$, we find that each cavity of size $\sim b$ contributes

$$\frac{Z_0^{\parallel}}{n}\ (\text{per cavity}) \approx 60\ \Omega \times \frac{b}{R}, \tag{2.122}$$

and that this carelessly designed accelerator has a total $Z_0^{\parallel}/n$ of

$$\frac{Z_0^{\parallel}}{n}\ (\text{total}) \approx 60\ \Omega \times \frac{b}{R} n_{\text{cav}} \approx 60\pi\ \Omega = \frac{1}{2} Z_0. \tag{2.123}$$

This *careless limit* (2.123) is independent of the accelerator size R and the pipe size b.

The impedance $Z_0^{\parallel}$ is a quantity integrated over the accelerator circumference, and tends to be proportional to R. The quantity $Z_0^{\parallel}/n$ has the significance of the impedance per unit length along the circumference, because it contains a factor of $n \propto R$ in the denominator. In addition, since the impedance is likely to be inductive and linear in ω at low frequencies, and since $n \propto \omega$, $Z_0^{\parallel}/n$ has also the significance that it gives the inductance at low frequencies. In other words, the beam dynamics respond more to the inductance than the resistance of the impedance, and the quantity $Z_0^{\parallel}/n$ has the significance of the *inductance per unit length* in the circular accelerator.[36] In particular, for a vacuum chamber structure much smaller than the bunch length, the impedance may be peaked at a frequency much higher than the frequency corresponding to the bunch length, but the effect on the beam may still be significant because of its inductive contribution at lower frequencies.

In case a fraction f of the accelerator is filled with cavities, one has

$$\frac{Z_0^{\parallel}}{n} \approx \frac{f}{2} Z_0. \tag{2.124}$$

In a typical modern accelerator, attempts are made to make $Z_0^{\parallel}/n$ less than $1\ \Omega$ or so. This means the vacuum chamber has to be sufficiently smooth to suppress the impedance by a factor of a few hundred compared with the careless limit.

[36] Put in another, somewhat exaggerated, way: what affects the beam dynamics is not measured in ohms; it is not even ohms per meter; it is henries per meter.

The rough estimate (2.117) can be extended to $m \neq 0$ cases. Consider a beam of length b with an mth moment I_m. The energy loss in the cavity can be estimated by the field energy contained in the same shaded region as in Figure 2.16(d), where the fields are given by Eq. (1.8) with the outer boundary located at $r \sim 2b$. This gives

$$\begin{aligned}\Delta\mathscr{E} &\approx -\frac{1}{8\pi}\int dV\left(E_r^2 + E_\theta^2 + B_r^2 + B_\theta^2\right) \\ &= -\frac{I_m^2}{mb^{2m+1}}\left(1 - \frac{1}{2^{4m}}\right) \approx -\frac{I_m^2}{mb^{2m+1}}.\end{aligned} \tag{2.125}$$

As before, the energy lost by the beam is approximately twice Eq. (2.125). By equating this energy loss to $-(b/c)J_m^2 Z_m^{\parallel}$ with $J_m = I_m c/b$, we obtain

$$Z_m^{\parallel} \approx \frac{2}{mcb^{2m}}. \tag{2.126}$$

This establishes Eq. (2.115) for $m \neq 0$.

The transverse impedance can then be obtained by relating it to the longitudinal impedance using Eq. (2.73). For example, for $m = 1$, we have for $\omega \lesssim c/b$

$$Z_1^{\perp} \approx \frac{2}{cb} \approx 60\ \Omega \times \frac{1}{b}. \tag{2.127}$$

A deep cavity in a $b = 5$ cm pipe, therefore, contributes approximately $Z_1^{\perp} \approx 1.2\ \text{k}\Omega/\text{m}$ in the neighborhood of $\omega/2\pi \lesssim 1$ GHz. In the same spirit as Eq. (2.121), a transverse broad-band resonator impedance [Eq. (2.87) with $m = 1$] that represents this cavity would have

$$R_S \approx 60\ \Omega \times \frac{1}{b^2}, \qquad Q \approx 1, \qquad \omega_R \approx \frac{c}{b} \tag{2.128}$$

Comparing Eqs. (2.121) and (2.128) with Eq. (2.107), we find that Eq. (2.107) is off by a factor of 2. This is not unreasonable in view of the approximate nature of the three equations involved.

Figure 2.18 shows the longitudinal and transverse wake functions corresponding to the broad-band impedances, (2.121) and (2.128). One should keep in mind that these wake functions do not apply to very short ($|z| \ll b$) or very long ($|z| \gg b$) ranges.

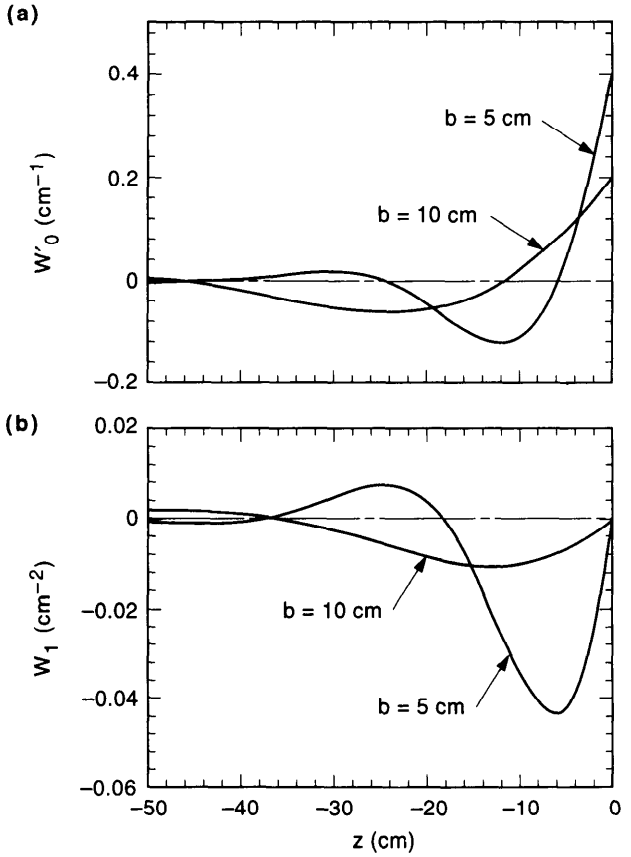

Figure 2.18. Wake functions of the broad-band impedances (2.121) and (2.128). (a) is longitudinal; (b) is transverse. Two values of b, 5 and 10 cm, are presented to indicate the scaling of the wake functions with respect to b.

Exercise 2.21 Consider a shallow cavity and the arrangement of Figure 2.17 except that $\rho(z)$ is the distribution of the dipole moment (instead of the charge) of the beam. Follow the argument (2.118–2.120) of the text to show that the transverse impedance $Z_1^{\perp}(\omega)$ at low frequencies $|\omega| \ll c/b$ is approximately given by

$$Z_1^{\perp}(\omega) \approx -iZ_0 \frac{gd}{\pi b^3} \tag{2.129}$$

Show that, aside from a numerical factor, this result is consistent with the broad-band resonator model (2.128). As can be expected, Eqs. (2.119) and (2.129) satisfy the condition (2.107).

Exercise 2.22

(a) Consider a cavity structure of length and depth g, where $g \ll b$, and consider a beam of length g. Follow the reasoning in the text to show

that this cavity has an impedance, at frequency $\omega \approx c/g$, given by

$$Z_0^{\parallel} \approx \frac{Z_0}{2\pi}\frac{g}{b}. \tag{2.130}$$

If the accelerator pipe is covered with these cavities, one has

$$\frac{Z_0^{\parallel}}{n} \approx \frac{Z_0}{2}\frac{g}{b}. \tag{2.131}$$

(b) Take g to be the skin depth δ_{skin}, and show that the result is consistent with the resistive-wall impedance (2.77). This means the resistive wall behaves almost like a continuum of small cavities of size $\sim \delta_{\text{skin}}$.

(c) Use Eq. (2.131) to estimate $Z_0^{\parallel}/n$ due to the roughness of the pipe wall. Show that

$$\frac{Z_0^{\parallel}}{n} \approx \frac{Z_0 g}{4b},$$

where g is the size of the granularities on the wall surface.

Exercise 2.23 The reasoning leading to the conclusion that the impedance of a cavity is mainly inductive at low frequencies and is given by Eq. (2.119) can also be applied to estimate the impedance of a perfectly smooth beam pipe of radius b with a small circular hole of radius $r \ll b$ on the pipe wall. Provide the reasoning that the low-frequency impedance can be roughly estimated by setting $g \sim d \sim r$ in Eq. (2.119) and multiplying the result by the factor $r/\pi b$, the fraction of the azimuthal extent of the hole. Compare the result with that obtained by an exact consideration,[37] which gives an inductance

$$L = \frac{Z_0}{6\pi^2 c}\frac{r^3}{b^2}. \tag{2.132}$$

Note the cubic dependence of the impedance on the hole size.

Exercise 2.24 Estimate $Z_0^{\parallel}/n$ and $Z_1^{\perp}$ for the accelerator sketched in Figure 2.19. Give a broad-band resonator representation of your estimates. Assume a resistive-wall aluminum pipe of radius $b = 5$ cm. Let there be 10 bellows (with depth $\Delta = 1$ cm), 10 stripline monitors (with characteristic resistance $R_{S0} = 3\ \Omega$ and length $d = 20$ cm), and 2 rf cavities. Consider an accelerator circumference of 200 m.

[37] H. A. Bethe, Phys. Rev. **66**, 163 (1944); M. Sands, SLAC Report PEP-253 (1977); S. S. Kurennoy, Part. Accel. **39**, 1 (1992); R. L. Gluckstern, Phys. Rev. A **46**, 1106 (1992) and Phys. Rev. A **46**, 1110 (1992).

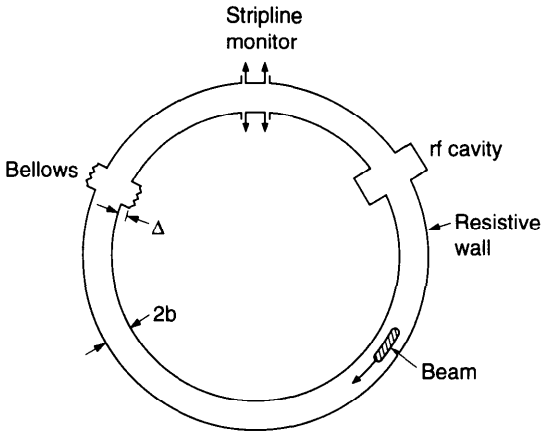

Figure 2.19. An accelerator with objects that contribute to impedances.

Exercise 2.25 Consider a circular accelerator with $b = 5$ cm and $|Z_0^{\parallel}/n| = 1\ \Omega$. Model the impedance as a number of cavities, each represented by the broad-band resonator (2.121). Show that the accelerator has one such cavity approximately every 25 m.

Diffraction Model

The broad-band resonator model addresses the impedance for frequencies $\omega \lesssim c/b$. It turns out that it is also possible to estimate the impedance at high frequencies $\omega \gg c/b$. The method used is called the diffraction model, and was first introduced by Lawson.[38]

To illustrate this method, we follow Bane and Sands to consider a single cavity in an infinitely long beam pipe as sketched in Figure 2.20. Since in this calculation we are interested in the frequency dependence of the impedance, we consider a sinusoidal beam current J_0 which is given by the real part of $\hat{J}_0 \exp[-i\omega(t - s/c)]$. In the region sufficiently upstream from the cavity, the electromagnetic field is given by a plane wave with the same sinusoidal t and s dependences as the beam current. At the pipe radius, we have $E_r = B_\theta = 2J_0/cb$. As the beam enters the cavity, this plane wave is diffracted by the entrance edge of the cavity as sketched in Figure 2.20. We let g be the longitudinal extent of the cavity.

At high frequencies $\omega \gg c/b$, according to the diffraction model, the electromagnetic field in the cavity region is the same as that produced by a plane wave impinging on an obscuring screen. Furthermore, at high frequen-

[38] J. D. Lawson, Rutherford Lab. Report RHEL/M 144 (1968), and Part. Accel. **25**, 107 (1990). See also G. Dome, IEEE Tran. Nucl. Sci. **NS-32**, 2531 (1985); S. A. Heifets and S. A. Kheifets, Part. Accel. **25**, 61 (1990); Karl Bane and Matthew Sands, Part. Accel. **25**, 73 (1990); R. B. Palmer, Part. Accel. **25**, 97 (1990); R. L. Gluckstern, *AIP Proc.* **249**, *Phys. Part. Accel.*, 1992, Vol. 1, p. 237.

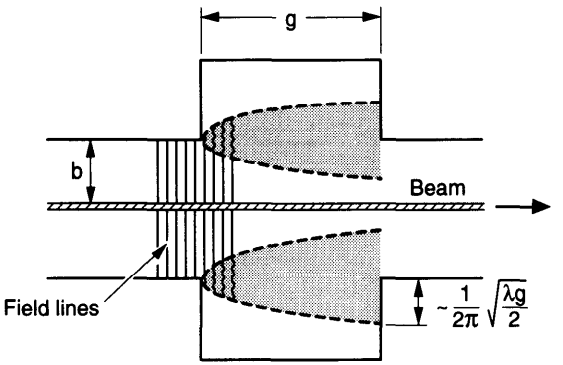

Figure 2.20. The diffraction model of high frequency impedance for a single cavity structure. The beam and the field lines are sketched. The shaded region between the dashed curves indicates the region where the fields are perturbed by diffraction. The depth of the cavity is assumed to be larger than $(1/2\pi)\sqrt{\lambda g/2}$. Approximately half the diffracted field energy is trapped in the cavity; the other half propagates down the vacuum chamber pipe.

cies the screen can be approximated as a semi-infinite plane with a straight edge, and the polar plane electromagnetic wave can be approximated as a Cartesian plane wave with $E_y = -B_x = -2J_0/cb$ and wavelength $\lambda = 2\pi c/\omega$. The beam-cavity system of Figure 2.20 is therefore modeled as shown in Figure 2.21. The incident wave carries an energy flux (energy flowing by per unit area per unit time)

$$F_0 = \frac{c}{8\pi}\left(E_y^2 + B_x^2\right) = \frac{J_0^2}{\pi c b^2}. \tag{2.133}$$

As it enters the cavity, the plane wave is diffracted at the edge of the obscuring screen (the entrance edge of the cavity) into the shadow region. By

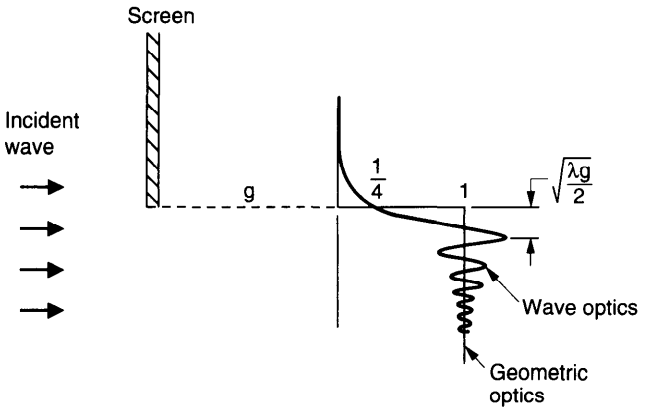

Figure 2.21. Geometry of the diffraction model. Energy flux behind the screen is shown on the right. Two curves are shown; one indicates what would happen with geometric optics without diffraction, the other is the result of wave optics.

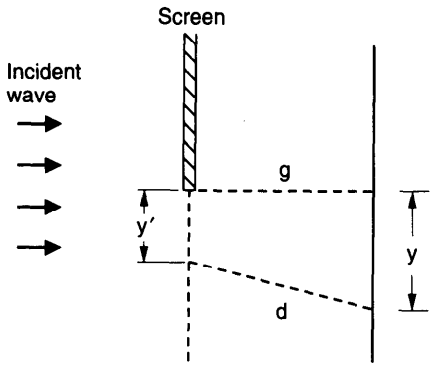

Figure 2.22. Geometry used to calculate the diffraction pattern.

the time the field reaches the exit edge of the cavity, the diffracted field has acquired a spread in the y-direction (the direction that lies in the plane of the screen and is perpendicular to the screen edge). The energy flux, as a function of y, is given by (see Exercise 2.26)

$$F(y) = F_0 \tfrac{1}{2}\left\{\left[C(u) + \tfrac{1}{2}\right]^2 + \left[S(u) + \tfrac{1}{2}\right]^2\right\} \equiv F_0\Phi(u), \quad (2.134)$$

where $u = y\sqrt{2/\lambda g}$, and $C(u)$ and $S(u)$ are the Fresnel integrals defined by

$$C(u) + iS(u) = \int_0^u dt\, e^{i(\pi/2)t^2}, \quad (2.135)$$

which are odd functions of u and have the properties $C(\pm\infty) = S(\pm\infty) = \pm\frac{1}{2}$.

Exercise 2.26 Consider the geometry shown in Figure 2.22. The diffracted field is proportional to $|a(y)|^2$, where

$$a(y) \propto \int_0^\infty dy'\, e^{i\omega d/c}, \quad (2.136)$$

where d, shown in Figure 2.22, is approximately given by $g + (y - y')^2/2g$. Derive Eq. (2.134) using Eqs. (2.135–2.136).

The energy loss from the beam is given by the energy contained in the diffracted fields. The power of this energy loss into the shadow region $y < 0$ is given by integrating Eq. (2.134) over the appropriate area:

$$\mathscr{P} = 2\pi b \int_{-\infty}^{0} dy\, F(y). \quad (2.137)$$

The integral can be evaluated to yield

$$\mathscr{P} = \frac{J_0^2}{\pi cb}\sqrt{\frac{\pi cg}{\omega}}, \quad (2.138)$$

where we have used $\int_{-\infty}^{0}\Phi(u)\,du = 1/2\pi$. As the wave is diffracted, half of the diffracted field energy goes into the shadow region, and represents the part of energy to be scraped off by the exit edge of the cavity. The other half is diffracted toward the pipe region and propagates down the pipe with the beam. The total loss of field energy by the beam is thus twice that given by Eq. (2.138). The effective depth that the field is diffracted into the shadow region is $\mathscr{P}/2\pi bF_0 = (1/2\pi)\sqrt{\lambda g/2}$.

Exercise 2.27 Show that:

(a) The wave energy flux at the shadow edge $y = 0$ is $\frac{1}{4}$ of the incident flux, i.e., $\Phi(0) = \frac{1}{4}$.

(b) The wave energy flux deep in the shadow region is given by $F(y) \approx \lambda g F_0/4\pi^2 y^2$.

(c) The total field energy contained in the diffracted wave pattern is the same as that contained in the geometrical optics pattern, i.e., total wave energy is conserved. [Hint: Show $\int_{-\infty}^{0} du\,\Phi(u) + \int_{0}^{\infty} du[\Phi(u) - 1] = 0$.]

(d) The energy lost by the plane wave in the shadow region $y < 0$ is equal to that in the region $y > 0$. [Hint: Show $\int_{-\infty}^{0} dy|a(y) - a(-\infty)|^2 = \int_{0}^{\infty} dy|a(y) - a(\infty)|^2$.]

The power loss (2.138), multiplied by 2, is then equated with $\operatorname{Re} Z_0^{\parallel} J_0^2$ to give the real part of the impedance at high frequencies,

$$\operatorname{Re} Z_0^{\parallel}(\omega) = \frac{Z_0}{2\pi^{3/2}}\frac{1}{b}\sqrt{\frac{cg}{\omega}}, \tag{2.139}$$

where $Z_0 = 4\pi/c = 377\ \Omega$. Causality requires a matching imaginary part of the impedance. The total impedance is

$$Z_0^{\parallel}(\omega) = [1 + \operatorname{sgn}(\omega)i]\frac{Z_0}{2\pi^{3/2}}\frac{1}{b}\sqrt{\frac{cg}{|\omega|}}. \tag{2.140}$$

The corresponding wake function is

$$W_0'(z < 0) = \frac{2\sqrt{2g}}{\pi b}|z|^{-1/2}. \tag{2.141}$$

Exercise 2.28 For a short Gaussian bunch with $\sigma_z \ll b$, use Eq. (2.139) to calculate the parasitic loss

$$\Delta\mathscr{E} = -\frac{1}{\pi}\Gamma\left(\frac{1}{4}\right)\frac{q^2}{b}\sqrt{\frac{g}{\pi\sigma_z}}. \tag{2.142}$$

Note that $\Delta\mathscr{E} \to \infty$ as $\sigma_z \to 0$. Setting $\sigma_z \sim g \sim b$ gives essentially Eq. (2.116) other than a numerical factor.

For $m \neq 0$, consider an mth moment current $J_m = \hat{J}_m \exp[-i\omega(t - s/c)]$. The electromagnetic field at the entrance edge of the cavity is $E_y = -B_x = -(4J_m \cos m\theta)/(cb^{m+1})$. The energy flux of the diffracted wave is given by

$$F(y,\theta) = \frac{4}{\pi}\frac{J_m^2}{cb^{2m+2}}\cos^2 m\theta\,\Phi(u), \tag{2.143}$$

where $\Phi(u)$ is defined in Eq. (2.134). The power lost by the beam in the shadow region is then

$$\mathscr{P} = b\int_{-\infty}^{0} dy \int_0^{2\pi} d\theta\, F(y,\theta) = \frac{Z_0}{2\pi^{3/2}}\frac{J_m^2}{b^{2m+1}}\sqrt{\frac{cg}{\omega}}\,. \tag{2.144}$$

Equating twice this amount to $\mathrm{Re}\, Z_m^{\parallel} J_m^2$ and matching an imaginary part to it, we obtain the impedance, for $m \neq 0$,

$$Z_m^{\parallel}(\omega) = \frac{\omega}{c}Z_m^{\perp}(\omega) = [1 + \mathrm{sgn}(\omega)i]\frac{Z_0}{\pi^{3/2}}\frac{1}{b^{2m+1}}\sqrt{\frac{cg}{|\omega|}}\,. \tag{2.145}$$

The corresponding wake functions are

$$\begin{aligned} W_m(z<0) &= -\frac{8\sqrt{2g}}{\pi b^{2m+1}}|z|^{1/2}, \\ W_m'(z<0) &= \frac{4\sqrt{2g}}{\pi b^{2m+1}}|z|^{-1/2}. \end{aligned} \tag{2.146}$$

Equation (2.140) and the $m = 1$ member of Eq. (2.145) satisfy Eq. (2.107) exactly. This is not surprising because the electrodynamics of the diffraction model are all happening near the pipe radius $r = b$. Furthermore, the generalized form (2.109) is also valid for the diffraction model.

According to the diffraction model, therefore, the longitudinal impedance $Z_m^{\parallel} \propto \omega^{-1/2}$ and the transverse impedance $Z_m^{\perp} \propto \omega^{-3/2}$ at high frequencies. At these high frequencies, we also find that the impedances are proportional to $\sqrt{g}$. By taking the lower end of the range of applicability, $\omega \approx c/b$, and setting $g = b$, we find the impedances are consistent with Eqs. (2.117) and (2.127), aside from a numerical factor of the order of unity. The diffraction impedance for $\omega \gg c/b$ therefore matches reasonably smoothly the broad-band resonator impedance for $\omega \lesssim c/b$. The wake function W_m' diverges as $z \to 0^-$. A point charge or a point multipole, therefore, loses an infinite

amount of energy to the cavity structure. At distance $|z| \approx b$, and $g = b$, we obtain Eq. (2.114).

The diffraction model applies to the case of a single cavity structure in an infinitely long smooth beam pipe. A beam pipe with a periodic array of cavities has an impedance whose high frequency behavior is very different from the diffraction model result. See Eq. (2.175) below.

2.4 CALCULATION OF WAKE FIELDS AND IMPEDANCES

In Section 2.1, we worked out in detail the wake fields of a resistive-wall pipe. The reason for using the resistive wall as an example is that it can be handled analytically and yet contains most of the important features of a general case. In most practical cases, the resistive-wall contribution is small compared with other wake fields found in an accelerator, such as those associated with discontinuities in the vacuum chamber pipe.

The computation of wake functions and impedances for practical accelerator applications is a rather demanding task. One encounters vacuum chamber components that require special attention of one kind or another (lack of axial symmetry, nonmetal material, vacuum pipe thinner than the skin depth, etc.). Practicality dictates the calculation to be performed, and sophisticated techniques have been developed to deal with these problems. Below we will describe two methods, one due to Condon[39] (the frequency domain approach), another by direct numerical solution of the Maxwell equations (the time domain approach). Not covered is for example a perturbation technique valid for smoothly varying wall boundaries.[40]

Frequency Domain

Consider a point charge q passing through a cavity with perfectly conducting walls. We suppose first the cavity is closed and the point charge traverses the cavity through infinitesimal holes. In the frequency domain, the cavity wake fields generated by the passage of the point charge are described in terms of a superposition of modes. Each mode can be specified by an equivalent LRC resonator impedance (2.85) and wake function (2.86) with its own mode frequency ω_R and R_S/Q.[41] The energy deposited by the point charge into a

[39] E. U. Condon, J. Appl. Phys. **12**, 129 (1941).

[40] M. Chatard-Moulin and A. Papiernik, Nucl. Instr. Meth. **205**, 37 (1983); R. K. Cooper, S. Krinsky, and P. L. Morton, Part. Accel. **12**, 1 (1982); S. Krinsky and R. L. Gluckstern, IEEE Trans. Nucl. Sci. **NS-28**, 2621 (1981).

[41] A resonator impedance is specified by three parameters: ω_R, R_S, and Q. But for a closed cavity with perfectly conducting walls assumed here, the analogy to an LRC circuit is meaningful only on setting $R_S \to \infty$, $Q \to \infty$ with R_S/Q fixed.

given mode after its passage through the cavity is given by

$$q^2\frac{W_0'(0^-)}{2} = q^2\frac{R_S\omega_R}{2Q} \equiv q^2k, \tag{2.147}$$

where the factor of $\frac{1}{2}$ is due to the fundamental theorem of beam loading. The quantity $k = R_S\omega_R/2Q$ is called the *loss factor*;[42] it is a property of the cavity and not of the beam.

The total longitudinal and transverse wake functions of the cavity are superpositions of (2.86) and (2.90) from all cavity modes. The λth mode is characterized by a mode frequency ω_λ and loss factor k_λ. Thus, for $z < 0$, we have

$$\begin{aligned} W_0'(z) &= 2\sum_\lambda k_\lambda \cos\frac{\omega_\lambda z}{c}, \\ W_0(z) &= 2\sum_\lambda \frac{k_\lambda c}{\omega_\lambda}\sin\frac{\omega_\lambda z}{c}. \end{aligned} \tag{2.148}$$

The corresponding impedances are given by Eqs. (2.85) and (2.89) with $R_S\omega_R/2Q$ replaced by k_λ. Computation of the wake functions and impedances is therefore reduced to computation of ω_λ and k_λ for all cavity modes. The total energy change of a point charge q is obtained by summing Eq. (2.147) over all modes:

$$\Delta\mathscr{E} = -q^2\sum_\lambda k_\lambda. \tag{2.149}$$

To proceed, we write the wake field generated by the beam as

$$\begin{aligned} \vec{E} &= -\nabla\Phi - \frac{1}{c}\frac{\partial\vec{A}}{\partial t}, \\ \vec{B} &= \nabla\times\vec{A}, \end{aligned} \tag{2.150}$$

where the scalar and vector potentials satisfy the Maxwell equations in Coulomb gauge,[43]

$$\begin{aligned} \nabla^2\Phi &= -4\pi\rho, \\ \nabla^2\vec{A} - \frac{1}{c^2}\frac{\partial^2\vec{A}}{\partial t^2} &= -\frac{4\pi}{c}\vec{j} + \frac{1}{c}\nabla\frac{\partial\Phi}{\partial t}. \end{aligned} \tag{2.151}$$

[42]R. F. Koontz, G. A. Loew, R. H. Miller, and P. B. Wilson, IEEE Trans. Nucl. Sci. **NS-24**, 1493 (1977); Perry B. Wilson, *AIP Proc.* **87**, *Phys. High Energy Accel.*, Fermilab, 1981, p. 450.
[43]J. D. Jackson, *Classical Electrodynamics*, 2nd ed., Wiley, New York, 1975.

To apply the *Condon method*, we expand the scalar and vector potentials in terms of the eigenmodes of the empty cavity according to

$$\begin{aligned} \vec{A}(\vec{x},t) &= \sum_{\lambda} q_\lambda(t)\vec{a}_\lambda(\vec{x}), \\ \Phi(\vec{x},t) &= \sum_{\lambda} r_\lambda(t)\phi_\lambda(\vec{x}), \end{aligned} \tag{2.152}$$

where the eigenmodes satisfy

$$\begin{aligned} \nabla^2\vec{a}_\lambda + \left(\frac{\omega_\lambda}{c}\right)^2 \vec{a}_\lambda &= 0, \\ \nabla^2\phi_\lambda + \left(\frac{\omega_\lambda}{c}\right)^2 \phi_\lambda &= 0, \end{aligned} \tag{2.153}$$

as well as the boundary conditions that $\vec{a}_\lambda$ is perpendicular to the conducting walls and that $\phi_\lambda = 0$ on the walls. We have adopted the Coulomb gauge $\nabla \cdot \vec{a}_\lambda = 0$ and the normalization conditions

$$\int_{\text{cavity}} dV \vec{a}_\lambda \cdot \vec{a}^*_{\lambda'} = \int_{\text{cavity}} dV \phi_\lambda \phi^*_{\lambda'} = \delta_{\lambda\lambda'}, \tag{2.154}$$

where $\delta_{\lambda\lambda'} = 1$ if $\lambda = \lambda'$ and 0 otherwise.

By a proper choice of a distance L, one can consider that the beam enters the cavity at location $s = 0$ at time $t = 0$, and exits the cavity at location $s = L$ at time $t = L/c$. By substituting Eq. (2.152) into Eq. (2.151) and applying the orthonormality condition (2.154), $r_\lambda(t)$ can be found readily:

$$r_\lambda(t) = \frac{4\pi c^2}{\omega_\lambda^2} \int_{\text{cavity}} dV \rho(\vec{x},t)\phi^*_\lambda(\vec{x}). \tag{2.155}$$

One also finds that $q_\lambda(t)$ satisfies

$$\ddot{q}_\lambda + \omega_\lambda^2 q_\lambda = 4\pi c \int_{\text{cavity}} dV \vec{j}(\vec{x},t) \cdot \vec{a}^*_\lambda(\vec{x}), \tag{2.156}$$

which has the explicit solution

$$q_\lambda(t) = \begin{cases} 0 & \text{if} \quad t < 0, \\ \dfrac{4\pi c}{\omega_\lambda} \displaystyle\int_0^{\min(t,\,L/c)} dt' \sin \omega_\lambda(t - t') & \\ \qquad \times \displaystyle\int_{\text{cavity}} dV \vec{j}(\vec{x},t') \cdot \vec{a}^*_\lambda(\vec{x}) & \text{if} \quad t > 0. \end{cases} \tag{2.157}$$

Knowing $\rho(\vec{x}, t)$ and $\vec{j}(\vec{x}, t)$, Eqs. (2.155) and (2.157) give directly the expansion coefficients $r_\lambda(t)$ and $q_\lambda(t)$. Note that r_λ (and therefore the scalar potential Φ) vanishes at times when the beam is absent, i.e., when $t < 0$ or $t > L/c$. The same is not true for the vector potential $\vec{A}$. Its expansion coefficients q_λ vanish before the beam enters the cavity ($t < 0$), but continue to "ring" after the beam has left the cavity.

We now consider the special case of a point charge,

$$\begin{aligned} \rho &= q\delta(x)\delta(y)\delta(s - ct), \\ \vec{j} &= c\rho\hat{s}. \end{aligned} \tag{2.158}$$

Substituting into Eqs. (2.155) and (2.157) gives

$$r_\lambda(t) = \begin{cases} \dfrac{4\pi c^2}{\omega_\lambda^2} q\phi_\lambda^*(0,0,ct) & \text{if } \dfrac{L}{c} > t > 0, \\ 0 & \text{otherwise,} \end{cases}$$

$$q_\lambda(t) = \begin{cases} 0 & \text{if } t < 0, \\ \dfrac{4\pi c^2 q}{\omega_\lambda} \displaystyle\int_0^{\min(t,\, L/c)} dt' \sin \omega_\lambda(t - t')\, a_{\lambda s}^*(0,0,ct') & \text{if } t > 0. \end{cases} \tag{2.159}$$

The energy loss of the point charge can be obtained by integrating the longitudinal electric field across the cavity:

$$\begin{aligned} \Delta\mathscr{E} &= qc\int_0^{L/c} dt\, E_s(0,0,ct) \\ &= -qc\sum_\lambda \int_0^{L/c} dt \left[r_\lambda(t) \frac{\partial\phi_\lambda(0,0,ct)}{c\partial t} + \frac{1}{c}\dot{q}_\lambda(t) a_{\lambda s}(0,0,ct) \right]. \end{aligned} \tag{2.160}$$

The loss factor k_λ is related to the energy deposited into the λth mode. On substituting (2.159) into (2.160), the first term on the right hand side vanishes after integrating over t due to the boundary condition of ϕ_λ. After some algebraic manipulations, the second term gives what we are looking for,[44]

$$k_\lambda = 2\pi \left| \int_0^{L/c} c\, dt\, e^{-i\omega_\lambda t}\, a_{\lambda s}(0,0,ct) \right|^2. \tag{2.161}$$

[44] For a guide to this derivation, see K. L. F. Bane, P. B. Wilson, and T. Weiland, *AIP Proc.* **127**, *Phys. of High Energy Accel.*, BNL/SUNY, 1983, p. 875.

Given the eigenmodes $a_\lambda(\vec{x})$ of the empty cavity, Eq. (2.161) gives the loss factors k_λ on integrating a_λ over the trajectory of the point charge along its path through the cavity. Knowing the mode frequencies and loss factors, the wake functions can be calculated using Eq. (2.148).

Exercise 2.29

(a) The loss factor (2.161) can also be obtained by calculating the field energy deposited in the cavity after the point charge has departed. Show that this derivation gives the same result, Eq. (2.161).

(b) By considering a test charge e a distance $|z|$ behind the point charge q, calculate the longitudinal wake function $W_0'(z)$ by using Eq. (2.50):

$$-eqW_0'(z) = \int_{-z/c}^{(L-z)/c} c\,dt\,eE_s(0,0,ct+z), \qquad z<0. \quad (2.162)$$

Verify explicitly that the wake function is given by Eq. (2.148).

So far we have been considering a closed cavity. In case of a periodic cavity array like that shown in Figure 2.1(a), the analysis can be applied if L is chosen to be the structure period and the modes are taken to be those with phase velocity equal to that of the beam, i.e., $v_{\text{ph}} = c$.

To calculate the wake functions for modes with $m \neq 0$, we consider a $\cos m\theta$ ring beam, Eq. (1.7), traversing the cavity. We assume the vacuum chamber pipe is axially symmetric, and switch to polar coordinates (r, θ, s). This gives, for $t > 0$,

$$r_\lambda(t) = \begin{cases} \dfrac{4c^2 I_m}{\omega_\lambda^2 a^m} \displaystyle\int_0^{2\pi} d\theta \cos m\theta\, \phi_\lambda^*(a,\theta,ct) & \text{if } \dfrac{L}{c} > t > 0, \\ 0 & \text{if } t > \dfrac{L}{c}, \end{cases} \quad (2.163)$$

$$q_\lambda(t) = \frac{4c^2 I_m}{\omega_\lambda a^m} \int_0^{\min(t,\,L/c)} dt' \sin\omega_\lambda(t-t') \times \int_0^{2\pi} d\theta \cos m\theta\, a_{\lambda s}^*(a,\theta,ct').$$

Note that it is the mth Fourier harmonic of the normal modes that drives the wake fields when the beam has a pure mth multipole moment.

Following similar steps to those for the point charge, Eqs. (2.160–2.161), we obtain the energy loss of the mth moment I_m,

$$\Delta\mathscr{E} = -I_m^2 \sum_\lambda k_\lambda^{(m)}, \quad (2.164)$$

where the loss factor is

$$k_\lambda^{(m)} = \frac{2\pi}{b^{2m}} \left| \int_0^{L/c} c\,dt\, e^{-i\omega_\lambda t} \frac{1}{(1+\delta_{m0})\pi} \int_0^{2\pi} d\theta \cos m\theta\, a_{\lambda s}(b,\theta,ct) \right|^2 . \tag{2.165}$$

Note that it is $a_{\lambda s}$ evaluated at the pipe radius $r = b$ that appears in the integral. The wake functions are then given, for $z < 0$, by

$$\begin{aligned} W'_m(z) &= 2\sum_\lambda k_\lambda^{(m)} \cos\frac{\omega_\lambda z}{c}, \\ W_m(z) &= 2\sum_\lambda \frac{k_\lambda^{(m)} c}{\omega_\lambda} \sin\frac{\omega_\lambda z}{c}. \end{aligned} \tag{2.166}$$

The dimensionalities of the loss factors k_λ and $k_\lambda^{(m)}$ are L^{-1} and L^{-2m-1}. To convert k_λ to other units, one can use

$$1\ \text{V/pC} = 1\ \text{k}\Omega\text{-GHz} = 1.11\ \text{cm}^{-1}. \tag{2.167}$$

As one application of the Condon method, below we calculate the electromagnetic fields generated by a point charge, Eq. (2.158), between two infinite, perfectly conducting plates located at $s = 0$ and $s = L$, as shown in Figure 2.23.[45] To do so, we first calculate the normal mode potentials for an empty cavity. These are found to be

$$\begin{aligned} \omega_\lambda &= c\sqrt{k_x^2 + k_y^2 + \left(\frac{p\pi}{L}\right)^2}, \\ \phi_\lambda &= \frac{1}{\pi\sqrt{2L}} e^{i(k_x x + k_y y)} \sin\frac{p\pi s}{L}, \\ \vec{a}_\lambda &= \frac{ce^{i(k_x x + k_y y)}}{\omega_\lambda \sqrt{2L\left(k_x^2 + k_y^2\right)(1+\delta_{p0})}} \\ &\quad \times \left[\hat{x}\left(\frac{-ipk_x}{L}\sin\frac{p\pi s}{L}\right) + \hat{y}\left(\frac{-ipk_y}{L}\sin\frac{p\pi s}{L}\right) + \hat{s}\left(\frac{k_x^2 + k_y^2}{\pi}\cos\frac{p\pi s}{L}\right)\right], \end{aligned} \tag{2.168}$$

where the mode index λ stands for the three mode numbers k_x, k_y, and p,

[45] This model ignores the effects of the outer boundary of the cavity walls which would be there if the cavity had the geometry of a pillbox. However, this simplification is strictly correct when the bunch length or distance of interest is sufficiently short so that causality precludes any effect of the wake fields reflected from the outer cavity walls.

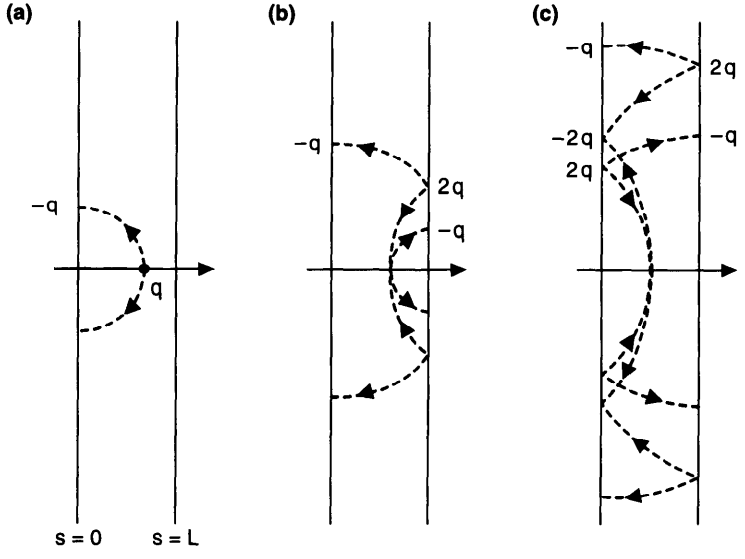

Figure 2.23. Wake field generated by a point charge passing through two perfectly conducting, infinite parallel plates. Dashed curves are the wake fields. Arrows indicate directions of the electric fields. (a) When the charge is between the plates; (b), (c) after the charge has left the cavity.

and

$$\sum_{\lambda} \to \int_{-\infty}^{\infty} dk_x \int_{-\infty}^{\infty} dk_y \sum_{p=0}^{\infty} . \tag{2.169}$$

It follows from Eqs. (2.155) and (2.157) that

$$r_\lambda(t) = \frac{4c^2 q}{\omega_\lambda^2 \sqrt{2L}} \begin{cases} \sin \dfrac{p\pi ct}{L}, \\ 0, \end{cases} \tag{2.170}$$

$$q_\lambda(t) = \frac{4cq}{\omega_\lambda \sqrt{2L\left(k_x^2 + k_y^2\right)(1 + \delta_{p0})}} \begin{cases} -\cos \omega_\lambda t + \cos \dfrac{p\pi ct}{L}, \\ -\cos \omega_\lambda t + (-1)^p \cos \omega_\lambda \left(t - \dfrac{L}{c}\right), \end{cases}$$

where the first entry refers to $L/c > t > 0$, the second to $t > L/c$.

After some algebraic manipulations, the field components are found using Eqs. (2.150) and (2.152):[46]

$$E_r = \begin{cases} \dfrac{2q}{r}A, \\ \dfrac{2q}{r}B_- - \dfrac{2q}{r}C_-, \end{cases}$$

$$E_s = \begin{cases} -\dfrac{2q}{\sqrt{c^2t^2 - r^2}}A, \\ -\dfrac{2q}{\sqrt{c^2t^2 - r^2}}B_+ + \dfrac{2q}{\sqrt{(ct - L)^2 - r^2}}C_+, \end{cases} \tag{2.171}$$

$$B_\theta = \begin{cases} \dfrac{2qct}{r\sqrt{c^2t^2 - r^2}}A, \\ \dfrac{2qct}{r\sqrt{c^2t^2 - r^2}}B_+ - \dfrac{2q(ct - L)}{r\sqrt{(ct - L)^2 - r^2}}C_+, \end{cases}$$

where $r^2 = x^2 + y^2$ and we have introduced the symbols

$$\begin{aligned} A &= H(ct - r)\delta\left(s - \sqrt{c^2t^2 - r^2}\right), \\ B_\pm &= H(ct - r)\sum_{n=-\infty}^{\infty}\Big[\delta\left(s - \sqrt{c^2t^2 - r^2} + 2nL\right) \\ &\qquad \pm\delta\left(s + \sqrt{c^2t^2 - r^2} - 2nL\right)\Big], \\ C_\pm &= H(ct - L - r)\sum_{n=-\infty}^{\infty}\left\{\delta\left[s - \sqrt{(ct - L)^2 - r^2} + (2n + 1)L\right]\right. \\ &\qquad \left.\pm\delta\left[s + \sqrt{(ct - L)^2 - r^2} - (2n + 1)L\right]\right\} \end{aligned} \tag{2.172}$$

with $H(x) = 1$ if $x > 0$, and 0 if $x < 0$.

As the point charge q enters the cavity, charges and currents are induced on the first conducting plate. These charges move out radially at the speed of light and stay on a circle of radius $r = ct$. The total charge on the plate is $-q$. The field due to these induced charges and currents plus the field due to

[46]For a guide to the derivation, see A. W. Chao and P. L. Morton, SLAC Report PEP-105/SPEAR-182 (1975).

the point charge and current is a δ-function wake field on the surface of the spherical shell $c^2t^2 = r^2 + s^2$. See Figure 2.23(a). The electric field is tangential to the shell surface, while the Poynting vector is perpendicular to the shell surface. The magnetic field is along the θ-direction and satisfies $|\vec{B}| = |\vec{E}|$. No field exists inside or outside the spherical shell surface.

At time $t = L/c$, both the point charge and the spherical wavefront of the field arrive at the second plate. At this time, drastic changes occur at the second plate. The net result is two sets of induced charges and currents. One set, with total charge $2q$, travels out radially on a circle $r^2 = c^2t^2 - L^2$ (with an apparent speed greater than the speed of light) and produces a reflection of the wave which reverses the sign of E_r but preserves the signs of E_s and B_θ. The second set of induced charges and currents, with a total charge of $-q$, travels out on a circle $r = ct - L$ at the speed of light. The field due to this second set is a δ-function signal on a new spherical shell $(ct - L)^2 = r^2 + (s - L)^2$. See Figure 2.23(b).

At time $t = 2L/c$, both of these wavefronts return to the first plate and are reflected by it, as shown in Figure 2.23(c). The wake fields then reflect between the two plates and are trapped by the cavity. Note that a test charge traveling behind the source charge along the axis will not experience any wake force until after the source charge q has passed through the second plate.

A moment's reflection indicates that we have also solved the case for a point charge penetrating a single perfectly conducting plate through an infinitesimal hole. The results are shown in Figure 2.24.

The loss factors for the case of two parallel plates are obtained from Eq. (2.161):

$$k_\lambda = \frac{2}{\pi L(1 + \delta_{p0})\left(k_x^2 + k_y^2\right)}\left[1 - (-1)^p \cos\frac{\omega_\lambda L}{c}\right]. \qquad (2.173)$$

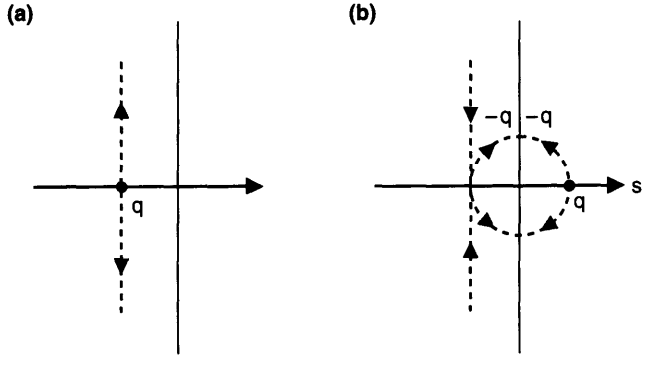

Figure 2.24. Wake field generated by a point charge penetrating through an infinitesimal hole on a perfectly conducting plate: (a) before penetration, (b) after penetration.

Similarly, from Eq. (2.165) we obtain

$$k_\lambda^{(m)} = \frac{8}{\pi L(1+\delta_{p0})(1+\delta_{m0})^2} \frac{k^{2m-2}}{(m!)^2 2^{2m}} \times \cos^2 m\phi \left[1 - (-1)^p \cos\frac{\omega_\lambda L}{c}\right], \tag{2.174}$$

where we have defined $k_x = k\cos\phi$ and $k_y = k\sin\phi$. In obtaining (2.174), we have let $b \to 0$ for the infinitesimal size of the entrance and exit holes of the cavity. For $m = 0$, Eq. (2.174) becomes (2.173).

As mentioned before, the wake functions can be obtained once we know the frequencies and loss factors of all normal modes of the empty cavity. For an idealized cavity geometry, such as two parallel plates, this can be done analytically. In general, however, no analytic solution is available and one has to resort to numerical calculations. If the vacuum chamber pipe is perfectly conducting, a commonly used approach is as follows. The region inside the pipe is first divided into subregions; in each subregion, the normal mode is expressed as an expansion in terms of functions that satisfy the wave equation and the boundary condition of that subregion. The expansion coefficients, as well as the mode frequency, are then determined by matching the fields across the junctions between subregions. The efficient implementation of the technique is a difficult research topic, and only becomes somewhat simplified if there is a symmetry (such as an axial symmetry) in the pipe geometry.

In Figure 2.25 we show the numerical results[47] for the SLAC linac structure, which is modeled as an infinite cavity array shown in Figure 2.25(a). A computer program KN7C[48] was used to obtain the loss factors of the $m = 0$ modes up to 150 GHz, and another program, TRANSVERS,[49] was used to calculate the loss factors of the $m = 1$ modes up to 75 GHz. In Figure 2.25(b) and (c), those loss factors are shown versus frequency.

Figure 2.25(b) and (c) can also be regarded as plots of the real parts of the impedances by recalling Eqs. (2.85) and (2.147). Note that it is only the real part of the impedance that contains the δ-function spikes shown in Figure 2.25(b) and (c). The imaginary part is a continuum; for each δ-function peak of $\mathrm{Re}\, Z_m^{\parallel}$ located at ω_λ, there is an imaginary part $\mathrm{Im}\, Z_m^{\parallel}$ that has a long $(\omega - \omega_\lambda)^{-1}$ tail around it.

The wake functions W_0' and W_1, obtained by Eqs. (2.148) and (2.166), are shown in Figure 2.26. They oscillate as functions of z, indicating the electromagnetic wake field "rings" in the cavity after being excited. The ringing wavelength is comparable to the cavity structure dimensions. The order of

[47] K. Bane and P. B. Wilson, *Proc. 11th Int. Conf. High Energy Accel.*, Geneva, 1980, p. 592.
[48] E. Keil, Nucl. Instr. Meth. **100**, 419 (1972).
[49] K. Bane and B. Zotter, *Proc. 11th Int. Conf. High Energy Accel.*, CERN, 1980, p. 581.

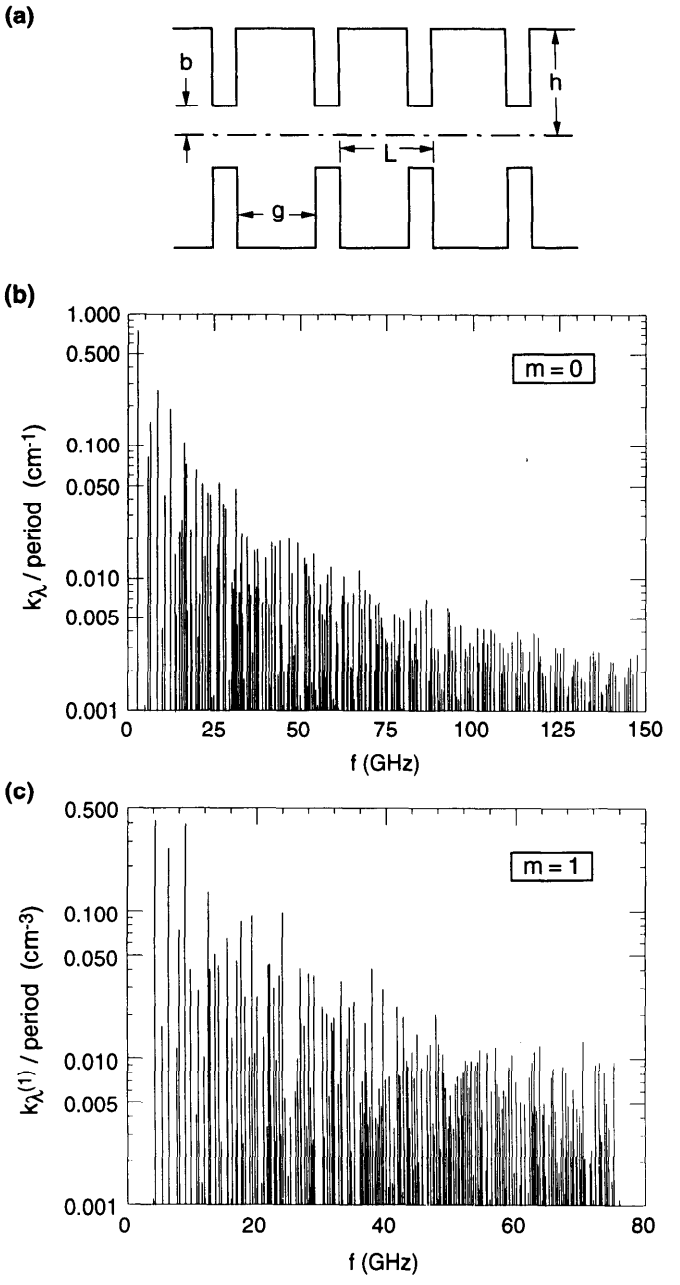

Figure 2.25. (a) The cavity model for the SLAC linac, $L = 3.499$ cm, $b = 1.163$ cm, $h = 4.134$ cm, $g = 2.915$ cm. (b) Loss factor k_λ per cavity period for the $m = 0$ modes versus frequency $f_\lambda = \omega_\lambda / 2\pi$, up to $f = 150$ GHz, for the SLAC linac. (c) Loss factor $k_\lambda^{(1)}$ per cavity period for the $m = 1$ modes up to $f = 75$ GHz.

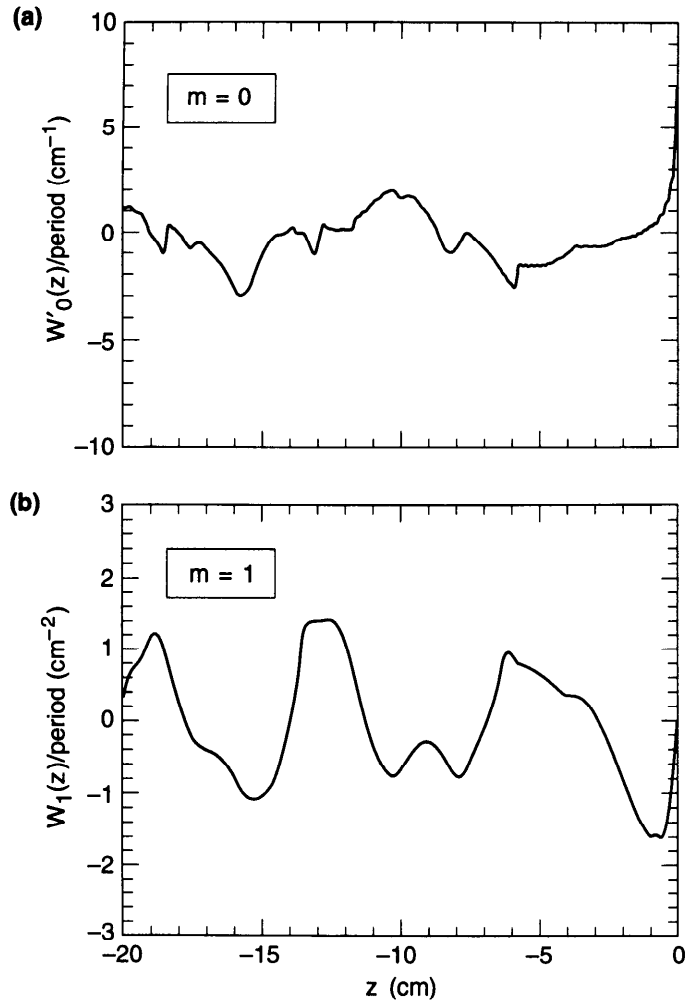

Figure 2.26. Wake functions per cavity period for the SLAC linac. (a) is for W'_0 and (b) is for W_1.

magnitude of these wakes agrees with the rough estimates (2.114) if we take b to be the disk hole radius, 1.163 cm.

The wake functions shown in Figure 2.26 are not accurate for short ranges ($|z| \lesssim 0.3$ mm). To calculate the short range behavior of the wake functions accurately, it is necessary to find modes whose frequencies are higher than 150 GHz. The behavior of the impedance at high frequencies much beyond the cutoff frequency $\omega \gg c/b$, or equivalently of wake fields at short distances $|z| \ll b$, is a difficult technical problem which we will not elaborate. It is particularly an important problem in the study of the dynamics of very short beam bunches. In addition to the calculational difficulty of requiring

more higher order modes, the crosstalk between adjacent cavity structures—which we have ignored—becomes relevant at high frequencies.

In the previous section, we introduced a diffraction model which predicted an impedance $Z_0^{\parallel} \propto \omega^{-1/2}$ at high frequencies for a single cavity structure in an infinitely long beam pipe. This $\omega^{-1/2}$ dependence of $Z_0^{\parallel}$ led to the conclusion that an ultrarelativistic point charge loses an infinite amount of energy due to the passage through the cavity structure. For an infinite cavity array—in contrast to a single standalone cavity—of Figure 2.25(a), however, the dependence of the impedance on ω is qualitatively different. In the steady state, a point charge traveling in the pipe cannot lose an infinite amount of energy per cavity, because the field that is available for the cavity to scrape was established only since the passage of the previous cavity. Calculation of the impedance at high frequencies for an infinite cavity array will not be given here.[50] The high-frequency impedance is found to be

$$Z_0^{\parallel}(\omega) \propto \omega^{-3/2}. \tag{2.175}$$

The ω-dependence (2.175) is confirmed numerically by the fact that the loss factor per unit frequency interval, $dk/d\omega$, in Figure 2.25(b) scales like $\omega^{-3/2}$ at high frequencies.[47]

One way to include the short-range behavior of the wake functions is to make an analytic extrapolation assuming $dk/d\omega$ is strictly proportional to $\omega^{-3/2}$ at high frequencies. This extension, if included, would change Figures 2.26(a) and (b) at short distances by about 10%.

The fact that the real parts of the impedances in Figure 2.25 consist of δ-function peaks is due to the assumptions that the vacuum chamber wall is infinitely conducting and that the cavity structure is infinitely periodic. When there are only a small number of cavity structures in the entire pipe or when the cavity walls are not perfectly conducting, the impedance actually looks like that sketched in Figure 2.27.

For modes whose frequencies are below the cutoff frequency $\sim c/b$, the wake fields are trapped by the cavity and ring in the cavity after the beam has departed. The widths of these modes are determined by the resistivity on the cavity wall and are described by the quality factor Q.

[50]Interested readers should read L. A. Veinshtein, Sov. Phys. JETP **17**, 709 (1963); A. M. Sessler, unpublished communication cited in E. Keil, Nucl. Instr. Meth. **100**, 419 (1972); D. Brandt and B. Zotter, CERN-ISR/TH/82-13 (1982). This approach is referred to in the literature as the *optical resonator model*. More discussions, including the transition from a single cavity to an infinite cavity array, can be found in R. L. Gluckstern, Phys. Rev. D **39**, 2733 (1989); H. Henke, Part. Accel. **25**, 183 (1990); P. B. Palmer, Part. Accel. **25**, 97 (1990); S. A. Heifets and S. A. Kheifets, Rev. Mod. Phys. **63**, 631 (1991); R. L. Gluckstern, *Proc. IEEE Part. Accel. Conf.*, Chicago, 1989, p. 1157.

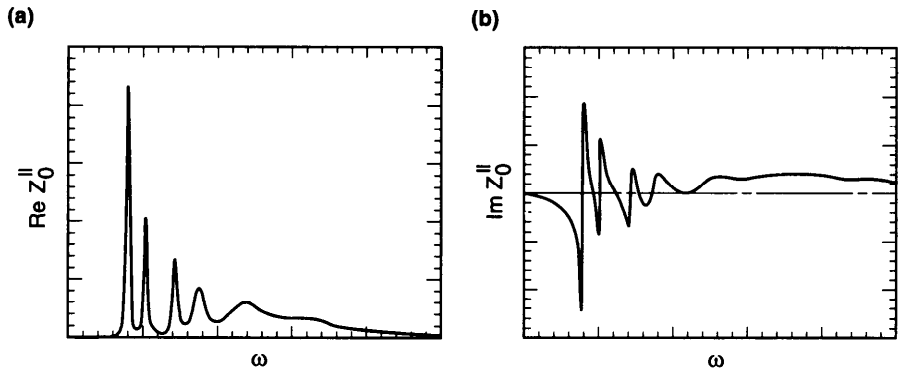

Figure 2.27. Sketch of the real and imaginary parts of a typical-looking impedance for a small number of cavities in series.

A rough estimate of Q for a cavity mode can be obtained by[43]

$$Q \approx \frac{V}{S\,\delta_{\text{skin}}}, \tag{2.176}$$

where V and S are the volume and the total surface area of the cavity, and δ_{skin} is the skin depth evaluated at the mode frequency. For the SLAC linac cavity, we have $V/S \approx 1$ cm and $f \approx 2.8$ GHz for the fundamental cavity mode. Taking $\sigma = 5 \times 10^{17}\ \text{s}^{-1}$ for copper, we find $\delta_{\text{skin}} \approx 1.3\ \mu\text{m}$ and $Q \approx 6 \times 10^3$. Larger cavities tend to have higher Q-values because of the larger value V/S (even though the lower mode frequency makes δ_{skin} larger). For superconducting cavities, Q can be as high as 10^9 or more.

Below the cutoff frequency c/b, the impedance consists more or less of discrete modes. Above cutoff, the wake field leaks out of the cavity and propagates in the pipe. The impedance in this region forms a continuum. Roughly, one can obtain this part of the impedance from that of Figure 2.25 by spreading each impedance peak over a width of $\Delta\omega/\omega \sim 1/N$, where N is the number of cavities in series. For this reason, the impedances are often either sharply peaked (below cutoff) or broad-banded (above cutoff) and not often in between. The corresponding wakes either ring for a long time or decohere quickly after being excited.

Time Domain

As mentioned at the beginning of this section, wake fields and impedances can also be calculated in the time domain by integrating the Maxwell equations. Below we will illustrate this technique by considering the $m = 0$ wake generated by an ultrarelativistic beam in an axially symmetric, perfectly conducting, vacuum chamber pipe. We will follow the illustration by

Weiland.[51] The beam is considered to be a ring charge moving along the pipe axis in the $\hat{s}$-direction with the speed of light c, i.e.,

$$\rho = \frac{1}{2\pi a}\delta(r-a)\lambda(s-ct) \quad \text{and} \quad \vec{j} = c\rho\hat{s}. \tag{2.177}$$

To proceed, we first write down the integral form of the Maxwell equations,

$$\begin{aligned}
&\oint d\vec{\mathscr{A}} \cdot \vec{E} = 4\pi \int dV \rho, \\
&\oint d\vec{\mathscr{A}} \cdot \vec{B} = 0, \\
&\oint d\vec{l} \cdot \vec{E} = -\frac{1}{c}\int d\vec{\mathscr{A}} \cdot \frac{\partial \vec{B}}{\partial t}, \\
&\oint d\vec{l} \cdot \vec{B} = \frac{1}{c}\int d\vec{\mathscr{A}} \cdot \frac{\partial \vec{E}}{\partial t} + \frac{4\pi}{c}\int d\vec{\mathscr{A}} \cdot \vec{j}.
\end{aligned} \tag{2.178}$$

The space inside the pipe is then divided into a grid of meshes. Because of the axial symmetry, each mesh accounts for a toroidal region axially symmetric around the axis. For simplicity, we assume the grids are divided evenly along the r- and the s-dimensions with grid sizes Δr and Δs. The ring beam size a in Eq. (2.177) is supposed smaller than the mesh size Δr.

The time t is also divided into discrete steps; the lth step occurs at time $t = l\,\Delta t$. The electromagnetic field components $E_r^{m,n,l}$, $E_s^{m,n,l}$, and $B_\theta^{m,n,l}$ (other field components vanish for $m = 0$) of the (m, n)th mesh, at the lth time step, are shown in Figure 2.28. The electric and magnetic field components are defined at interleaving, discrete locations as shown. Having defined the fields on the mesh grid, we are now ready to apply the Maxwell equations (2.178).

Take the third member of Eq. (2.178) first. Integrating around the rectangle of the (m, n)th mesh gives

$$\Delta s E_s^{m,n,l} + \Delta r E_r^{m+1,n,l} - \Delta s E_s^{m,n+1,l} - \Delta r E_r^{m,n,l} = -\frac{1}{c}\Delta s\,\Delta r\left(\frac{\partial B_\theta}{\partial t}\right)^{m,n,l}. \tag{2.179}$$

On the right hand side of Eq. (2.179) appears the time derivative of the

[51] T. Weiland, CERN/ISR-TH/80-07 (1980); Thomas Weiland, Part. Accel. **15**, 245 (1984).

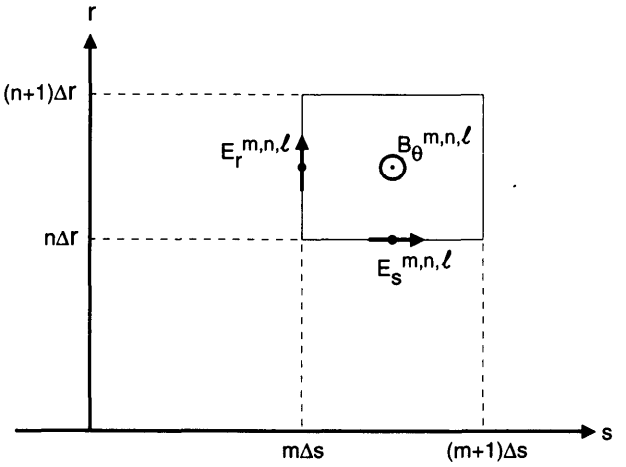

Figure 2.28. The (m, n)th mesh in the calculation of the axially symmetric time-domain wake field. The meshes are generated in the half plane defined by $\theta = 0$. For simplicity, we assume uniform mesh sizes Δr and Δs. The electromagnetic field components E_r, E_s, and B_θ at the lth time step $t = l\Delta t$ are defined at positions indicated.

magnetic field. To evaluate this time derivative, the magnetic field is evaluated at times $\Delta t/2$ away from the electric fields, and the time derivative can be written as

$$\left(\frac{\partial B_\theta}{\partial t}\right)^{m,n,l} = \frac{1}{\Delta t}\left(B_\theta^{m,n,l+1/2} - B_\theta^{m,n,l-1/2}\right). \tag{2.180}$$

This method of alternating the time steps between electric and magnetic fields is referred to in the literature as the *alternating explicit time scheme*, and was suggested by Yee.[52] Substituting Eq. (2.180) into (2.179) gives an expression for B_θ in terms of field components at earlier times according to

$$B_\theta^{m,n,l+1/2} = B_\theta^{m,n,l-1/2} - c\,\Delta t\left(\frac{E_s^{m,n,l} - E_s^{m,n+1,l}}{\Delta r} + \frac{E_r^{m+1,n,l} - E_r^{m,n,l}}{\Delta s}\right). \tag{2.181}$$

We now turn to the fourth member of Eq. (2.178). This equation gives two equations according to the choice of the integration surface. If we choose the integration surface to be the one generated by rotating the line segment between the centers of the (m, n)th mesh and the $(m + 1, n)$th mesh around

[52] Kane S. Yee, IEEE Trans. Antennas & Propagation **SP-14**, 302 (1966).

the axis, we obtain, at time $(l + \frac{1}{2})\Delta t$,

$$B_\theta^{m,n,l+1/2} 2\pi\left(n + \frac{1}{2}\right)\Delta r - B_\theta^{m+1,n,l+1/2} 2\pi\left(n + \frac{1}{2}\right)\Delta r = \frac{1}{c}\Delta s\, 2\pi\left(n + \frac{1}{2}\right)\Delta r\left(\frac{\partial E_r}{\partial t}\right)^{m+1,n,l+1/2}. \tag{2.182}$$

The time derivative of the electric field component is written as

$$\left(\frac{\partial E_r}{\partial t}\right)^{m+1,n,l+1/2} = \frac{1}{\Delta t}\left(E_r^{m+1,n,l+1} - E_r^{m+1,n,l}\right). \tag{2.183}$$

Combining Eqs. (2.182–2.183) gives an expression of E_r in terms of the field components at earlier times

$$E_r^{m+1,n,l+1} = E_r^{m+1,n,l} + \frac{c\,\Delta t}{\Delta s}\left(B_\theta^{m,n,l+1/2} - B_\theta^{m+1,n,l+1/2}\right). \tag{2.184}$$

If we choose the surface generated by rotating the line segment between the centers of the (m, n)th mesh and the $(m, n + 1)$th mesh around the axis, we obtain at time $t = (l + \frac{1}{2})\Delta t$ (except for the case $n = -1$, which contains the beam)

$$-B_\theta^{m,n,l+1/2} 2\pi\left(n + \frac{1}{2}\right)\Delta r + B_\theta^{m,n+1,l+1/2} 2\pi\left(n + \frac{3}{2}\right)\Delta r = \frac{1}{c}\left[\pi\left(n + \frac{3}{2}\right)^2 \Delta r^2 - \pi\left(n + \frac{1}{2}\right)^2 \Delta r^2\right]\left(\frac{\partial E_s}{\partial t}\right)^{m,n+1,l+1/2}. \tag{2.185}$$

Expressing the time derivative as in Eqs. (2.180) and (2.183), we arrive at an expression for E_s $(n \neq -1)$:

$$E_s^{m,n+1,l+1} = E_s^{m,n+1,l} + \frac{c\,\Delta t}{\Delta r}\left(-\frac{n + \frac{1}{2}}{n+1} B_\theta^{m,n,l+1/2} + \frac{n + \frac{3}{2}}{n+1} B_\theta^{m,n+1,l+1/2}\right). \tag{2.186}$$

For the meshes with $n = -1$, which contain the beam, the surface is the circular disk of radius $\Delta r/2$ oriented perpendicularly to the axis. Let the beam current be defined at the discrete locations $s = (m + \frac{1}{2})\Delta s$ along the axis. Let $\lambda^{m,l+1/2}\Delta s$ be the beam charge between $s = m\,\Delta s$ and $(m + 1)\Delta s$

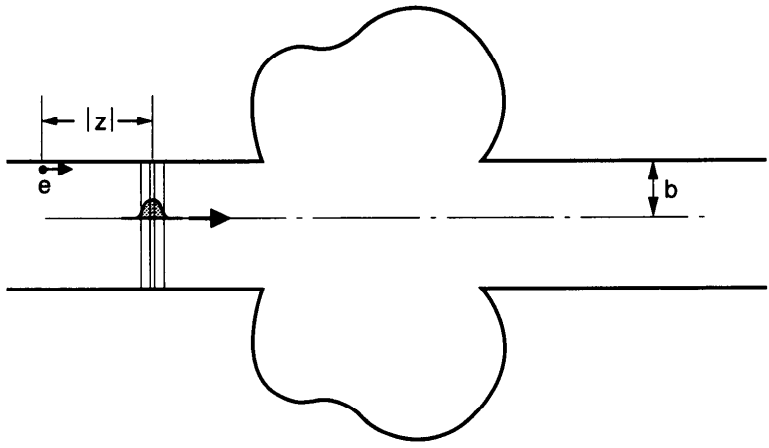

Figure 2.29. Configuration of the beam, the cavity, and the electromagnetic fields when the numerical integration of the Maxwell equations is launched. A test charge e is included in order to calculate the wake function $W_0'(z)$.

at time $(l + \frac{1}{2})\,\Delta t$. An application of the fourth member of Eq. (2.178) gives

$$B_\theta^{m,0,l+1/2} 2\pi \frac{\Delta r}{2} = \frac{\pi}{c}\left(\frac{\Delta r}{2}\right)^2 \left(\frac{\partial E_s}{\partial t}\right)^{m,0,l+1/2} + 4\pi\lambda^{m,l+1/2}, \quad (2.187)$$

which in turn gives

$$E_s^{m,0,l+1} = E_s^{m,0,l} + \frac{4c\,\Delta t}{\Delta r} B_\theta^{m,0,l+1/2} - \frac{16c\,\Delta t}{\Delta r^2}\lambda^{m,l+1/2}. \quad (2.188)$$

Equations (2.181), (2.184), (2.186), and (2.188) are our time domain numerical representation of the Maxwell equations. The remaining members of Eq. (2.178) are automatically satisfied. The meshes have to be distorted near the pipe wall to match the wall geometry. The boundary conditions that the electric field must be perpendicular to the wall surface and that the magnetic field must be tangential to the surface are straightforward to incorporate.

To start the numerical integration, at times $t = 0$ and $t = \Delta t/2$, the field configuration in the beam pipe is prepared as shown in Figure 2.29. The electromagnetic fields are just the pancake fields, and the cavity is empty. The Maxwell equations are then integrated in subsequent time steps to obtain the fields at all times and locations.

To account for the beam charges properly, Δs is chosen to be an integral multiple of $c\,\Delta t$, i.e.,

$$\Delta s = Nc\,\Delta t. \quad (2.189)$$

To assure numerical convergence,[53] we need to have

$$c\,\Delta t \leq \frac{1}{\sqrt{\frac{1}{\Delta r^2} + \frac{1}{\Delta s^2}}}. \tag{2.190}$$

Combining Eqs. (2.189–2.190), we obtain a limit on the number of time steps per longitudinal step,

$$N \geq \sqrt{\left(\frac{\Delta s}{\Delta r}\right)^2 + 1}\,. \tag{2.191}$$

For example, one may choose $\Delta r = \Delta s = 2c\,\Delta t$.

Calculation of wake functions is most difficult at short distances. To calculate the wake functions down to a small distance d, the mesh sizes must be chosen smaller than or equal to d. The total number of meshes, and therefore the computer memory required, is proportional to d^{-2} (d^{-3} without axial symmetry). Since the total number of time steps is proportional to d^{-1}, the computer CPU time to perform the field calculation is then proportional to d^{-3} (d^{-4} without axial symmetry). The computational expense escalates very rapidly if short range wake information is needed.

To calculate the wake functions, a beam bunch (say a Gaussian bunch) of length σ_z in the configuration shown in Figure 2.29 is launched to drive the wake fields. The bunch length is chosen to be comparable to d. The wake fields are calculated at all grid points and all time steps as prescribed above. Also shown in Figure 2.29 is a test charge e that trails the driving bunch by a fixed longitudinal distance $|z|$. The longitudinal force experienced by this test charge is integrated as it traverses the vacuum chamber structure. As we proved in Eq. (2.50), the integrated longitudinal force on the test charge depends on z, but not on the radial position r of the test charge for the $m = 0$ mode. This powerful property gives us the freedom of locating the test charge at any r and obtaining the same result. In Figure 2.29, the test charge is located immediately inside the vacuum chamber pipe boundary $r = b$. This has the advantage that, because the longitudinal electric field vanishes on the pipe wall, the integration of the wake force needs to be performed only in the cavity region. The wake function $W_0'(z)$ is then obtained by integrating the force on the test charges at varying distances $|z|$ behind the driving beam. The impedance $Z_0^{\parallel}(\omega)$ follows by performing a Fourier transformation on $W_0'(z)$.

The above calculation was implemented, for example, in the program BCI of Weiland.[54] It can be generalized to the $m \neq 0$ modes. In those cases, all

[53]Allen Taflove and Morris E. Brodwin, IEEE Trans. Microwave Theory & Techniques **MTT-23**, 623 (1975).

[54]T. Weiland, *Proc. 11th Int. Conf. High Energy Accel.*, CERN, 1980, p. 570.

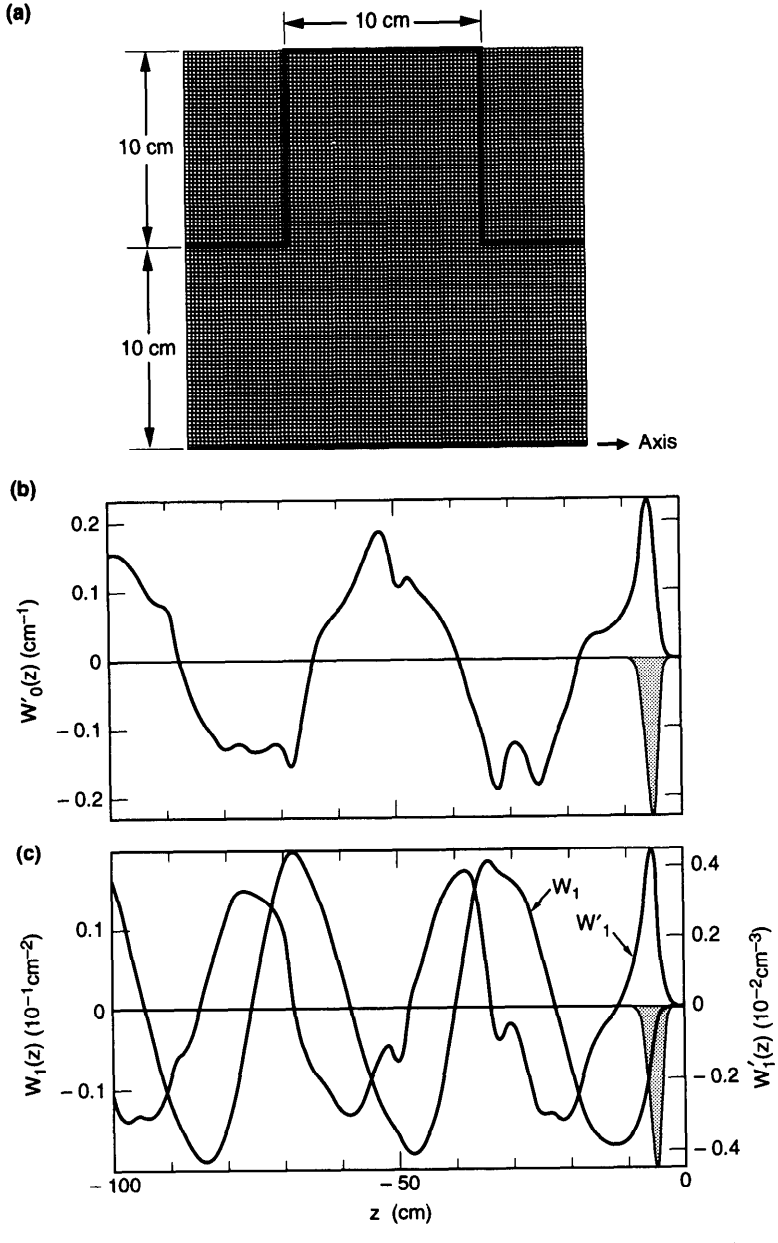

Figure 2.30. A time domain calculation of wake functions for a single cavity using the program TBCI. (a) The cavity geometry and the mesh used for the calculation. (b) The wake function $W_0'(z)$ calculated using a Gaussian driving beam (shaded curve) with $\sigma_z = 1$ cm. The peak of the driving beam is located at $z = -5$ cm. (c) Wake function $W_1(z)$ and $W_1'(z)$. (Courtesy Tom Weiland, Weiren Chou, and Bo Chen, 1991.)

six field components have to be included. This has been implemented for example in the program TBCI.[55] Although in the $m \neq 0$ cases one is most likely interested in the transverse wake functions, the integration being performed is the longitudinal wake on the test charge e. The transverse wake is obtained by integrating the longitudinal wake over z.

Shown in Figure 2.30 are some results of a wake function calculation using TBCI for a single cavity. These results are to be compared with the $b = 10$ cm case shown in Figure 2.18 using the broad-band resonator model. The agreement at short distance $|z| \lesssim b$ is reasonable. In the range between b and a few times b, the broad-band model somewhat underestimates the wakes. At long ranges, the model of course misrepresents the ringing part of the wakes, as seen in Figure 2.30.

Exercise 2.30 There is an error associated with using a bunch of finite length to derive the wake functions numerically. Suppose $\overline{W}(z)$ is the wake function found numerically by using a Gaussian beam of rms length σ_z, and $\overline{Z}(\omega)$ is the impedance obtained by Fourier transforming $\overline{W}(z)$. Show that the actual impedance is given by

$$Z(\omega) = \overline{Z}(\omega)\, e^{\omega^2\sigma_z^2/2c^2}. \tag{2.192}$$

Although Eq. (2.192) means in principle one can obtain $Z(\omega)$ by using a Gaussian beam of arbitrary length, the numerical accuracy becomes doubtful when $\omega \gtrsim c/\sigma_z$.

2.5 PARASITIC LOSS

As a beam traverses an impedance, it loses a certain amount of energy to the impedance. This energy loss, given by Eqs. (2.102–2.103), is referred to as the *parasitic loss* of the beam. For example, the space charge force does not cause any net parasitic loss on a beam, because its impedance is purely imaginary. Physically this is because particles exert forces on each other; energy gain of one particle necessarily means energy loss of an equal amount by another particle. The total energy loss of the beam, the parasitic loss, is therefore zero. A resistive wall, on the other hand, does induce parasitic losses. For a Gaussian bunch with

$$\rho(z) = \frac{q}{\sqrt{2\pi}\,\sigma_z} e^{-z^2/2\sigma_z^2} \quad \text{and} \quad \tilde{\rho}(\omega) = q\, e^{-\omega^2\sigma_z^2/2c^2}, \tag{2.193}$$

the parasitic loss rate is obtained by substituting the impedance (2.75) into

[55] T. Weiland, Nucl. Instr. Meth. **212**, 13 (1983).

Eq. (2.103). The result is

$$\frac{\Delta \mathscr{E}}{L} = \begin{cases} -\dfrac{2q^2}{b^2} & \text{if} \quad \sigma_z \ll \chi^{1/3} b, \\ -\dfrac{1}{2\pi}\Gamma\left(\dfrac{3}{4}\right)\dfrac{q^2}{b\sigma_z^{3/2}}\sqrt{\dfrac{c}{2\pi\sigma}} & \text{if} \quad \sigma_z \gg \chi^{1/3} b, \end{cases} \tag{2.194}$$

where χ is the small parameter defined by Eq. (2.10) and $\Gamma(x)$ is the gamma function. Take for example $q = 10^{11}\, e$, $\sigma_z = 10$ cm, $b = 5$ cm, $\Gamma(\frac{3}{4}) = 1.23$, and an aluminum pipe with $\sigma = 3 \times 10^{17}\ \text{s}^{-1}$; the long bunch limit of Eq. (2.194) applies, and the average energy loss rate per particle in the bunch is about 0.2 eV/m. Although this is a small energy loss, the heating of the vacuum chamber walls may not be negligible for superconducting accelerators if this heat is to be removed at liquid helium temperature. This is one reason why it is sometimes desirable to coat the inside of the vacuum chamber with copper for these accelerators.[56]

The short bunch result for $\sigma_z \ll \chi^{1/3} b$ in Eq. (2.194) is just Eq. (2.27) reproduced. Aside from a numerical factor, the long bunch ($\sigma_z \gg \chi^{1/3} b$) result, which is more relevant in practice, can be understood from

$$\frac{\Delta \mathscr{E}}{L} \sim \frac{1}{\sigma A} J^2 \Delta t, \tag{2.195}$$

where the heating is generated by a current $J \sim qc/\sigma_z$ that flows in a cross-sectional area of $A \sim 2\pi b\, \delta_{\text{skin}}$ (where δ_{skin} is the skin depth evaluated at frequency $\omega \sim c/\sigma_z$) and lasts for a time $\Delta t \sim \sigma_z/c$. See Figure 2.10. The long bunch loss is smaller than the point bunch limit by a factor of $\sim (\chi^{1/3} b/\sigma_z)^{3/2}$.

Exercise 2.31 Consider a beam (not necessarily Gaussian) which travels with a transverse offset a from the pipe axis. By summing over all multipole moments of order m, show that, in the long bunch limit, the resistive wall heating is increased from that of a centered beam by a factor of $(b^2 + a^2)/(b^2 - a^2)$. The loss becomes infinite as a approaches the pipe radius b. The short bunch limit was obtained before in Eq. (2.45).

In case the vacuum chamber pipe contains a structure which is modeled by the resonator impedance (2.82) with the corresponding wake function (2.84),

[56] Particularly if the vacuum chamber pipe is made of stainless steel.

the energy loss of a Gaussian bunch as it traverses the structure is

$$\Delta\mathscr{E} = -\frac{q^2 R_S c}{\pi\sigma_z} f\left(\frac{\omega_R \sigma_z}{c}, Q\right), \tag{2.196}$$

where we have defined a dimensionless function[57]

$$f(u, Q) = \int_0^\infty dx \frac{e^{-x^2}}{1 + Q^2\left(\frac{u}{x} - \frac{x}{u}\right)^2}. \tag{2.197}$$

If the bunch length is much longer than the resonant wavelength of the impedance, i.e., $\sigma_z \gg c/\omega_R$, the energy loss becomes

$$\Delta\mathscr{E} \approx -\frac{q^2 R_S c^3}{4\sqrt{\pi} Q^2 \omega_R^2 \sigma_z^3}. \tag{2.198}$$

The parasitic loss is proportional to σ_z^{-3} for long bunches. For short bunches, $\sigma_z \ll c/\omega_R$, one finds the point charge limit [Cf. Eq. (2.149)]

$$\Delta\mathscr{E} \approx -\frac{q^2 R_S \omega_R}{2Q}. \tag{2.199}$$

which is independent of σ_z, because $\Delta\mathscr{E}$ is simply related to the area under Re $Z_0^\parallel$ [Eq. (2.83)].

Figure 2.31 shows the function $f(u, Q)$. The dashed curves are the long bunch and short bunch limits (2.198–2.199). One observes that for the $Q = 1$ case the long bunch approximation is already reasonably accurate when $u = \omega_R \sigma_z / c \approx 1$. With a broad-band resonator (2.121) for a cavity size ~ 5 cm, and a beam bunch with $q = 10^{11}\, e$ and $\sigma_z = 20$ cm, the average energy loss of a particle in the bunch is 60 eV per traversal of the cavity. The total energy loss from the beam bunch is 10 erg, and, recalling the discussion leading from Eq. (2.116) to (2.117), about half of that energy is deposited in the cavity proper.

In a circular accelerator, one could also express Eqs. (2.198–2.199) in terms of $Z_0^\parallel/n$ of the resonator. To do this, one might identify $|Z_0^\parallel/n|$ as the slope of Im $Z_0^\parallel$ with respect to $n = \omega/\omega_0$ for small ω,

$$\left|\frac{Z_0^\parallel}{n}\right| \approx \frac{R_S \omega_0}{Q\omega_R}, \tag{2.200}$$

[57] $f(u, Q)$ can also be expressed in terms of the complex error function. See M. Furman, H. Lee, and B. Zotter, *Proc. IEEE Part. Accel. Conf.*, Washington, 1987, p. 1049.

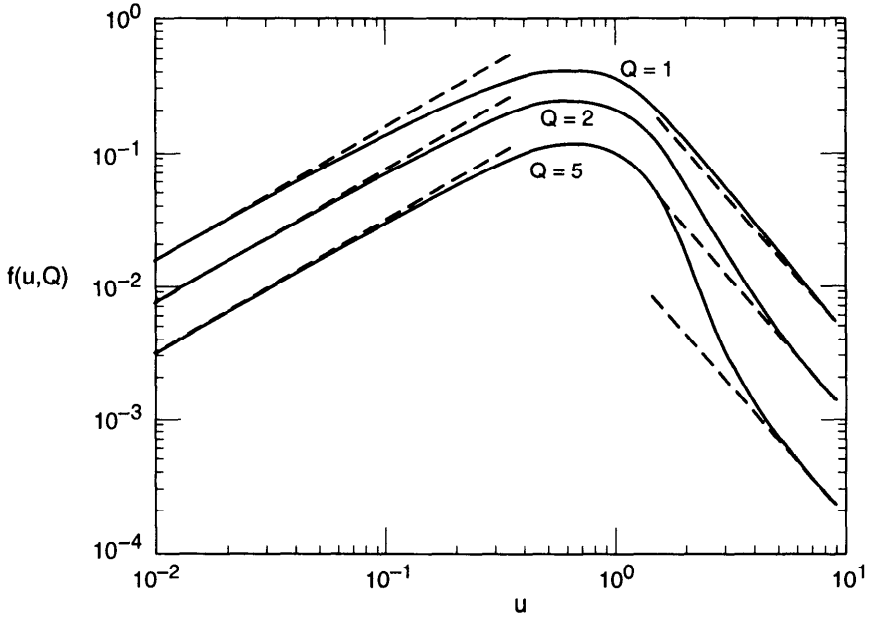

Figure 2.31. The function $f(\upsilon, Q)$ of Eq. (2.197) versus $\upsilon = \omega_R \sigma_z / c$ for $Q = 1, 2, 5$. Dashed curves are the approximations $f(\upsilon, Q) \approx \sqrt{\pi} / (4Q^2\upsilon^2)$ for $\upsilon \gg 1$ (the long bunch limit) and $f \approx \pi\upsilon / 2Q$ for $\upsilon \ll 1$ (the short bunch limit).

which in turn gives the parasitic loss power

$$P_{\text{parasitic}} = -\frac{\Delta\mathscr{E}}{T_0} \approx \begin{cases} -\dfrac{q^2c^3}{8\pi^{3/2}Q\omega_R\sigma_z^3}\left|\dfrac{Z_0^{\parallel}}{n}\right|, & \text{long bunch,} \\ -\dfrac{q^2\omega_R^2}{4\pi}\left|\dfrac{Z_0^{\parallel}}{n}\right|, & \text{short bunch,} \end{cases} \tag{2.201}$$

where $T_0 = 2\pi/\omega_0 = 2\pi R/c$ is the period of revolution of the beam around the accelerator. Taking $\omega_R = 3$ GHz, $q = 10^{11}\,e$, $\sigma_z = 20$ cm, and $Z_0^{\parallel}/n = 1\ \Omega$ (one 60 Ω broad-band resonator impedance every 38 m), we have $P_{\text{parasitic}} = 8$ W.

Conversely, Eq. (2.201) can be used to estimate the impedance $|Z_0^{\parallel}/n|$ of an accelerator by measuring the parasitic loss of a stored beam. (See also footnote 16 of Chapter 6.) Take the electron storage ring SPEAR II, for example; the loss factor $k = \Delta\mathscr{E}/q^2$ was measured to be 8 V/pC when $\sigma_z = 4.5$ cm.[58] Taking $2\pi R = 240$ m, $\omega_R = 8$ GHz, and $Q = 1$, and using the

[58] P. B. Wilson et al., IEEE Trans. Nucl. Sci. **NS-24**, 1211 (1977).

long bunch formula, one obtains $|Z_0^{\parallel}/n| = 12\ \Omega$. (SPEAR II had a relatively large impedance because it has an early vacuum chamber design.) An equivalent of 6% of the circumference is occupied by cavity-like objects according to Eq. (2.124).

When the wake function is expressed in mode expansion [Eq. (2.148)], the parasitic loss is given by

$$\Delta\mathscr{E} = -\sum_{\lambda} k_{\lambda} |\tilde{\rho}(\omega_{\lambda})|^2. \tag{2.202}$$

For a Gaussian bunch,

$$\Delta\mathscr{E} \equiv -q^2 k_{\text{Gauss}} = -q^2 \sum_{\lambda} k_{\lambda}\, e^{-\omega_{\lambda}^2 \sigma_z^2/c^2}. \tag{2.203}$$

For a point charge ($\sigma_z = 0$), we recover Eq. (2.149). When the cavity structure and the bunch length are both comparable to the vacuum chamber pipe radius b, the parasitic loss of the beam is roughly $\sim q^2/b$.

Using the loss factor k_{λ} in Eq. (2.173), we can calculate the parasitic loss of a Gaussian bunch traversing a closed cavity modeled as two parallel plates. This gives

$$\Delta\mathscr{E} = -q^2 \sum_{p=0}^{\infty} \int_{-\infty}^{\infty} dk_x \int_{-\infty}^{\infty} dk_y\, k_{\lambda}\, e^{-\omega_{\lambda}^2 \sigma_z^2/c^2} = -\frac{q^2}{L} f\left(\frac{\sigma_z}{L}\right), \tag{2.204}$$

where

$$f(u) = 2\int_0^{\infty} \frac{d\alpha}{\alpha} e^{-\alpha^2 u^2}(1 - \cos\alpha) + 4\sum_{p=1}^{\infty} \int_0^{\infty} \frac{d\alpha}{\alpha} e^{-p^2\pi^2 u^2(1+\alpha^2)}\left[1 - (-1)^p \cos\left(p\pi\sqrt{1+\alpha^2}\right)\right]. \tag{2.205}$$

The first term in $f(u)$ comes from the lowest longitudinal $p = 0$ mode in the cavity. Figure 2.32 shows the behavior of $f(u)$. For $u \gtrsim 0.5$, almost all energy deposited in the cavity is in the $p = 0$ mode. For a point bunch, $u \to 0$, the parasitic loss is infinite. In case $u \gtrsim 1$, the first term in $f(u)$ is approximately

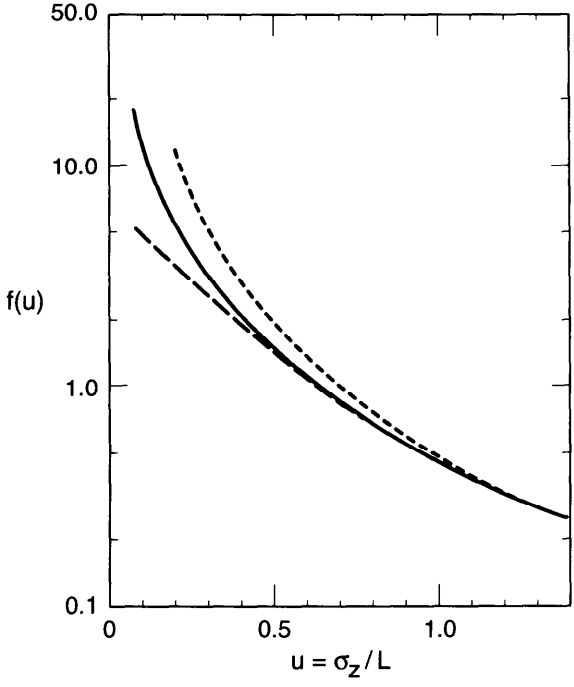

Figure 2.32. The function $f(u)$ of Eq. (2.205) versus $u = \sigma_z / L$. The dashed curve is the first term on the right hand side of Eq. (2.205), representing the energy deposited into the $p = 0$ mode only. The dotted curve is the approximation $f(u) \approx 1 / 2u^2$ for $u \gg 1$.

equal to $1/2u^2$. Therefore, when $\sigma_z \gtrsim L$, the parasitic loss is approximately

$$\Delta\mathscr{E} \approx -\frac{q^2 L}{2\sigma_z^2}. \tag{2.206}$$

Taking $q = 10^{11}\, e$, $L = 10$ cm, $\sigma_z = 20$ cm, the average energy loss per particle going through this cavity is 170 eV.

Let us examine the structure of Eqs. (2.198) and (2.206), both applicable for long bunches. Consider a broad-band resonator with $Q \sim 1$, and write $\Delta\mathscr{E}$ of Eq. (2.198) as $\sim J^2 Z_0^{\parallel} \Delta t$, where $J \sim qc/\sigma_z$ and $\Delta t \sim \sigma_z/c$. We obtain $Z_0^{\parallel} \sim R_S (L/\sigma_z)^2$, where $L = c/\omega_R$ is the characteristic dimension of the cavity. This means the long bunch has introduced a suppression form factor $(L/\sigma_z)^2$ on the effective impedance. Similar analysis of Eq. (2.206) leads to a suppression factor of L/σ_z. Closed cavities suppress less and tend to overestimate the parasitic loss for long bunches.

Exercise 2.32

(a) Use Eqs. (2.164) and (2.174) to show that the parasitic loss deposited in the two-parallel-plate cavity by a Gaussian bunch with a net mth

moment I_m is given by

$$\Delta\mathscr{E} = -\frac{I_m^2}{L}\frac{4}{(1+\delta_{m0})(m!)^2 2^{2m}} \times\left\{\int_0^\infty \frac{d\alpha}{\alpha}\left(\frac{\alpha}{L}\right)^{2m} e^{-\sigma_z^2\alpha^2/L^2}(1-\cos\alpha) +2\sum_{p=1}^{\infty}\int_0^\infty \frac{d\alpha}{\alpha}\left(\frac{\alpha p\pi}{L}\right)^{2m} e^{-\sigma_z^2 x^2/L^2}\left[1-(-1)^p\cos x\right]\right\}, \tag{2.207}$$

where $x = p\pi\sqrt{1+\alpha^2}$.

(b) Consider a Gaussian bunch with total charge q traversing the two-parallel-plate cavity with a transverse displacement a. Represent this bunch going through the infinitesimal openings as a superposition of multipole modes m and show that the parasitic loss of the off-centered bunch is

$$\Delta\mathscr{E} = -\frac{2q^2}{L}\left\{\int_0^\infty \frac{d\alpha}{\alpha}\left[2I_0\left(\frac{a\alpha}{L}\right)-1\right]e^{-\sigma_z^2\alpha^2/L^2}(1-\cos\alpha) +2\sum_{p-1}^{\infty}\int_0^\infty \frac{d\alpha}{\alpha}\left[2I_0\left(\frac{a\alpha p\pi}{L}\right)-1\right] \times e^{-\sigma_z^2 x^2/L^2}\left[1-(-1)^p\cos x\right]\right\}, \tag{2.208}$$

where $x = p\pi\sqrt{1+\alpha^2}$ and $I_0(x)$ is the Bessel function.

(c) Show that, in the long bunch limit $\sigma_z \gtrsim L$, if $L \gg a$, the parasitic loss of the offset bunch is larger than that of the centered bunch, Eq. (2.206), by a factor of $1 + a^2/2\sigma_z^2$.

Figure 2.33 shows the net loss factor k_{Gauss} per cavity as a function of bunch length σ_z for the SLAC linac using the loss factors k_λ in Figure 2.25(b) and Eq. (2.203). The parasitic loss is sensitive to the bunch length, especially for short bunches. For bunches longer than the wavelength of the fundamental cavity mode, the parasitic loss is small because the bunch tail recovers part of the energy lost by the bunch head.

Figure 2.33 is based on the calculated cavity modes up to 150 GHz. Results shown for bunch lengths $\sigma_z \lesssim 0.03$ cm or so assume the contribution from higher order modes is negligible, which will be true if the high

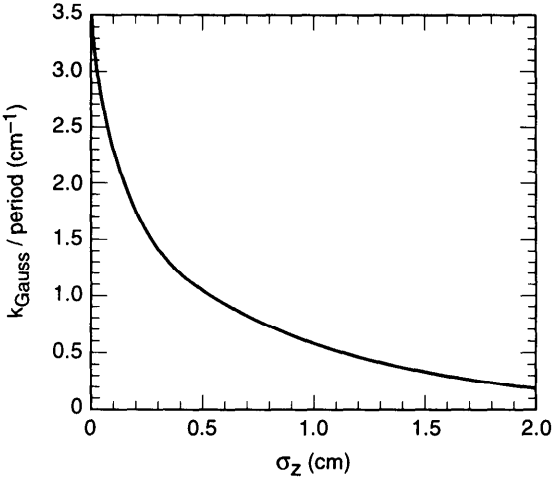

Figure 2.33. Loss factor k_{Gauss} per cavity as a function of bunch length σ_z for the SLAC linac. Shorter bunches suffer larger parasitic losses.

frequency impedance behaves according to Eq. (2.175). If so, $k_{\text{Gauss}}(\sigma_z = 0) = \frac{1}{2}W_0'(0^-) \approx 3.5\ \text{cm}^{-1}$, as shown in Figures 2.26(a) and 2.33. Taking for example $\sigma_z = 1$ mm, $q = 5 \times 10^{10}e$, and cavity length $L = 3.5$ cm, the average parasitic loss per particle of the bunch propagating down the length of the SLAC linac of 3000 m is about 1.5 GeV.

Exercise 2.33 Consider a 10 km linac with a fundamental accelerating mode frequency of $\omega_R = 2\pi \times 20$ GHz. Estimate the parasitic loss per particle in a beam bunch with $q = 10^{10}e$. [Hint: Take cavity structure dimension ~ pipe radius $b \sim c/\omega_R$, W_0' per cavity $\sim 1/b$, and $\Delta\mathscr{E}$ per cavity $\sim -q^2W_0'/2$.]

Equations (2.102–2.103) are valid for a beam traversing the impedance once. In a circular accelerator, the situation is somewhat different. As the beam traverses an impedance, it sees not only the wake field generated during this traversal, but also all traversals made in previous revolutions. The energy loss can then be written as (take $m = 0$)

$$\Delta\mathscr{E} = -\int_{-\infty}^{\infty} dz'\,\rho(z')\int_{-\infty}^{\infty} dz\,\rho(z)\sum_{k=-\infty}^{\infty} W_0'(kC + z' - z), \quad (2.209)$$

where C is the circumference of the accelerator, k sums over revolutions, and we have used the fact that $W_0'(z) = 0$ if $z > 0$.

It is more convenient to express Eq. (2.209) in terms of impedance. To do so, we will use the following identity (the Poisson sum formula):

$$\sum_{k=-\infty}^{\infty} F(kC) = \frac{1}{C} \sum_{p=-\infty}^{\infty} \tilde{F}\left(\frac{2\pi p}{C}\right), \tag{2.210}$$

where $F(z), \tilde{F}(k)$ are arbitrary Fourier transform pairs. In other words, summing a function at a regular interval C is equal to summing over its Fourier transform at the regular intervals $2\pi/C$. A particularly useful special case of Eq. (2.210) is

$$\sum_{k=-\infty}^{\infty} e^{ikx} = 2\pi \sum_{p=-\infty}^{\infty} \delta(x - 2\pi p). \tag{2.211}$$

Using Eq. (2.210), the summation over W_0' in Eq. (2.209) becomes a summation over the total impedance $Z_0^{\parallel}$ in a circular accelerator. The energy loss of a beam per revolution then becomes

$$\Delta\mathscr{E} = -\frac{\omega_0}{2\pi} \sum_{p=-\infty}^{\infty} |\tilde{\rho}(p\omega_0)|^2 \operatorname{Re} Z_0^{\parallel}(p\omega_0), \tag{2.212}$$

where $\omega_0 = 2\pi c/C$ is the revolution frequency and $\tilde{\rho}(\omega)$ is the Fourier transform of $\rho(z)$ according to Eq. (2.104). Here we see one manifestation of the usefulness of the impedance concept; Eq. (2.212) contains a single summation, but Eq. (2.209) involves a summation and a double integral.

In case the range of the wake field is shorter than the accelerator circumference, one would expect the difference between the multiturn and single-pass results to disappear. To demonstrate this, note that in this case the impedance $Z_0^{\parallel}(\omega)$ cannot have sharp structures in any frequency interval $\Delta\omega \lesssim \omega_0$. This means the summation over p in Eq. (2.212) can be replaced by an integration over p. Equation (2.212) then reduces to Eq. (2.103), as it should. In case the wake field lasts for distances $\gtrsim C$, Eq. (2.212) must be used instead of Eq. (2.103).

Exercise 2.34 Consider a narrow-band resonator impedance with $\omega_R/Q \ll \omega_0$. Let h be the closest integer such that $\omega_R \approx h\omega_0$, and define $\Delta = (h\omega_0 - \omega_R)/\omega_R$. Show that, for a Gaussian bunch with $\sigma_z \ll c/\omega_R|\Delta|$,

$$\Delta\mathscr{E} \approx -\frac{\omega_0 q^2 R_S}{2\pi} \frac{e^{-\omega_R^2\sigma_z^2/c^2}}{1 + 4Q^2\Delta^2}. \tag{2.213}$$

Most of the parasitic loss occurs as the beam traverses a discontinuous structure in the vacuum chamber pipe. Part of the wake field gets trapped by the structure if the structure is cavity-like and if the wake field frequency is

below the cutoff frequency of the pipe. This trapped field energy is eventually deposited as heat on the cavity walls. The rest of the wake field, with frequency higher than the cutoff frequency, propagates down the pipe and eventually deposits its energy on lossy material elsewhere in the vacuum chamber, much like heating a potato in a microwave oven.[59]

The parasitic energy lost by the beam goes into the wake fields. Typically, only a small fraction of the particle energy is depleted to produce the wake fields, and most of the energy stored in the wake fields ends up as heat on the vacuum chamber walls; but under unfavorable conditions, the wake field energy can be transferred systematically back to beam motion, causing beam instabilities. The parasitic loss, therefore, is ultimately responsible for the various collective beam instabilities. How the wake fields affect the beam dynamics and what are the mechanisms of the various collective beam instabilities are subjects to which we will devote the following chapters. The parasitic energy loss, of course, will have to be supplied back to the beam by an rf accelerating voltage.

[59]Next time you put a potato into a microwave oven, think of it as the impedance.